Investigation of Sinonasal Airflow and Transport

by

Catherine E. Rennie

Department of Aeronautics

Imperial College of Science, Technology and Medicine

Prince Consort Road

London SW7 2BY

This thesis is submitted for the degree of Doctor of Philosophy of Imperial College London

2013

Abstract

This work comprises an investigation of airflow and transport in the human upper airways, which not only perform essential air conditioning physiological functions (heat and water exchange and primary filtration) but also house the olfactory receptors. The conflicting requirements posed by efficient air transit on the one hand and sampling for olfaction on the other renders the geometry of the upper airways complex.

Knowledge of the geometry and flow conditions are primary requirements for understanding the physiological mechanics of the airways. This work describes the application of imaging and experimental measurement techniques to determine the variations in nasal airway geometry and the characteristics of nasal inspiratory flow. Whilst the results are relevant to a host of applications, the particular case of sinonasal ventilation well illustrates the interrelation between form, flow and function as well as motivating the development of improved techniques for clinical management.

Specifically 3T MR imaging has been investigated as a means to define the anatomy in congested and decongested states. Results show very large changes in nasal airway calibre and moreover allow the variation in mucosal engorgement throughout the nasal cavity to be mapped. Highly time resolved hot wire measurements of inspiratory flow profiles revealed for the first time the rapid temporal development of inspiratory flow during normal inspiration and dramatically so during sniffing. Variations in flow profile were recorded across a cohort of subjects for conditions of normal inspiration, sniffing and smelling.

Sinonasal gas exchange is of particular interest given the common occurrence of sinus pathologies. Here short half-life Krypton imaging has been used to investigate gas exchange between the maxillary sinus and the nasal cavity. It has been shown that the technique can provide quantitative assessment of volume flow rate in a model, demonstrating the rapid venting associated with an accessory ostium.

Declaration of Originality

I declare that the work presented in this thesis is my own, and any work done by others is explicitly attributed.

Catherine Rennie

Copyright Declaration

Acknowledgements

I would like to acknowledge my supervisors, Prof. Denis J. Doorly and Mr Neil S. Tolley, who have been a constant source of guidance and expertise throughout my research.

Furthermore, I would like to thank Dr. Christina M. Hood, Dr. Donal J. Taylor and Dr. Kevin Gouder for their support, advice and encouragement.

I also extend my appreciation to Prof. Robert C. Schroter, Dr. Hazel Jones, Dr. David Towey, Esther J.S.M. Blenke and Raul Cetto for their help and guidance.

Finally I am indebted to my family and friends for their invaluable support throughout what has been an enjoyable, if eventful and testing, period.

Contents

List of Figures

List of Tables

Chapter 1

Introduction

1.1 Motivation for studying sinonasal airflow and transport

The nose is the entrance to the airway and has multiple functions: it provides the first line of defence against infection, it is a sensory organ and perhaps most importantly a remarkably efficient air conditioner that protects the delicate alveolar environment. The nasal cavity is enclosed by four groups of air filled paranasal sinuses, which connect to the nasal airway (Figure 1.1). In contrast to the nose the function of the sinuses remains a mystery, many theories have been proposed but none are universally accepted.

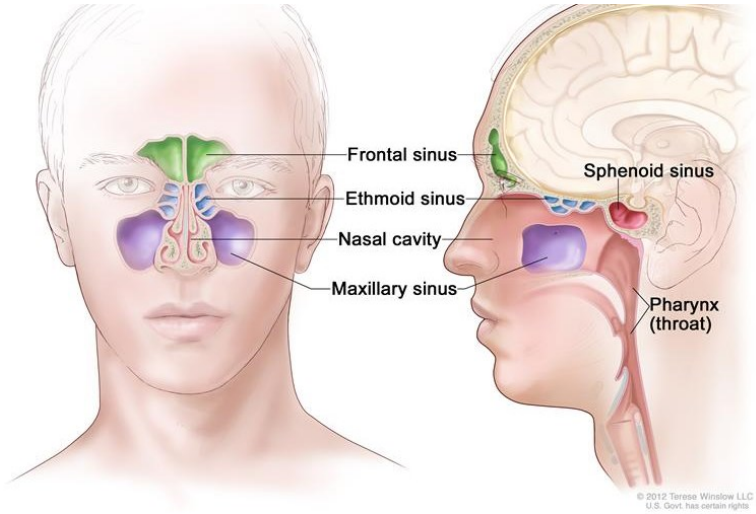

Figure 1.1 Anatomy of the nose and paranasal sinuses[1].

The lung requires air to be warmed to near to 37^0C with 100% relative humidity. Inspiration through the nasal cavity conditions the ambient air to nearly alveolar requirements by the time it reaches the pharynx and is able to do this even in extremes of environment such as sub-Saharan Africa or the Antarctic[1,2]. This involves humidification, temperature modification, particle filtration, with olfaction and phonation as secondary functions.

Whilst we appreciate the multiple and varied functions of the nose our knowledge of the fundamental physiology underlying them remains limited. In vivo measurements of the conditions within the sinonasal airway are hampered by its inaccessibility. The complex geometry, narrow calibre and sensitivity of the tissues preclude direct measurement, as the placement of even a small probe would not only be difficult, but would also obstruct the airflow it was intended to measure. Our knowledge of functional parameters is limited to point wise measures of local quantities (e.g., velocity, temperature, humidity) or global measurements (e.g., pressure drop) up- or down-stream of the sinonasal airway. Experimental and computational simulations have provided an insight into the interaction of nasal airflow with anatomical form, however, modelling relies on clinically derived data to enhance modelling capabilities.

Regrettably there are limited detailed in vivo measurements available to provide a rigorous characterisation of nasal inspiration. To date the time-dependent evolution of the volume flow rate waveform during inspiration (which is important in understanding the disparate and complex functions of the respiratory airways) has largely been ignored, or for modelling studies, greatly simplified (e.g., assumed sinusoidal profile). However, for many applications these assumptions may be inappropriate and could provide misleading results. The transient dynamics of inspiration will strongly impact on the intended application e.g., temporal oscillations of the inspiration flow rate profile could dramatically increase mixing and hence enhance olfactory perception or further distribute patterns of drug deposition. Determination of the characteristic features of the nasal profile is thus needed to improve physiological understanding and for applications requiring detailed knowledge of the transport properties of the flow.

A small number of studies have investigated airflow in the same patient before and after surgery[3,4]. However, there has been little investigation of the normal intra-individual variations in nasal anatomy due to the nasal cycle. There is currently little available data to detail the anatomical changes during the nasal cycle or with decongestion. These changes could lead to alterations in the transport of inhaled substances and the processes of heat and water exchange at the nasal mucosal surface.

In contrast to the nose the functions of the paranasal sinuses remain an enigma. In the 1960's Blanton and Biggs[5] published a review entitled "Eighteen hundred years of controversy: The paranasal sinuses" in which they document years of speculation over the physiological function of the sinuses. Forty years later, in a recent review by Keir (2009) "Why do we have paranasal sinuses?"[6], it would appear that little has improved in the understanding of sinus function. The Greek physician and philosopher Galen (130-201 AD) is credited with the original description of the paranasal sinuses[7], however the first documented evidence is provided by the notebooks of Leonardo da Vinci where his illustrations 'View of the Skull' and 'Two views of the skull' (circa 1489) show sagittally and coronally sectioned human skulls with the frontal and maxillary sinuses exposed[8] (see figures 1.2+1.3 pg 18). One of the earliest theories of sinus function was proposed by Da Vinci who postulated that the maxillary sinus 'contains the humor which nourishes the teeth'[9]. Keir (2009)[6] discusses the validity of each proposed function and theoretically or scientifically discounts all theories, except the hypothesis that the sinuses function to enhance immune and antimicrobial function. Whilst this may give a function to sinuses it does not necessarily explain why we have sinuses.

Studies investigating comparative anatomy between species have been unable to elucidate sinus function as the presence, size and shape of paranasal sinuses appear to be randomly distributed between species[10]. Lund (1988), found no statistically significant differences in skull size or environment when comparing species in the same genus with and without sinuses[11]. It is possible that the sinuses arose as an aid to facial growth and architecture[12], or that they persist as residual remnants of an evolutionary structure [13] with an as yet unknown purpose, and in doing so have found an additional role as an adjunct to the nasal cavity. Whilst we may never find a single function or purpose for the sinuses an increased understanding of the physiology may help to support or refute the numerous hypotheses.

Rhinosinusitis is a common condition affecting ~15% of the western population and is a major reason for medical consultation worldwide[14-18]. It is defined as inflammation of the mucosa lining the nasal cavity and paranasal sinuses resulting in two or more symptoms either: nasal blockage or discharge and pain or loss of smell[19,20]. Treatment for rhinosinusitis is estimated to cost more than $5.8 billion annually in the USA[21] and it is ranked in the top ten most expensive conditions for US employers based on combined healthcare and productivity costs[22]. These huge costs make sinus disease a significant public health issue[23-25]. In addition to the financial costs studies have shown that chronic rhinosinusitis (CRS) significantly impacts quality of life, even in comparison to chronic debilitating diseases, with perceived bodily pain and impact on social functioning worse than for angina pectoris, congestive heart failure,

chronic obstructive pulmonary disease, and chronic back pain[26]. CRS not only causes significant physical symptoms but also results in substantial functional and emotional impairment[27].

Despite the vast socioeconomic impact of sinusitis the causes are not well understood. Important factors in the pathogenesis of sinusitis are reduced sinus ventilation and impaired mucociliary transport.

Improved sinus ventilation is often a goal of clinical interventions; however, the links among sinus geometry, ventilation, and clinical outcomes are still poorly understood. An improved insight into normal sinus function is critical to furthering our understanding of the pathophysiological processes that mediate sinus disease.

Though this work is primarily motivated by a desire to better understand the complex sinonasal physiology, it also impacts on many other research areas including: planning and assessment of surgical interventions, the design of drug delivery devices, and toxicological research.

1.2 Anatomy

The nose and paranasal sinuses are complex three dimensional structures. The nose is subdivided into the external nose and nasal cavity for anatomical purposes. The visible external nose represents only a small portion of the nasal airways. The nasal cavity extends from the nostrils anteriorly to the posterior choanae (the opening between the nasal cavity and nasopharynx) and is divided sagittally by the nasal septum into asymmetrical (even in the decongested state) left and right passageways. The efficiency of healthy nasal function is strongly dependent on the nasal anatomy which controls and distributes airflow.

The paranasal sinuses are air-filled pockets located within the bones of the face and around the nasal cavity. The sinuses are named after the bones in which they are located; maxillary (one sinus located in each cheek), ethmoid (approximately 6-12 small sinuses per side, located between the eyes), frontal (one sinus per side, located in the forehead) and sphenoid (one sinus per side, located behind the ethmoid sinuses, near the middle of the skull). The sinuses connect to the nose through openings called ostia[28,29].

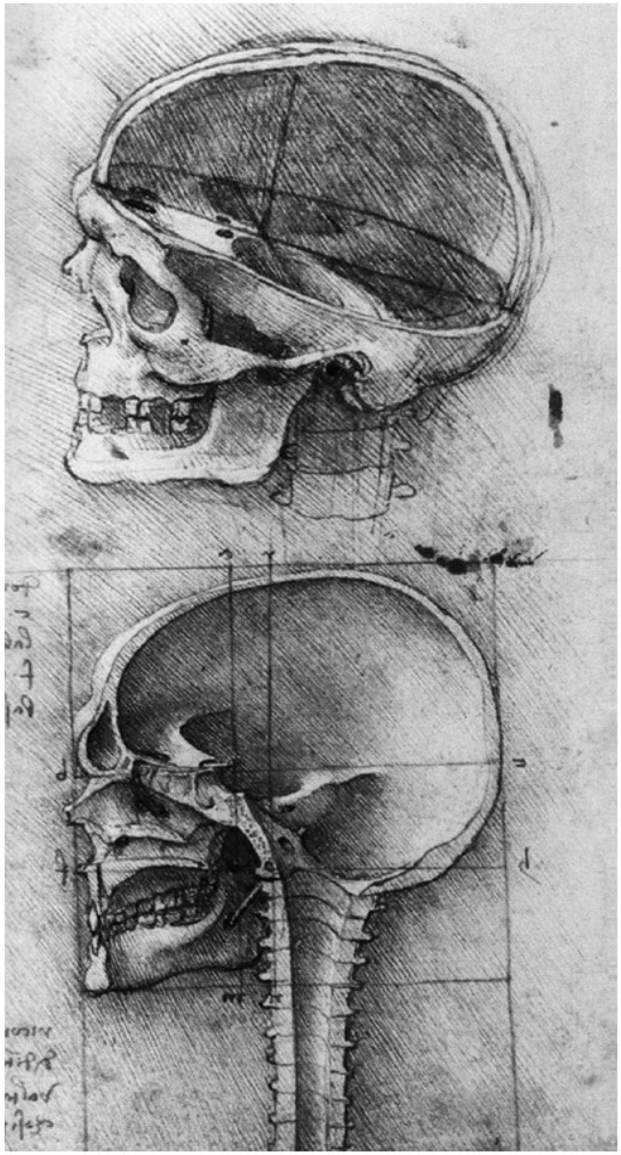

Figure 1.2 'Two views of the skull' by Leonardo Da Vinci, circa 1489

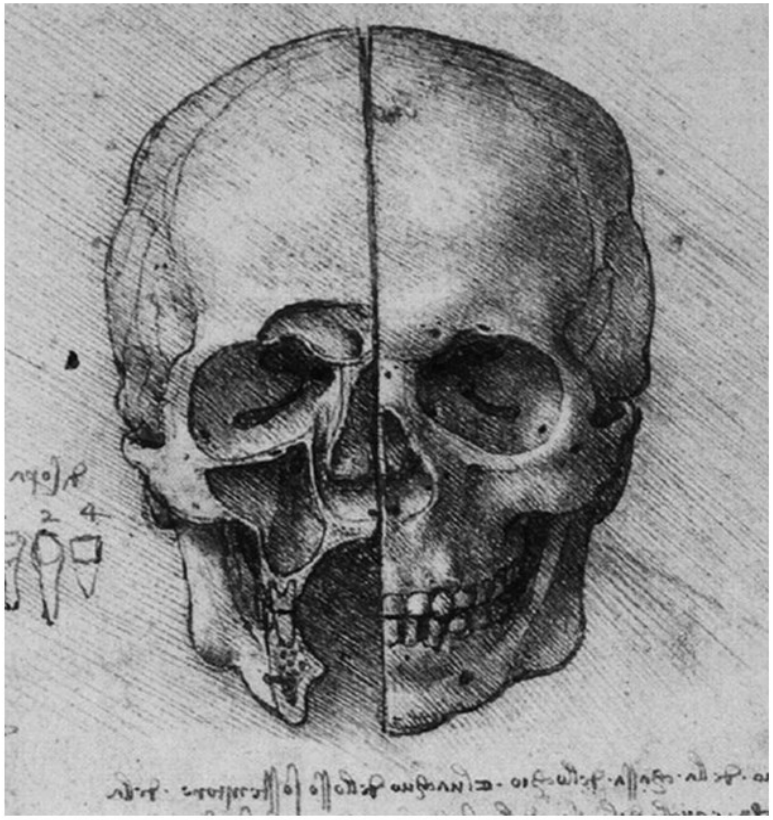

Figure 1.3 'View of a skull' by Leonardo Da Vinci, circa 1489

1.2.1 Nasal Cavity

The anatomy of the nasal cavity is the most important factor in determining the mechanics of nasal air flow[30]. It extends from the nostrils or nares anteriorly to the choanae posteriorly; it is divided into two by the nasal septum. Each side has a roof, floor, medial and lateral wall. The roof is narrow and formed of the body of the sphenoid and the cribiform plate of the ethmoid through which the delicate olfactory fibres pass more anteriorly. The floor is formed by the palatine process of the maxilla and the horizontal plate of the palatine bone. The medial wall is the nasal septum an osseocartilaginous partition separating the two sides. The lateral nasal wall (Figure 1.4) has three important structures, which are known as the superior, middle and inferior turbinates. Each turbinate is a rounded shelf like projection that extends the length of the nasal cavity. The area between each turbinate is referred to as a meatus.

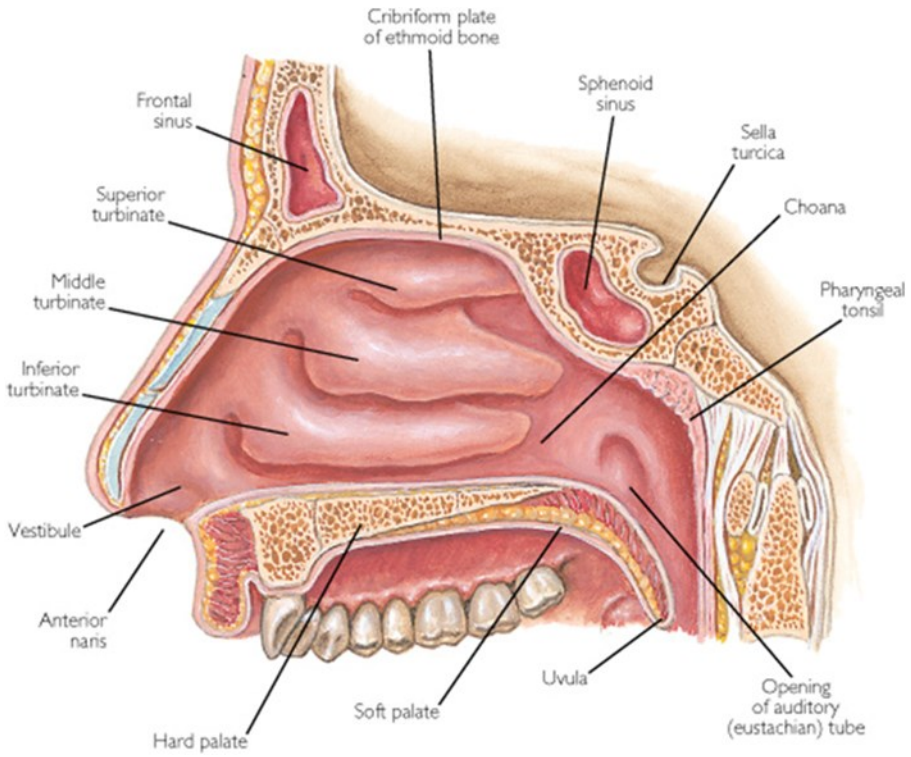

Figure 1.4 Schematic representation of the lateral nasal wall anatomy, viewed through the omitted septal wall[31].

The nasal vestibule is the most anterior part of the nasal cavity and is bounded internally by the region of the nasal valve. It is lined by stratified squamous, keratinized epithelium (skin), in contrast the remainder of the nasal cavity is lined by the respiratory epithelium. Inside the vestibule are short thick hairs (vibrissae), which aid in the filtration of

large particulate matter. The nasal valve region, formed by the junction of the upper lateral cartilages, the nasal septum and the inferior turbinate, is typically the narrowest point in the nasal cavity and accounts for up to 50% of total airway resistance in quiet breathing conditions[2]. Beyond the nasal valve the airways expand rapidly until the turbinates are reached.

The inferior turbinate, which is the largest turbinate, occupies a significant proportion of the nasal cavity, it is responsible for the majority of humidification, heating, and filtering of air inhaled through the nose. It is made up of dense lamellar bone from the maxilla and is covered with erectile tissue. The surface of the turbinate is covered with a pseudostratified columnar, ciliated respiratory epithelium; beneath this the submucosa contains numerous seromucinous glands and vascular channels containing cavernous sinusoids. Nasal airflow is regulated through volume changes in these sinusoids. These channels are under autonomic control and are the end targets for decongestant medications. Beneath the inferior turbinate is the inferior meatus into which the nasolacrimal duct drains. The middle turbinate is located above the inferior turbinate. The maxillary sinus, anterior ethmoids and the frontal sinus via the frontal recess open into the middle meatus. The superior turbinate, the smallest turbinate, lies above the middle turbinate. The posterior ethmoid cells and sphenoid sinus drain into the superior meatus. The turbinates end at the posterior choanae and the two nasal cavities join to form the nasopharynx.

The nasal anatomy is not fixed and may change dynamically in response to either vigorous respiration, stimulus or the nasal cycle. The latter represents a reciprocating cycle of congestion and decongestion of alternate sides of the nose that has been recognized for over a century[32], and although its exact function is unknown it has been suggested that it plays a role in respiratory defence[33]. The autonomic nervous system affects changes in regional airway calibre through congestion and decongestion of the nasal venous sinusoids. Early studies reported a frequency of approximately 80% in the general population[34,35]. More recent work has shown that the nasal cycle is much less common, and may only occur in 21-39% of the population[36,37]. These fluctuations occur on a timescale orders of magnitude larger than the typical breathing cycle, although the period and extent of change shows considerable inter-subject variability[37]. Recent studies using acoustic rhinometry have demonstrated that the cycle is present in children as young as 3 years, and that it persists after cessation of nasal airflow. It may, however, be overridden or modulated by many environmental and pathological situations.

Variations in airway calibre can also be facilitated by the facial nerve, as an increase of tone in the dilator alae muscles results in nasal flaring and an increase in anterior nasal cross sectional area. However, increased negative pressure during forced inspiration can cause the nasal vestibule to collapse inwards and decrease the cross sectional area.

1.2.2 Embryology

The nose develops in the fourth intrauterine week. Three facial prominences from the 1st pharyngeal arch develop on the ventral surface of the embryo, and paired thickenings forming the nasal placodes appear in the cranial ectoderm above the stomatodeum (primitive mouth). These nasal placodes invaginate to form nasal pits and then subsequently nasal sacs by the fifth week. In doing so ridges of tissue surrounding each pit form the medial and lateral nasal prominences which eventually form the columella, tip and alae of the nose. The nasal sacs deepen and thin the bucconasal membrane until it ruptures to form the posterior choanae. The nasal septum continues to form from contributions made by the frontonasal process and the forebrain capsule[38]. Diverticulae develop from the lateral nasal walls into the maxillary, ethmoid, frontal and sphenoid bones, forming the paranasal sinuses. The maxillary sinus is the first sinus to develop (seven to ten weeks) and is filled with fluid at birth[11]. It grows according to a biphasic pattern, in which the first phase occurs during years 0-3 and the second during years 6-12[39]. The ethmoid sinuses are a collection of fluid-filled cells at birth that grow and pneumatise until the age of 12. The sphenoid sinus reaches its full size by the late teenage years, it is variably pneumatised and may extend as far as the foramen magnum in some patients. The frontal sinus is formed by the upward movement of anterior ethmoid cells after the age of 2. Growth of this sinus increases at the age of 6 and continues until the late teenage years [40].

1.2.3 External Nose

The frame work of the nose consists of a bony upper third and cartilaginous lower third (Figure 1.5). The upper third is made up of the nasal bones, the frontal process of the maxilla and nasal process of the frontal bones. The cartilaginous lower third comprises of the upper laterals, lower laterals and septal cartilages. The upper lateral cartilages are overlapped superiorly by the nasal bones, they fuse in the midline with the septum and inferiorly with the lower lateral cartilages. The lower lateral cartilages have a medial crus that forms the columella and a lateral crus that forms the nasal alae. Nasal flaring is controlled by two important muscles in the lower nose, the compressor naris and dilator naris. Both of these muscles are supplied by the buccal branch of the facial nerve.

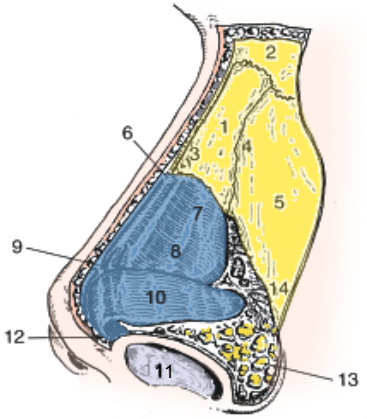

1 - nasal bone
2 - nasion (nasofrontal suture line)
3 - internasal suture line
4 - nasomaxillary suture line
5 - ascending process of maxilla
6 - rhinion (osseocartilaginous junction)
7 - upper lateral cartilage
8 - caudal edge of upper lateral cartilage
9 - anterior septal angle
10 - lower lateral cartilage - lateral crus
11 - medial crural footplate
12 - intermediate crus
13 - sesamoid cartilage
14 - pyriform aperture

Figure 1.5 Nasal anatomy adapted from Revision Rhinoplasty[41].

1.2.4 Maxillary sinus

The pyramid shaped maxillary sinus (or antrum of Highmore) is the largest of the paranasal sinuses, is situated in the body of the maxilla. The apex of the sinus extends into the zygomatic process of the maxilla and the lateral wall of the nose forms the base. The ostium for drainage is located high on the medial wall and opens into the middle meatus on the lateral wall of the nasal cavity (Figure 1.6). The position of the ostium prevents drainage of the maxillary sinus contents by gravity when the head is erect. The sinus is lined with mucoperiosteum, with cilia that beat toward the ostia, this mucociliary clearance is essential to expel mucus and pathogens from the sinus. The lack of gravity dependent drainage renders the maxillary sinus particularly susceptible to sinusitis.

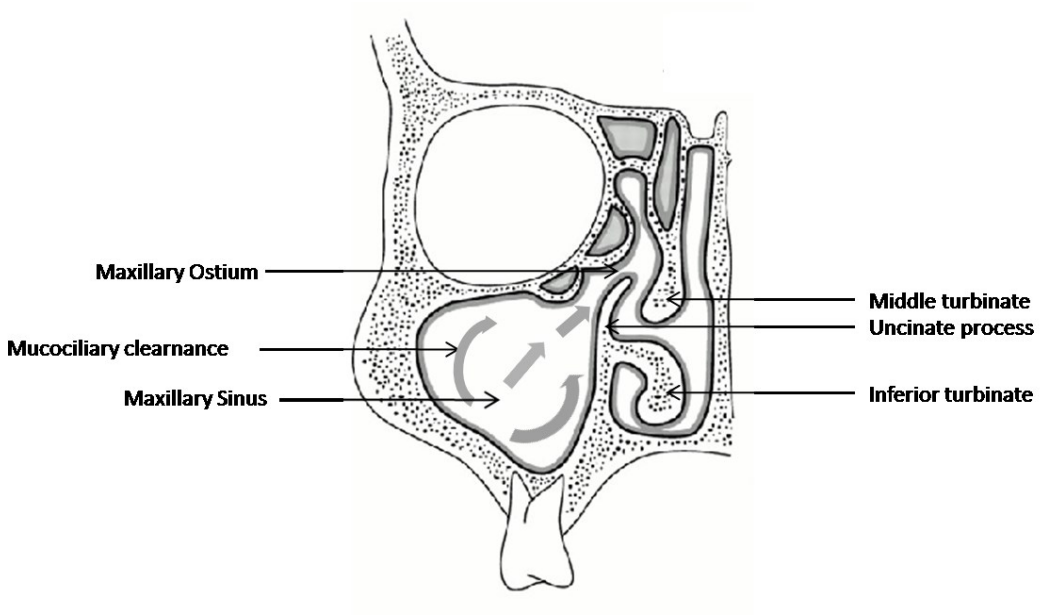

Figure 1.6 Coronal section through the maxillary sinus adapted from Hosemann W. (2000)[42].

Studies of sinus anatomy have been reported from 1880 onwards, although it has not been possible to get some of the original papers their results have been quoted in later papers and table 1.1 gives a summary of the values found for maxillary sinus volume, ostial diameter, ostial length and presence of accessory ostia. Measurements of ostial size and the presence of accessory ostia are hampered by the inaccessibility and complex geometry of the sinuses and as a result many studies have been performed in cadavers. However, cadavers are subject to dehydration and shrinkage of the mucosa which could result in greater dimensions for sinus volume and ostial diameter. Higher proportions of accessory ostia are seen in cadaveric studies and this is likely to be because the fontanelles where the majority of accessory ostia are found are particularly sensitive to damage when drying out[43].

A relationship between rhinosinusitis and the presence of accessory ostia has been reported in the literature but the causal link is unclear. It has been proposed that infections may damage the fontanelle membranes and create accessory ostia[28,44] and that accessory ostia disrupt mucociliary clearance pathways and result in sinusitis[45,46].

Table 1.1 Summary of the findings from anatomical studies of maxillary sinus and ostial dimensions[47,48].

Author	Year	Cadaveric, healthy or pathological	No. studied	Sinus Vol (ml)	Ostium diam (mm)	Ostium length (mm)	Accessory ostia present (%)	Cited by
Neivert	-	Cadaver		-		-	25	Van Alyea (1936)[49]
Zuckerkandl	1882-3	Cadaver			2-19	7-11	10	Rantanen (1974)[50]; Lang (1989)[28]
Oppikofer	1906	Cadaver			2-17	-	11	Myerson (1932)[51,52]; Rantanen (1974)[50]
Skillern	1913	Cadaver			2-17	-	-	Simon 1939[53]
Schaeffer[7]	1920	Cadaver			1-22	-	44	Simon (1939)[54]; Rantanen (1974)[50]
Myerson[51,52]	1932	Cadaver	170		1-13	-	31	
Van Alyea[49]	1936	Cadaver	163				23	
Simon[53]	1939	Cadaver	102			1-15 Av 5.55	20	
Flottes et al[55]	1960	Cadaver		10				Aust and Drettner (1974)[56]
Wagemann	1964	Cadaver		2-30 av 15	-	-	-	Aust and Drettner (1974)[57]
Aust[57]	1974	Cadaver		9-23	0.4-5+	(6)	-	
May[58]	1990	Cadaver and Sinus surgery patients	10 cadaver 100 sinus surgery	-	-	-	10	
Earwaker[59]	1993	CT scans of FESS referrals	800	-	-	-	14	
Jog et al[60]	2003	Healthy and rhinology patients	113 healthy 91 patients	-	-	-	2 (healthy) 8 (Rhinol Pts)	

1.3 Physiology

At rest, humans and other primates respire mainly through the nose even though the tortuous anatomy imposes a significantly higher resistance than mouth breathing. This resistance, which accounts for between half and two thirds of total airway resistance, facilitates temperature regulation and humidification by slowing down air flow and increasing the time spent in contact with the highly vascularised nasal mucosa. At a normal respiratory rate of 12-15 breaths per minute with a tidal volume of 500ml we respire about 10,000L per day[2,61], resulting in a typical inspiratory flow rate of 250ml.s^{-1} distributed between the two nasal cavities. At increased respiratory rates, for example during exercise, humans revert to mouth breathing as partial collapse of the nasal airway increases the work of the lungs[62].

There is growing evidence to support the concept that the respiratory tract functions as an integrated unit "the unified airway". Hence, changes in the physiology of the nose and paranasal sinuses can and will affect the lower airways and vice versa[63]. Support for this relationship can be found in epidemiological studies, in shared pathophysiological mechanisms, and in observed interactive treatment effects. Rhinosinusitis and asthma have common inflammatory mechanisms and often coexist in the same patients[64]. Treating rhinosinusitis and other upper respiratory tract disorders, has been shown to improve asthmatic control and reduce the need for asthma medications[65,66].

1.3.1 Nasal Airway

The nasal airway is a remarkably complex biological conduit that plays a key role in the filtration, warming and humidification of inspired air. It also provides the first line in respiratory defence, is an important chemosensor and acts as a phonation chamber.

1.3.1.1 Nasal Function

Air conditioning

The nose is an exceptionally efficient air conditioner, the mucosa with its rich blood supply heats and humidifies ambient air to near core conditions over a remarkably short distance[67,68,69] and irrespective of environmental extremes[1]. The relationship between humidity and temperature in the ambient air and core air is dynamic over a breath cycle and varies according

to the respiratory rate and force, whether nasal or mouth breathing is predominant or if there is underlying respiratory pathology[70]. A healthy adult requires 350kcal and 400ml of water per day to condition air at average environmental conditions (22°C and a relative humidity of 50%). Water conservation during expiration recovers about a third of that used up in inspiration[71-73]. The air conditioning capacity of the nasal cavity is facilitated by its high surface area to volume ratio, and is sensitive to the nasal inspiratory flow profile[74] .

Filtration

The nose provides the only means through which warm, humidified and filtered air can reach the lower respiratory tract. It is an efficient filter for particulate matter, and it also serves to provide the first line in respiratory immune defence by bringing trapped particles in contact with the Immunoglobulin A (IgA) rich nasal mucous. The nose removes all particulate matter >5μm and around 50% of material of 2-4 μm^2. There are four elements to nasal filtration these include: impingement, electrostatic charge, vibrissae and mucociliary blanket. Impingement is the process whereby particles suspended in a gas are deposited on walls downstream from a bend. As a result of impingement between 85-90% of particulate matter > 5 μm are deposited on the nasal cavity walls. The positive electrostatic charge of the mucociliary blanket attracts and traps negatively charged matter. The vibrissae within the nasal vestibule trap larger particles and are a sensitive stimulus for the sneeze reflex. Finally the mucociliary blanket transports entrapped matter towards the nasopharynx with a clearance within 15 minutes[72]. The mucus layer is biphasic with a serous, sol layer in which the cilia beat and a superficial gel layer. The viscosity of this upper mucous layer means that the tips of the cilia catch in the layer and propel it along the nasal cavity[75]. Mucociliary clearance can be disrupted by pathogens, inflammatory processes, exposure to toxins, cystic fibrosis and primary ciliary dysfunction (e.g. Kartagener's syndrome)[76].

The filtration capacity of the nose can be exploited in metered dose drug delivery, as yet an underutilised administration route. The nose has a large mucosal surface area for deposition and the highly-vascularised mucosa allows for rapid absorption and hence rapid onset of action. It is a non-invasive method of drug delivery making it possible for self-administration with its improved convenience and compliance. Other advantages are that it avoids the first-pass metabolism of the gastrointestinal tract and it can offer pharmacokinetic profiles similar to intravenous drug delivery with bioavailability approaching 100%[77]. However to date there have been difficulties with repeatability of dosage for nasal drug delivery. Model studies could identify delivery modes and particle size to optimise targeted deposition.

Olfaction

The olfactory apparatus enables humans to sense the external environment for either beneficial or defence purposes[78]. Olfactory neuroepithelum, which covers an area approximately the size of a postage stamp on the dorsal aspect of the nasal roof, contains several million olfactory neurons and is unique in central nervous system as it is the only part in direct contact with the external environment[79]. Inspired volatile compounds (odorants) stimulate this region resulting in the perception of smell. Humans can detect approximately 10,000 odours and the sense of smell also affects the ability to taste.

Phonation

The sinonasal airway also acts a resonance chamber for voice production[80] affecting the pitch and timbre of the voice. This is most obvious in the production of vowels and soft consonants where the sinonasal airway acts as an escape valve[81,82].

1.3.1.2 Nasal airflow

Many of our current concepts of nasal airflow characteristics are based upon experiments involving relatively a small number of nasal cavities.

Nasal airflow

A flow can be laminar, turbulent or transitional in nature. This classification is succinctly demonstrated by the experiment conducted by Osborne Reynolds (1842 - 1912)[83]. A dye was injected into a flow through a glass tube in order to observe the nature of the flow (Figure 1.7). At low flow rates the flow seemed to follow a straight line path (with only a slight blurring due to dye diffusion). As the flow rate was increased the dye fluctuated and intermittent bursts were observed. As the flow speed is further increased the dye is blurred and fills the entire pipe.

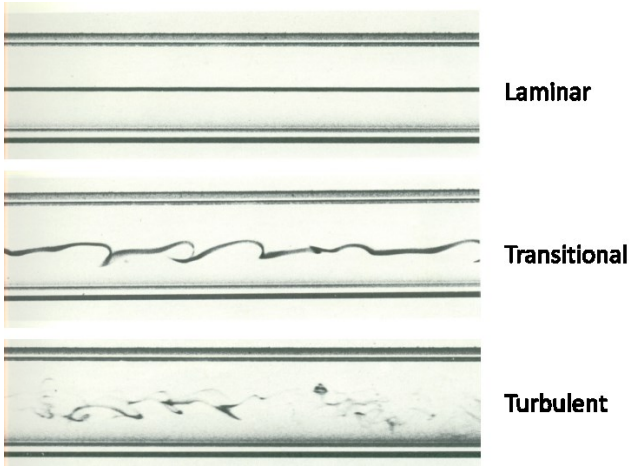

Figure 1.7 Reynolds experiment[83].

Laminar flow occurs when the flow of fluid through a straight pipe follows a predictable manner. The motion of the particles of fluid is very orderly with all particles moving in straight lines parallel to the pipe walls. Fluid adjacent to the walls of the pipe is nearly still, whereas in the central lumen flows more rapidly. In a Newtonian fluid, viscosity is assumed to be constant; fortunately for airflow this is a suitable assumption whereas for blood flow, it may not be appropriate. Laminar flow of a Newtonian fluid in a pipe of circular cross-section obeys Poiseuille's law.

$$Q = \frac{\Delta P \pi r^4}{8 \mu L}$$

Equation 1.1

Where:
Q is flow
P is pressure drop along tube
r is radius
μ is dynamic viscosity of the fluid
L is length of the tube.

When flow enters a pipe, the velocity distribution at first is approximately constant across the cross-section, requiring a certain distance before the equilibrium velocity profile becomes established. This is known as the entry length; it is relevant for the hot wire measurements as described in materials and methods in Chapter 5.

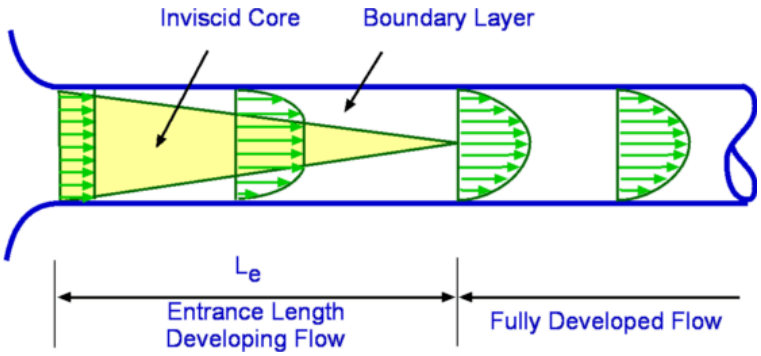

Figure 1.8 Developing flow in a pipe[84].

Turbulent flow is characterized by chaotic and random property changes. This includes rapid variation of pressure and velocity in space and time. It is dominated by inertial forces which produce chaotic eddies, vortices and other flow instabilities.

From his experiments in 1883, Reynolds went on to introduce the concept of a Reynolds number (Re). This is a dimensionless number that indicates the ratio of inertial forces to viscous forces in a fluid. Laminar flow occurs at low Reynolds numbers, where viscous forces are dominant, and is characterised by smooth, constant fluid motion; turbulent flow occurs at high Reynolds numbers and is dominated by inertial forces, which tend to produce chaotic eddies, vortices and other flow instabilities. For pipe flow, a Reynolds number above about 4000 indicates that the flow is likely to be turbulent, while a Reynolds number below 2100 indicates laminar flow. The region in between ($2100 < Re < 4000$) is called the transition region[85,86].

For flow in a pipe, the Reynolds number is defined as

$$\mathrm{Re} = \frac{\rho \upsilon D_H}{\mu} = \frac{\upsilon D_H}{\nu} = \frac{Q D_H}{\nu A}$$

Equation 1.2

Where:

D_H is the hydraulic diameter of the pipe

Q is the volumetric flow rate (m^3/s)

A is the cross-sectional area (m^2)

υ is the mean velocity

μ is the dynamic viscosity of the fluid

ν is the kinematic viscosity ($kg/(m \cdot s)$)

ρ is the density of the fluid (kg/m^3)

Experimental evidence indicates that nasal airflow at rest is predominantly laminar in the strict physical sense[87-91], however it is always complex as the flow does not follow a straight pathway through the nasal cavity. In contrast to turbulent flow it does not have random fluctuating velocities across a broad range of spatial frequencies. A flow may be unsteady, and display eddying flow paths but unless it possessed a broad range of random fluctuations it would be classified as laminar.

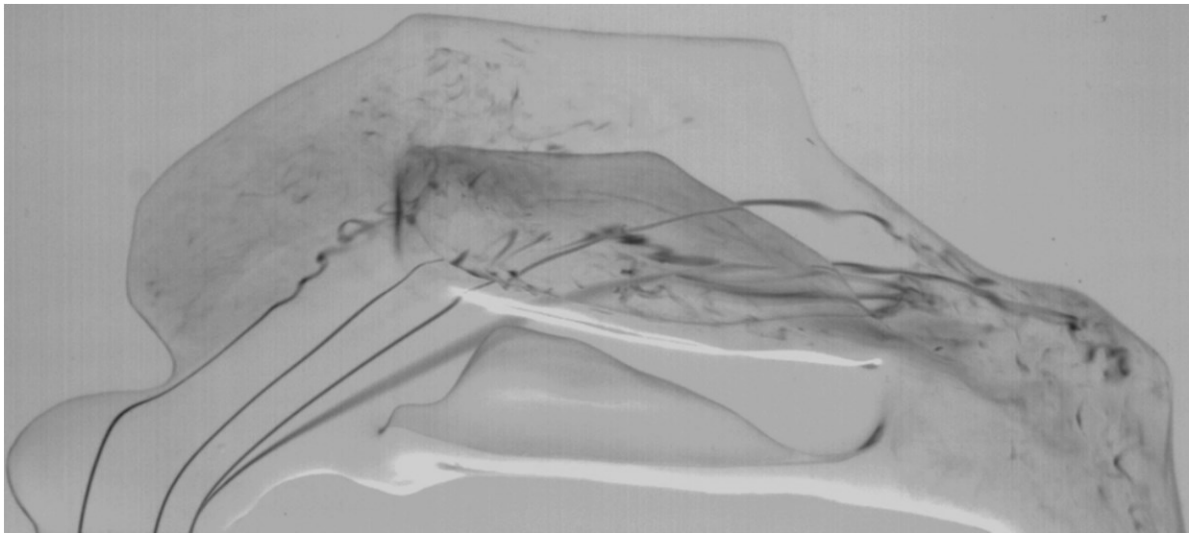

Figure 1.9 High speed dye visualisation experiments reveal nasal airflow pathways. Courtesy of Dr D Taylor[90].

The nasal inspiratory pathway follows an arc through the nasal cavity. Air enters through the external naris and accelerates through the nasal valve as a high velocity jet which then impacts on the middle turbinate. The main flow of air is through the middle meatus towards the posterior end of the inferior turbinate and into the post nasal space. Behind the nasal valve the passage area expands sharply and flow separation occurs, here regions of slow recirculation develop. It is important to note that these instabilities are not random, but are periodic in keeping with the disturbances in a flow, which though unsteady is predominantly laminar at least to the nasal choanae. Low flow rates have been observed in the region of the olfactory cleft which would allow prolonged exposure of air to the olfactory mucosa[90,91].

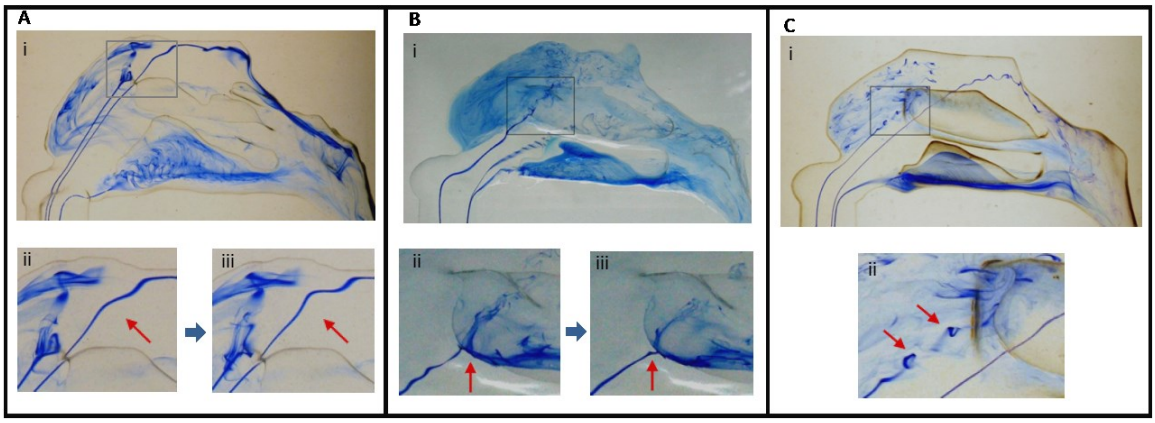

Figure 1.10 Dye visualization depicting flow irregularity and middle turbinate impact[92].

The dye visualisation experiments above (performed by Dr D Taylor[92]), depict onset of unsteadiness of inspiratory flow and impact on the middle turbinate in three optically clear silicone models. Creation and validation of the twice life-scale replica models and procedures for dye visualization are described by Doorly *et al.* (2008)[92]. Flow rates correspond to the equivalent values for a real nose. Airflow at quiet inspiratory flow rates is predominantly laminar, though small-scale instabilities may profoundly enhance mixing (as visualised by dye dispersion).

(A) (i)–(iii) Relatively stable flow 150 ml/s. The large passageway calibre reduces velocity, delaying the appearance of instability until the filaments reach the upper parts of the airway; this is shown using two sequential magnified views of the inspiratory jet.

(B) (i)–(iii) The instability of flow at 170 ml/s. Though the dye filaments appear dispersed and well mixed, flow is not truly turbulent. The magnified sequential images (ii), (iii) indicate dramatic effects on mixing and dispersion due to minor fluctuations of the inspiratory jet where it impacts on the middle meatus.

(c) (i), (ii) Filaments as they pass through the model at 150 ml/s. Shear-layer instability at the edge of the inspiratory jet is shown by successive roll-up of the dye in this region, with a detail of this region magnified in (ii). There is enhanced dispersion of dye in the anterior cavity due to the jet boundary instability and the variation in the orientation of flow approaching the middle turbinate. Note the relatively undisturbed trajectory of the major portion of flow until near the middle turbinate where filaments can be seen to oscillate as they pass through the region containing the olfactory receptors, and as they encroach on the middle turbinate.

1. 4 Aims of Current Work and outline of the thesis

It can be seen from background above that the geometry of the sinonasal airway is complex, and the manner in which it controls the airflow to accomplish its conflicting physiological functions is not fully understood. A detailed knowledge of both the geometry and flow conditions is key to improving our understanding the physiological mechanics of the upper airways.

To date cadaveric studies, CT and MRI scans have been used to detail the nasal geometry. Cadavers offer an opportunity to examine the nasal anatomy in fine detail however cannot be used to investigate *in vivo* changes in the nasal mucosa. Each nasal cavity differs not only in size and shape but is also temporally variable, and the size of the airway is probably significantly smaller than those of human cadavers. This is in part due to the absence of blood engorging the venous sinusoids of the nasal turbinates and part due to tissue shrinkage as a result of fixation increasing the size of the nasal airways beyond the normal physiological range. *In vivo* measurements are hampered by the complex geometry, narrow calibre and sensitivity of the tissues.

CT has been shown to be an excellent modality for demonstrating bony architecture within the nose and paranasal sinuses however MRI is the preferred modality for demonstrating mucosal changes as it images the air mucosal interface directly. Studies looking at the changes in the nasal airway morphology with MRI are few[93-97] and have used early MRI scanners which had poor resolution. 3T MRI offers the opportunity to determine *in vivo* changes in the nasal mucosa in far greater detail than previously studied. Changes seen with congestion and decongestion will affect how airflow is distributed throughout the nose and hence impact on the processes of heat and water exchange as well as the deposition of aerosols. The aim of this study was to determine the dimensions of human nasal airways in vivo using 3T MRI, a technique that images the air mucosa interface directly, and to compare the quantitative measurements of airway cross-sectional areas and perimeters to those that have previously been published. This comparison provides an indication of the realism of the physical and computational models that have been used previously for studies of nasal air flow mechanics. No previous work using 3T MRI scanning to determine changes in the nasal airway mucosa with decongestion is known.

In addition to a detailed knowledge of in vivo variations in the nasal anatomy, a rigorous characterisation of nasal airflow profiles is required to improve our understanding of the normal physiological functions of the nose. Accumulative processes such as air conditioning, olfactory sensation, drug delivery, and toxicology are highly sensitive to the characteristics of the assumed inspiratory profile used, for simplicity most studies to date[98,99] have assumed

constant volumetric inspiration. However recent experiments in nasal replica models and computational predictions indicate that rapid flow initiation can destabilise flow patterns[89-91]. This can lead to an alteration from laminar to transitional flow with consequential alterations to the transport of inhaled substances and the processes of heat and water exchange at the nasal mucosal surface. This study aims to investigate and characterise the variation in the temporal profiles of nasal inspiration within a cohort of healthy subjects. Furthermore, both the effect of nasal decongestion and mode of inspiration (inspiration at rest, smelling and sniffing), are also considered for all subjects. The experimental modalities will enable bilateral volume flow rates to be captured simultaneously in high temporal detail (5000 Hz using hot-wire anemometry), which will be complemented by measures acquired using clinically available tools.

Whilst an increased understanding of the in vivo nasal geometry and inspiratory flow patterns are relevant to a host of applications in this study we look at the specific example of sinonasal ventilation to illustrate the relationship between form, flow and function. Sinus ventilation is often associated with sinusitis, a common condition causing significant pain and reduced quality of life. Clinical implications of the diverse anatomy of ostia connecting sinus to nose and the efficacy of surgical intervention in chronic sinusitis are poorly understood. Although this work focuses on sinus ventilation it should be noted that is only one factor in the pathogenesis of a multifactorial disease. Mucociliary transport plays a significant role in sinus health as illustrated by the chronic sinusitis Kartageners patients (who have immotile cilia) suffer[100]. This study aims to measure sinus ventilation and explore variables in physical and mathematical models. ɣ-scintigraphy will be used to investigate gas exchange between the maxillary sinus and the nasal cavity using short half-life Krypton 81M. It has been shown that the technique can provide quantitative assessment of volume flow rate in the lower respiratory tract but has not previously been applied to sinus ventilation. It is hoped that an increased understanding of the relationship between geometry, ventilation and clinical outcome will improve our understanding of the pathological process that leads to rhinosinusitis help to direct future interventions in the treatment of rhinosinusitis.

Chapter 2

Background to sinonasal air flow and assessment

2.1 Nasal Airway Assessment

2.1.1 Clinical

Accurate diagnosis of nasal pathologies begins with a thorough clinical history, concentrating on symptoms such as obstruction, rhinorrhoea, post nasal drip, sneezing, nasal itching, facial pain, epistaxis and anosmia. It is important to establish the frequency, duration, temporal relationship, and precipitating factors of the symptoms. The impact of the symptoms on the patient's quality of life should be recorded. A social history, including use of cigarettes, alcohol and drugs (prescription, over-the-counter and recreational), as well as details of occupation and hobbies may provide important diagnostic information. Finally, the past medical history should include the history of trauma, surgery (including aesthetic procedures), asthma, pregnancy, oral contraceptive pills, hormone replacement therapy and thyroid diseases.

A full examination of the head and neck follows the history. Inspection may reveal midface deformities associated with chronic mouth breathing, the allergic salute of allergic rhinitis, tip ptosis, alar collapse or facial nerve palsy. A depressed bridge may indicate previous

surgery, Wegeners or cocaine misuse, a widened bridge is suggestive of polyps whereas an overly narrow nasal bridge may be the result of previous osteotomies. A crude assessment of nasal airflow can be made by looking at metal spatula misting. Relief of airflow obstruction with Cottle's manoeuvre may indicate a problem in the valve region. Anterior rhinoscopy with a thudicum's speculum may reveal septal deviations, rhinitic mucosa or gross polyposis. It is important not to forget an ear examination as a middle ear effusion may indicate a nasopharyngeal mass, inflammation or adenoidal hypertrophy

Nasal endoscopy should be performed both pre and post decongestant to assess the septum, turbinates, meati and internal valve. It is important to rule out tumours and recognise inflammatory diseases. The history and examination will direct further investigations.

2.1.2 Radiologic evaluation

Both CT and MRI can be useful to document polyps, tumours and chronic rhinosinusitis. Contrast-enhanced CT scan is the current radiologic standard for the evaluation of the sinonasal airway.

CT scans are usually indicated after failure of maximal medical therapy for chronic rhinosinusitis, before surgical planning and in exclusion of possible neoplasms. A coronal CT scan of the sinus correlates best with the surgical approach, permitting visualization of the ostiomeatal complex and sinus cavities. Surrounding structures such as the orbit, cribriform plate and dental pathologies are visualized well. The main disadvantage of CT scanning is the associated radiation dose and therefore most centres now offer limited sinus CT scans which have reduced radiation doses and spare the ocular lens and thyroid gland[101-103]. It is important to note that a significant degree of incidental change can be found on CT in around a third of 'normal' adults and 45% of children probably related to recent viral upper respiratory tract infections.

MRI is generally reserved only for complex cases. Soft tissue contrast is better with MRI. Neoplasms, orbital and intracranial complications as well fungal sinusitis can be better evaluated[104]. The advantage of MRI scanning is that there is no associated radiation dose. However traditionally the MRI scans of the nose and sinuses have only been able to take very thick slices and had long acquisition times and hence suffered from movement artefact during

the scan. The introduction of 3T MRI scanners into clinical practice has increased the resolution of scans obtained and reduced the acquisition time.

2.2 Nasal airway tests

Measures of nasal obstruction can be either subjective or objective. The difficulty in interpreting objective measures is that they do not always correlate well with the patient's symptoms[105]. A comparison of methods of evaluation of nasal assessment is given in table 2.1 pg 42.

2.2.1 Objective evaluation

Peak Nasal Inspiratory Flow

PNIF is a cheap, quick and easy to perform method for assessing nasal patency which is reproducible[106-109] and sensitive[110,111]. It has a good correlation with total nasal resistance measured by active anterior rhinomanometry[43,112,107] and statistically significant associations with nasal cavity dimensions recorded by acoustic rhinometry[113]. PNIF has been used in the evaluation of medical therapy for rhinitis[114], to assess the efficacy of intranasal corticosteroids for nasal polyposis[115,116] and to show improvements after surgery[117]. PNIF has also been used to determine the reaction threshold or cut off value to determine the endpoint in nasal challenge testing. Limitations with this technique are that it is not sensitive to small changes in nasal patency[118,119]. It requires patient cooperation and respiratory co-morbidities as well as alar collapse can influence measurements. PNIF in contrast to acoustic rhinometry provides no information on the structure of the nose or location of the obstruction.

Peak nasal inspiratory flow in L/min
<50 severe nasal obstruction
50-80 moderate nasal obstruction
80-120 mild nasal obstruction
>120 no obstruction

Acoustic Rhinometry

Acoustic rhinometry (AR) is a validated technique for assessing the cross-sectional area of the nose and the volume of the nasal cavity by analysis of incident reflected sound waves[120-122]. This technique is useful for estimating the location of nasal obstruction and documenting changes in nasal patency caused by medications or surgical interventions[123,124]. However, a number of assumptions are made about the characteristics of the nasal cavity in order to process acoustic rhinometry results;

1. The walls are rigid and exhibit no radial motion, i.e. compliance
2. There is no loss of sound energy as it propagates down the tube
3. Branching within the nasal cavity is symmetrical
4. The acoustic waves propagate in one direction.

All of these assumptions are flawed within the nasal cavity and could potentially lead to inaccuracies in the results. Also early validation studies comparing acoustic rhinometry results with CT and MRI used coronal cross sectional areas from imaging to compare to the acoustic cross sectional areas[95,125,126] however coronal imaging is not representative of the curved path of the acoustic pulse. Terheyden *et al.* (2005)[122] used CAD software to create a more realistic acoustic path and determine the perpendicular cross sectional areas from this path. They found a good correlation between AR and CT in the anterior nasal cavity but by the mid turbinate region there was a consistent overestimation of area with AR. More recently Tarhan *et al*. (2005)[121] performed a comprehensive study that compared AR data to CT data to evaluate the accuracy of AR measurements in estimating nasal passage area and to assess its ability of quantifying paranasal sinus volume and ostium size in humans. In the anterior nasal cavity, there was good agreement between the cross-sectional areas determined by AR and CT. However, posterior to the sinus ostia, AR overestimated cross-sectional area. This effect was independent of sinus volume. Therefore, the diagnostic value of this method is limited to the anterior nasal cavity as beyond the sinus ostia it becomes unreliable[121].

The advantages of AR are that it is minimally invasive, quick to perform, and requires little patient cooperation. There are published standards for age, race, ethnicity and sex for the use of AR[127,128]. In 2005 and 2010, the European Rhinology Society's Standardisation Committee on Objective Assessment of the Nasal Airway published a consensus report with comprehensive recommendations regarding the use of AR and rhinomanometry[129,130].

Rhinomanometry

Rhinomanometry measures nasal airway resistance by making quantitative measurements of nasal airflow and pressure. Although the nose is not a simple tube, nasal airflow follows the laws of fluid dynamics, with flow rate depending on the pressure gradient and being inversely dependent on nasal resistance. For a pipe of fixed radius, the relation between pressure loss and flow can be expressed either in terms of a simple proportionality (for laminar flow) or a power law (for turbulent flow). In such cases the resistance has a simple form. However the relation between flow and pressure loss is not as simple where flow separation occurs. Flow separation results in additional losses associated with the mixing of fluid momentum. For example, where the nasal valve creates a pronounced inspiratory jet that enters the nasal cavity, there is a loss associated with the jet dispersal by mixing. It is thus important to recognise that nasal resistance cannot be assumed to be simply proportional to flow rate.

In terms of mechanics, the pressure differential in the nose is created by respiratory effort altering the post nasal space pressure relative to the ambient pressure[130]. In rhinomanometry, measurements are made via two pressure transducers and a pneumotachograph and nasal resistance is calculated by the equation:

$$R = \frac{\Delta P}{V}$$

Equation 2.1

where;
R = nasal resistance ($Pa/cm^3/s$)
ΔP = transnasal pressure
V = nasal airflow (cm^3/s).

However this equation does not take account of airflow characteristics (laminar v turbulent) and therefore may not be completely representative of in vivo resistance[131]. The calculations are further complicated by the relationship between pressure and flow. This follows a curvilinear pattern and therefore the resistance can't simply be read by the slope of the graph. As a result the European committee for standardisation of rhinomanometry have set criteria for performing rhinomanometry in order to allow comparison of results and the setting of normal ranges[129,132].

Different techniques for rhinomanometry complicate matters further. Rhinomanometry can be performed actively (during normal respiration) or passively (using a standard flow rate generated by a pump), and by either anterior (at the nostril) or posterior (at the nasopharynx) approaches. Active anterior rhinomanometry is the most commonly used, being the most physiological. Pressure is recorded in one sealed nostril while flow is recorded in the other open nostril. The results are presented graphically as a sigmoid shaped curve, each nostril is measured 5 times and the mean value is used. The resistance at a fixed pressure of 150Pa is expressed in SI units.

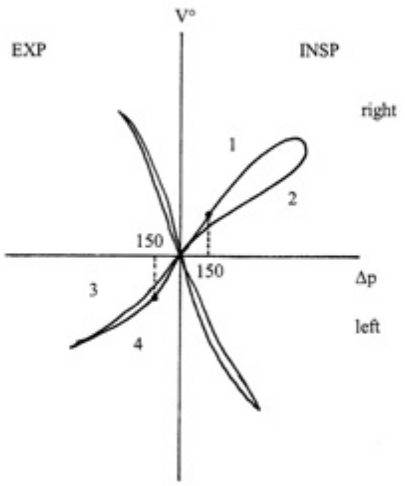

Figure 2.1 Four phases rhinomanometry: assessment of the flow at 150 Pa in order to determine the resistance[129]. For the four phases rhinomanometry, resistance is determined for phase 1 (ascending inspiratory phase) and phase 4 (descending expiratory phase) of the four loop rhinomanometry by using the "highest possible flow" at a pressure of 150 Pa (the ascending inspiratory and the descending expiratory curve parts are much more consistent and reproducible[129]).

There are several disadvantages of rhinomanometry. The machine must be calibrated with each use and calibration varies with temperature and humidity. The placement of the probes/masks requires patient cooperation and is often uncomfortable. It is also relatively time consuming and the reproducibility of results can vary by 20-25%. It cannot be used when the nose is completely blocked or if there is a septal perforation and does not assess the site of an obstruction. Despite these drawbacks, rhinomanometry is still used and standards for reading rhinomanometry are readily available[129,130].

2.2.2 Subjective measures

Along with objective measurements, it is important to assess the patients' perception of nasal symptoms. Visual analogue scales and psychometrically validated surveys are useful tools for evaluating patients' perception.

Visual Analogue Scores (VAS)

For evaluating patients' subjective experience of nasal obstruction VAS are commonly used, however, they often show inconsistent correspondence to other objective measures. However, they are inexpensive and quick to perform. In rhinosinusitis the severity of the disease can be divided into mild, moderate and severe based on visual analogue score (VAS) (0-10cm)

Mild= VAS 0-3

Moderate=VAS>3-7

Severe= VAS>7-10

To evaluate the total severity the patient is asked to indicate on VAS the answer to

the question:

HOW TROUBLESOME ARE YOUR SYMPTOMS OF RHINOSINUSITIS?

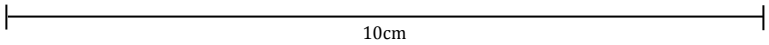

Not troublesome Worst imaginable

A VAS>5 is considered to affect quality of life.

Patient recorded outcome measures (PROMS)

Psychometrically validated symptom questionnaires for sinonasal symptoms offer statistically validated measures for the assessment of general health and disease specific conditions.

The most frequently utilised psychometrically validated questionnaires include the 22-question sinonasal outcome test (SNOT-22)[133,134], the rhinitis quality of life questionnaire (RQLQ)[135], and the rhinosinusitis disability index (RSDI)[136]. The SNOT and RQLQ are the most commonly cited validated psychometric surveys.

Other tests

The saccharin test evaluates ciliary function by measuring the time it takes for a drop of saccharin to be tasted in the back of the throat when applied to the anterior tip of the inferior turbinate. A transport time of between seven and fifteen minutes is considered normal and a time over thirty minutes is suggestive of a disruption of ciliary transport.

Multiple tests of olfaction are available, but the University of Pennsylvania Smell Identification Test (UPSIT) is used most commonly. The UPSIT is a 40-item scratch-and-sniff test and is highly validated by age and sex[137-140].

Recent research into exhaled nitric oxide suggests that in the future, these measurements may prove valuable as non-invasive objective tools for the assessment and management of normal nasal physiology and sinonasal disorders[141-143].

Table 2.1 Comparison of methods of evaluation of nasal assessment [144]

Method of evaluation	Measures	Advantage	Disadvantage
Visual analog scale (VAS)	Patient perception	• Inexpensive	• Variable correlation with objective measures
Validated questionnaires	Patients perception of quality of life	• Statistically valid • Can be used to assess outcome • Assess importance to patients	• Limited number of validated questionnaires available
Video endoscopic photo-documentation	• Anatomy • Colour • Secretions	• Provides colour image of internal anatomy • Can be recorded for later evaluation	• Colour may vary • Non-standardized reading scale
Nasal peak flow	Inspired air flow	• Quick • Inexpensive • Reliable results	• Requires patient cooperation • "Snapshot" measurement
Acoustic rhinometry	Reflected sound waves	• Quick • Localizes area of blockage • Painless • Non-invasive • Requires no subject cooperation	• Availability of equipment
Rhinomanometry	Pressure/flow	• Gives functional result of blockage	• Machine must be calibrated with each use • Calibration varies with temperature and humidity • Probes/marks require patient cooperation and are often uncomfortable

2.3 Maxillary Sinus

2.3.1 Sinus function

Throughout history, conjecture on sinus function has provided numerous and diverse hypotheses and whilst many have now been scientifically discredited, there remains no predominant accepted theory. Table (2.2) lists the numerous hypotheses of sinus function over the years.

The recent discovery of high NO concentrations in the maxillary sinuses[145], has triggered speculation that the sinuses play a role in the immune defence of the nasal cavity, and lower respiratory tract. NO has been shown to act as an anti-microbial agent[146], a neurotransmitter, a bronchodilator[147] and a regulator of mucociliary function[148,149]. Altered concentrations of NO in the nose and sinuses have been linked to the pathogenesis of chronic rhinosinusitis[141,142,150]. It has been proposed that the sinuses are responsible for producing NO for the nose. However the nasal mucosa also produces NO and transport estimates based on measured NO concentrations and modelling suggest that it would not be possible for enough NO to leave the sinuses to explain the nasal NO levels during normal breathing[151]. Although the sinuses cannot supply the entire nasal NO, the high sinus NO concentrations may be important in maintaining a sterile environment in the sinuses and preventing sinus infections. Frequently, in sinus surgery the natural sinus ostium is widened to improve sinus ventilation, however this is likely to impact on the sinus NO concentration. In this thesis the effect of changing ostial size on sinonasal transport is investigated. (Chapter 6, Section 6.2.1 page 113)

Table 2.2 Historical overview of the proposed functions of the paranasal sinuses. Adapted from Marquez (2008)[10].

Proposed function of paranasal sinuses	Studies
Non-functional role	
Exists as evolutionary remains of useless air spaces	Ingersoll,(1906)[152],(1922)[153]; Negus,(1957)[154],(1958)[155]; Takahashi,(1983)[156]; Lund,(1988)[11]
Physiological role	
Contain nourishment for teeth	Da Vinci; (circ 1489)[157]
Increase olfactory mucosa surface area	Braune and Clasen, (1877)[158]
Provides even distribution of inspired air, which aids in olfaction	Strickland,(1932)[159]
An adjunct in air conditioning of inspired air	O'Malley,(1924)[160]; Eckert-Mobius,(1933)[161]; Sato,(1938)[162]; Proetz,(1922)[163],(1938)[164],(1941)[165]; Gannon *et al*.(1997)[166]
Imparting resonance to the voice	Cleland,(1862)[167]; Bignon,(1889)[168]; Zuckerkandl,(1892)[169]; Dieulafé,(1906)[170]; Hartz,(1909)[171]; O'Malley,(1924)[160]; Eckert-Mobius,(1933)[161]; Wegner,(1958)[172]; Dyce *et al*.(1987); Leakey and Walker,(1997)[173].
Regulating intranasal pressure	Coffin,(1905)[174]; Neumayer,(1901)[175], Suarez,(1952)[176]; Del Cañizo,(1959)[177]
Reservoirs for mucus secretions	Alger,(1943)[178]
Assist in flotation at some point in time aquatic evolution	Bignon,(1889)[168]; Proetz,(1953)[12]; Wegner,(1958)[172]; Rhys Evans,(1992)[13]
Nasal cavity immune defence and production of nitric oxide gas	Lundberg *et al*.(1994)[179]
Structural role	
Reduce cranial weight	Galen (circ. 130 AD)[5]; Cleland,(1862)[167]; Onodi,(1908)[180]; Nemours,(1931)[181]; Shea,(1936)[182];
Assist in facial growth and architecture	Eckley,(1904)[183]; Dieulafé,(1906)[170]; Blaney,(1986)[184];(1990)[185]; Davis *et al*.(1996)[186]
Part of normal skull pneumatisation	Witmer,(1995)[187],(1995)[188],(1997)[189]
Protection for the brain and sensory organs	Rui *et al*.(1960)[190]; Davis *et al*.(1996)[186], Kelman, (2009)[191]
Provide thermal insulation for CNS and sense organs	Bignon,(1889)[168]; Bremer,(1940)[192]; Proetz,(1953)[12]

2.3.2 Sinonasal airflow

Pressure Measurements

Early work on sinonasal pressure measurements by Braune and Clasen (1877)[158] and Proetz (1932)[193] showing that the pressure changes in the sinus exactly follow those in the nose still holds true today. Later experiments by Drettner (1965)[194], Rantanen (1974)[50] and Bachert (1986)[195] confirm these results, therefore, since the pressure in the sinus follows that in the nasal cavity, sinus ventilation cannot be driven by pressure differences as suggested by Tornberg *et al*. (2002)[196]. There is no published evidence to show differences between sinus and nasal pressure with open ostia.

The pressure in the nose varies with the breathing cycle, this variation has been calculated as around ±10 mmH2O (100 Pa). The sinus follows these pressure changes and expands and contracts according to Boyles law leading to a very small movement of air. Proetz (1932)[193] calculated this to be 1/1026 of the sinus volume and Svanholm *et al*. (1981)[197] quantified it as 20µl for a 15ml sinus. A typical ostium with a 3mm diameter and 6mm length has a volume of around 42 µl so the air movement as a result of this mechanism would be the equivalent of dead space ventilation in the respiratory tract.

Velocity Measurements

The inaccessibility of the maxillary sinus has limited direct measurement of velocities within the sinus, as the placement of even a small probe would not only be difficult, but would also result in perturbations of the flow. The most detailed experimental results of maxillary sinus velocities are provided by Musebeck and Rosenberg (1978)[198,199] who used a small hot-film anemometer inserted into the sinus via puncture of the canine fossa to measure velocities. Velocities in the region of the maxillary sinus ostium were found to be 40-50 times less than those in the nasal cavity, and the velocities reduced further with increasing distance from the ostium.

Assessment of Ventilation

Sinus ventilation has previously been investigated both in vivo and in vitro. Early experiments were carried out by Aust and Drettner[56] who investigated the recovery of oxygen concentration in sinuses where air had been replaced by pure nitrogen. They found that the rate of return of oxygen into the sinus is inversely related to sinus volume and ostium length but varies proportionally with the cross-sectional area of the ostium, as would be expected for diffusive

transport. They found the typical time taken to restore a normal concentration of oxygen in a healthy maxillary sinus to be around 5 minutes. Two isotopes of xenon have also been used in conjunction with imaging: xenon-133 is a β and γ emitter which can be detected by Single Photon Emission Computed Tomography (SPECT) cameras, used for example by Zippel *et al.* (1979)[200], and Paulsson *et al.*[201-203] while xenon-129 is radiodense rather than radioactive and has been used with Computational Tomography (CT) imaging, for example by Marcucci *et al.* (2001)[204,205]. The disadvantages with Xe are that it is lipophilic and a powerful general anaesthetic which cannot be used in high concentrations or for long exposures, as it leads to side-effects such as dizziness and nausea for experimental subjects. Hence experiments have often had problems with non-invasively introducing sufficient quantities of the tracer gas into the sinuses for clear images and quantitative results. Experimental results from Marcucci *et al.* (2001)[204] found similar exchange times to the earlier Aust (1974)[56] studies. Hyperpolarised helium (He) gas has been developed as a contrast agent for Magnetic Resonance Imaging (MRI) and has been used to study sinus ventilation[206,207]. 3He causes far fewer side-effects than Xe and using hyperpolarised He with MRI does not expose subjects to radiation, however the production, transport and storage of pure and hyperpolarised 3He are complex and extremely expensive so this method seems unlikely to come into widespread use either for research or for clinical purposes. Recently Möller *et al.*[208-212] have used 81mKr to image human sinuses and investigate the effects of pulsating airflow but did not quantify the ventilation of the sinuses under normal breathing conditions. Early pilot studies by our group suggested that it would be possible to quantify sinus ventilation using 81mKr[213].

81mKr is a γ emitter with a half-life of 13s which is currently used clinically in ventilation-perfusion imaging of the lungs[214]. The short half-life means that little time is needed for the counts in the model to reduce to background between experimental runs and minimal radiation protection is required. In contrast to xenon, which is lipophilic and anaesthetic and can cause complications for both in vitro and in vivo investigations, krypton is chemically inert and does not interact with the materials of a physical model or with biological tissues. Technetium aerosols are also commonly used as a contrast agent for respiratory imaging but are less appropriate for physiological transport measurements as aerosols follow different transport processes to gases.

Until recently little experimental work had been published on the effects of accessory ostia on sinus ventilation. The work of Proetz (1953)[12] has frequently been taken out of context when saying an accessory ostium would not influence exchange times. His conclusion is based upon a thought experiment in which suction was applied to the nostril while the nasopharynx was closed, however this is not representative of the normal physiological state.

More recent work has confirmed that the addition of a second or accessory ostium to the maxillary sinus does result in a net flow in the sinus and thus speeds up exchange processes[151,215] by several orders of magnitude. This concept may have implications for the way endoscopic sinus surgery is performed, as enlarging the existing ostium (middle meatal antrostomy) and/or creating a second ostium (inferior meatal antrostomy) will affect sinonasal exchange processes in different ways.

2.4 Pathophysiology of Rhinosinusitis

The ostiomeatal complex plays a fundamental role in the pathogenesis of rhinosinusitis, as it is the functional unit that comprises maxillary sinus ostia, anterior ethmoid cells and their ostia, ethmoid infundibulum, hiatus semilunaris and middle meatus. The key element in the prevention of rhinosinusitis is the maintenance of ostial patency. The ostial patency will affect both the composition and secretion of mucus, and an open ostium allows mucociliary clearance to remove debris and bacteria from within the sinus[19,216].

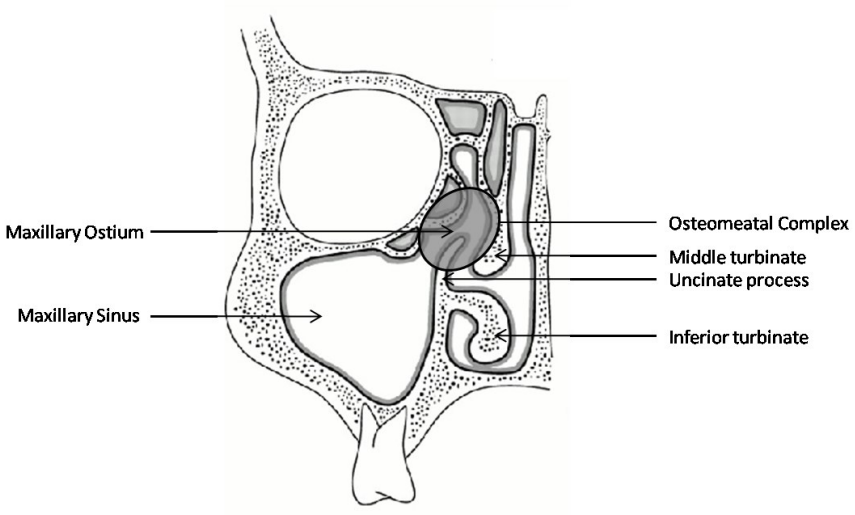

Figure 2.2 Coronal section through the maxillary sinus illustrating the osteomeatal complex adapted from Hosemann (2000)[42].

Problems occur if the orifice is too small for the amount of mucus, if mucus production is increased, for instance during an upper respiratory tract infection (URTI), or if ciliary function is impaired. Stasis of secretions follows and bacterial export ceases, causing or exacerbating inflammation of the mucosa whilst aeration of the mucosa is decreased, causing even more

ciliary dysfunction. This vicious cycle can be difficult to break, and if the condition persists, it can result in chronic rhinosinusitis. Chronic rhinosinusitis (CRS) is defined as symptoms persisting for more than 12 weeks.

The diagnosis of sinus disease is typically made by clinical history and examination in conjunction with nasoendoscopy and CT imaging. Treatments range from pharmacological interventions, with steroids and decongestants, to both short and long term antibiotic therapy, to functional endoscopic sinus surgery when medical therapy fails. Currently we are unable to objectively assess the efficacy of pharmacological or surgical treatment and rely on patient recorded outcome measures. Some patients with profound clinical disability have apparently normal CT scans and conversely some patients with significantly abnormal CT scans are symptom free. It is thought that patients with recurrent rhinosinusitis have poor gas exchange in one or more of their sinuses. Also patients who do not improve after medical or surgical therapy may have too much or too little sinus ventilation[204]. There are no quantitative non-invasive methods for assessing the ventilatory function of the paranasal sinuses in clinical use. Development and validation of a technique to assess dynamic sinus ventilation would be of great clinical and research significance.

Surgical interventions for CRS aim to improve sinus ventilation, however the mechanisms involved require further clarification. An increased understanding of the relationship between sinus geometry, ventilation and clinical outcome will help to direct future interventions. Smith *et al.* showed that Endoscopic Sinus Surgery (ESS) significantly improves the quality of life in patients with CRS[217], however with revision rates approaching 20% within 5 years of the initial procedure[218] there remains an opportunity for improvement in the treatment of CRS.

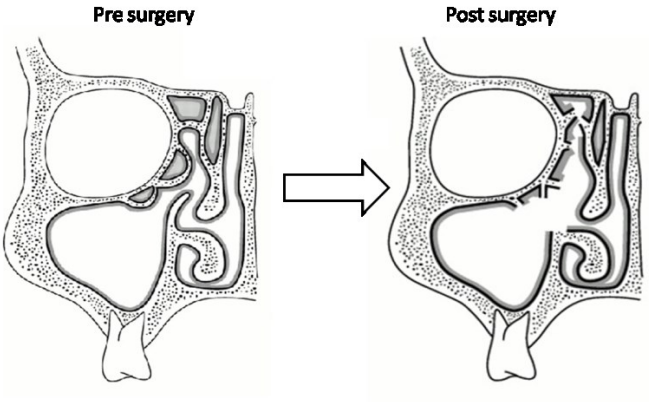

Figure 2.3 Diagram of sinus anatomy pre and post endoscopic sinus surgery adapted from Hosemann (2000)[42].

Chapter 3

Research Methodologies

3.1 Introduction

A number of varied techniques from different fields, including: 3T MRI and image processing (radiology); hot-wire anemometry (aeronautics); acoustic rhinometry (ENT surgery) and γ-scintigraphy (nuclear medicine), have been employed to systematically investigate the mucosal changes in the nasal geometry, the time dependent profile of nasal inspiration and sinonasal transport mechanisms. This chapter details and discusses each of the techniques. As with any experimental investigation, attention was paid to reducing experimental errors and hence increasing the reliability of the results by examining repeatability, variability and extended calibration where possible.

3.1.1 Ethical approval

This thesis comprises three main studies;

1. Definition of the nasal anatomy and congestion/decongestion patterns
2. Nasal inspiratory air flow profiles
3. Sinus ventilation

Since the first two studies involve procedures on healthy volunteers, ethical approval was therefore obtained from the Outer North East London Research Ethics Committee (REC reference: 06/Q0602/18). The studies were conducted in accordance with the International

Conference of Harmonization's Guidelines for Good Clinical Practice and the World Medical Association's Declaration of Helsinki.

3.2 Common Assessment Tools

Common assessment tools have been employed for the first two studies described (congestion/decongestion, inspiratory airflow profiles) in which healthy volunteers were involved. The subjects were screened to ensure they had no nasal complaints and no obvious rhinoscopic abnormalities. Tobacco, alcohol, coffee, drugs, physical activities, changes of temperature and food or beverages were avoided during the study. All subjects were acclimatised in a resting position in the laboratory for approximately 30 minutes prior to each study.

3.2.1 Sino-Nasal Outcome Test and visual analogue scores

All subjects completed a Sino-Nasal Outcome Test (SNOT-22) questionnaire to ensure they had no significant nasal symptoms. The SNOT-22 is a rhinosinusitis specific assessment tool based on the previous SNOT-20 but with the addition of 2 questions relating to nasal blockage and loss of olfactory sensitivity (see appendix). Gillet *et al.* (2009) have investigated SNOT scores in the normal population i.e. without sinonasal disease and found that a SNOT 22 score of 7 could be used a guide for "normal", and that care should be taken when suggesting treatment on patients with a score below this level[219]. Therefore our inclusion criteria included a SNOT score of 7 or less. The degree of nasal obstruction of each volunteer was also recorded with Visual Analogue Scores (VAS) using a line (0-10cm) with 0 representing no obstruction to 10 complete obstruction.

3.2.2 Peak Nasal Inspiratory Flow

Peak Nasal Inspiratory Flow (PNIF) measurements were taken using a Nasal Inspiratory flow meter (In-Check, Clement Clarke International, Essex, UK). The meter has a nozzle connected to a cushioned face mask (figure 3.1). This mask covers the nose and the soft cushion prevents any distortion of the nasal contours which compromise the readings. The subject is asked to empty

their lungs and hold their breath. The meter is then applied around the nose applying adequate pressure to obtain an airtight seal but not distort the nasal contours. The subject is asked to sniff air maximally through the nose without opening their mouth. Three satisfactory maximal nasal inspirations were obtained with the patient in an upright position and the highest value was taken for subsequent analysis in accordance with clinical guidelines. The unit of measurement is litres/minute (L/min).

Figure 3.1 Peak Nasal Inspiratory Flow[220]

3.2.3 Acoustic Rhinometry

The Acoustic Rhinometry (AR) measurements were obtained using an EccoVision Acoustic Rhinometer (Hood Laboratories, Pembroke, Massachusetts USA). Measurements were performed by a single trained operator in accordance with published protocols [128-130]). Inter-reading variability was kept below 10%. The following measures were recorded in all cases: minimum cross-sectional area (MCA - in cm^2) and nasal cavity volume (NCV - in cm^3) between 0 and 5.0 cm. (See appendix for the acoustic rhinometry protocol.)

Figure 3.2 Acoustic rhinometry

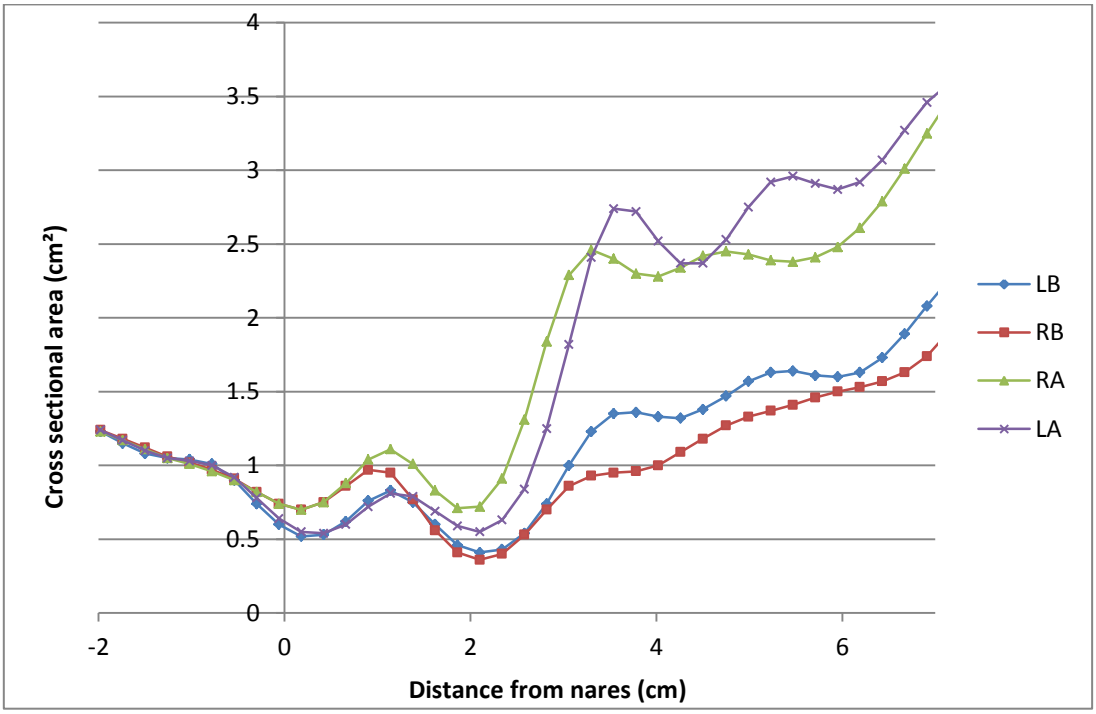

Figure 3.3 Rhinogram; The lines represent the cross sectional area against distance through the nasal cavity, LB = left nostril pre decongestion, RB = right nostril pre decongestion, RA = right nostril post decongestion and LA = left nostril post decongestion. The greatest change in cross sectional area is seen in the region of the turbinates i.e. 3-7cm from the nares. (Data from results in Chapter 5)

3.3 Methods employed to assess Congestion/Decongestion Patterns

This study investigated the effect of decongestion on nasal airway dimensions in normal subjects using high resolution 3T MRI scanning. High resolution 3T MRI scans are fast, non-invasive and provide a detailed 3D geometry. Acoustic rhinometry was used for comparison with the MRI data as it has previously been shown to correlate well with MRI.

3.3.1 Experimental Overview

Seven healthy volunteers (ages ranging from 21-44 years, mean 28) were selected for inclusion in this study. The subjects were screened by an otolaryngologist to ensure they had no nasal complaints and no obvious rhinoscopic abnormalities. The exclusion criteria were;

1. The presence of nasal disease (nasal polyps, rhinosinusitis, severe septal deviation, septal perforations etc.) or other clinically significant disease
2. Medication
3. Ingestion of any food or drink within the previous hour.
4. Pregnancy
5. Claustrophobia (MRI scanner environment is claustrophobic and noisy)
6. Smokers
7. Age <18 years
8. Coryzal symptoms within the previous 2 weeks

Informed consent was obtained from each participant. All volunteers completed a SNOT 22 questionnaire and visual analogue score. Acoustic rhinometry and nasal peak inspiratory flow measurements were performed on all subjects by a single trained operator in accordance with published protocols.

Each subject underwent 2 MRI scans one pre and one post decongestion. Scans were performed on a 3 Tesla, MRI scanner (Discovery MR750, GE Medical Systems). Each scan took less than 3 minutes and a series of 120 contiguous 1.2mm thick coronal sections was obtained. All subjects remained immobilised following the scan and were decongested with Xylometazoline. Decongestion of the nasal mucosa was performed in a standardised manner as per Clements *et al.* consensus document 2005 [129,130]. Djupesland *et al.* found a one-step approach to be insufficient for decongestion[221]. Hence, three sprays of an α2 mimetic

(Xylometazoline) were sprayed into each nostril and repeated after 5 minutes with a single spray [222-225].

A second MRI scan was taken after 25 minutes allowing time for the decongestant to take full effect and acoustic rhinometry and PNIF measures were repeated after the scan. The MRI scans were delineated using Amira (Visage Imaging) and the virtual airways were analysed using a computer aided design package. See appendix for the MRI protocol.

3.3.2 MRI

Although both magnetic resonance imaging (MRI) and computed tomography (CT) are used clinically to image the nasal cavity (see section 1.4 pg 30 and section 2.1.2 pg 33) MRI was selected for this study due to its superiority in visualising the soft tissue enabling better delineation of the changes in the mucosal thickness during the nasal cycle. Another advantage of MRI is that subjects can undergo repeat scanning without the associated risks of exposure to ionising radiation seen with CT. The previous disadvantage of using MRI for the segmentation work was the lengthy duration of the scan. As a consequence the scans often suffered from movement artefact if the subject moved or swallowed. Also only a limited number of thick slices were possible in one scan (20-30). This in turn leads to significant problems with loss of resolution, particularly in areas where the anatomical detail is intricate. The recent introduction of 3 tesla MRI scanners into clinical practice has significantly reduced the scanning time and increased the number of slices possible per scan hence dramatically improving the quality of any segmentation work based on MRI scans. Figure 3.4 below illustrates the difference in CT and MRI imaging.

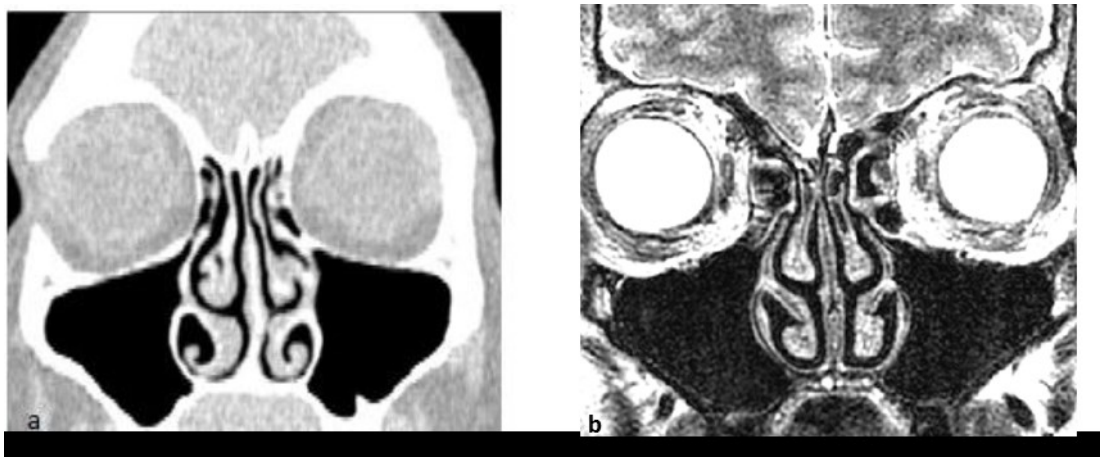

Figure 3.4 Comparison of a coronal CT (a) and MRI (b) T2 image of a different patient, showing the same area.

MRI utilises the fact that much of the body is comprised of water, and hence protons (H+ ions). When a person is inside an MRI scanner these protons become aligned with the direction of the magnetic field. If the protons are then hit with a short, precisely tuned burst of radio waves, they will momentarily flip around. Then, in the process of returning to their original orientation, they resound with a brief radio signal of their own. The intensity of this emission reflects the number of protons in a particular region.

Additional magnetic fields can be applied during the scan to determine the origin of the signal in 3D space. These fields are generated by passing electric currents through gradient coils, which vary the strength of the magnetic field depending on the position within the magnet. Since the frequency of the released radio signal is dependent on its origin in a predictable manner, the distribution of protons in the body can be mathematically recovered from the signal by the use of the inverse Fourier transform. In this study we have utilised head coils to improve the imaging of the choanae and post nasal space.

Contrast between different tissues can be enhanced by exploiting different tissue variables, such as spin density, T1 and T2 relaxation times, and flow and spectral shifts. T1 is the longitudinal relaxation time. It indicates the time required to regain longitudinal magnetization following a radio frequency pulse. T2 is the "transverse" relaxation time. It is a measure of how long transverse magnetization would last in a perfectly uniform external magnetic field. T1 images cause fat to appear bright, e.g. myelin in white matter. T2 weighted images cause water to appear bright like CSF and fat is dark. For this study we selected T2 weighted image for superiority at imaging tissue oedema and hence the engorgement of the nasal turbinates.

Following analysis of the images from a number of MRI sequences on one healthy volunteer a sequence known as a "Cube" sequence was selected for this study. Conventional MR imaging has typically provided discrete slices in one plane only. This requires repeating the acquisition for every additional plane or evaluating images without the benefit of data provided from different angles. However, the Cube sequence replaces several slice-by-slice, plane-after-plane 2D acquisitions with a single 3D volume scan. The scan time is short hence minimising movement artefact and the high definition, high contrast images with a slice thickness of only 1.2mm, permit detailed segmentation work. Therefore the Cube sequence provided the best sequence option for this study. Please see the appendix for the MRI settings.

3.3.3 Image Segmentation

Segmentation is the process of dividing image data into different domains or segments (e.g. anatomic structures or tissues). Each voxel is assigned a label describing the domain to which they belong, i.e. airway or tissue, and these labelled voxels function as building blocks so that the region of interest (ROI) can be extracted for 3D reconstruction (see figure 3.5). A segmentation process was used in preference to the volume rendering techniques which are frequently used for virtual endoscopies as detailed volumetric data was required to investigate the changes with decongestion. Segmentation leads to a 3D reconstruction model based on volume data, whereas the volume rendering process leads to the creation of simply an image, by using a threshold method combined with edge detection algorithms to form an isosurface (a surface of equal voxel value)[226]. The MRI scans were segmented in coronal-section using Amira 4.1 (Mercury Computer Systems, Berlin), a specialist software package.

The image segmentation was performed using a thresholding method. This method uses a threshold value to turn a gray-scale image into a binary image. The intricate architecture of the nasal passages precluded fully automatic segmentation procedures as the resolution of the image renders automatic identification of the boundaries difficult particularly in the fine nasal channels, where partial volume effects become significant. The partial volume effect is an artefact of the imaging process whereby only part of the imaging pixel overlaps the anatomy, and hence it has a reduced overall intensity. However, its neighbouring pixels may be fully overlapped and have a significantly higher intensity[227]. This is illustrated in the enlarged inset figure 3.5.

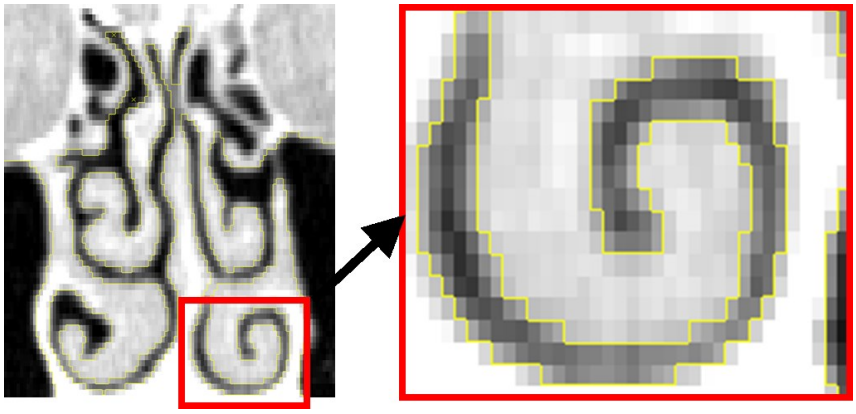

Figure 3.5 The partial volume effect. On the left a coronal CT scan of the nose and paranasal sinuses has been segmented. The magnification on the right highlights the partial volume effect with non-uniform shades of grey filling the nasal airway pixels blurring the boundary between tissue and air[213].

The problems in defining a boundary were addressed by adjusting the viewing window threshold to increase the visibility of thin bony structures, following them in consecutive slices, and by reviewing the ROI in different viewing planes (coronal, axial and sagittal), before a decision was made about manually assigning a pixel to the tissue or air-containing space. Since selection of a single threshold value could have a significant influence on the airway dimensions a segmentation threshold analysis was performed as described by[48]. The segmentation threshold was defined as:

$$Segmentation\ threshold = Mean\ AI\ \left(\frac{Mean\ TI - Mean\ AI}{2}\right)$$

Equation 3.1

where AI is the voxel intensity of the voxel in air space adjacent to the segmentation boundary and TI is the intensity value of the voxel opposite in the tissue domain. The segmentation threshold for each stack of images was determined by taking 20 random samples in 20 random slices. The threshold for the nasal cavity was found to be very consistent (+/- 6%) however there was greater variation in the level around the olfactory cleft and middle meatus areas (+/- 22%) which would be less affected by decongestion. Inter operator variability in segmentation was assessed comparing the nasal airways independently segmented by three different persons (two ENT surgeons and a radiologist). The table below shows a comparison of the results of the 3 different segmentations.

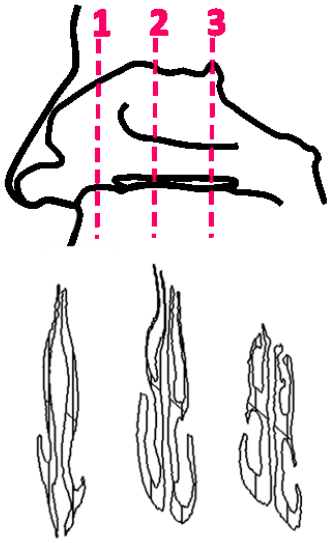

Measure	MRI A		MRI B	
	R	L	R	L
Total anterior nasal cavity volume mm^3	4472 (+/- 7%)	4628 (+/- 5%)	6417 (+/- 2%)	5330 (+/- 3%)
1. Cross sectional area head of inferior turbinate mm^2	36.3 (+/- 4%)	92.2 (+/- 1%)	170.7 (+/- 2%)	132 (+/- 3%)
2. Cross sectional area mid inferior turbinate mm^2	52.8 (+/- 6%)	128.7 (+/- 4%)	177.6 (+/- 1%)	184 (+/-1%)
3. Cross sectional area posterior inferior turbinate mm^2	35.1 (+/- 7%)	144.1 (+/- 5%)	166 (+/-2%)	197.2 (+/-1%)

Figure 3.6. Operator variability in segmentation. The table above compares the total anterior nasal cavity volume and cross sectional area at 1. the head of the inferior turbinate, 2. mid inferior turbinate and 3. posterior inferior turbinate, for a single subject pre and post decongestion, as measured by 3 independent operators. The largest difference between operators is seen when the cross sectional area is smallest as here slight difference in segmentation threshold would have a larger effect on the cross sectional area.

3.4 Nasal airflow profiles

The hot-wire technique was used to acquire simultaneous bilateral measurements of the time-varying inspiratory flow rate at each nostril. This method relies upon capturing the centerline velocity within a pipe attached to an anatomical nasal adaptor positioned against each nostril. Using this velocity signature the volume flow rate within the pipe (which represents that entering the nostril i.e., inspiratory flow rate) can be determined.

3.4.1 Study Design

A total of 14 healthy subjects (ages ranging from 21 to 38 years; mean 28 years) were selected for inclusion in this study. The subjects (6 male, 8 female) were screened to ensure they had no nasal complaints and no obvious rhinoscopic abnormalities. Following baseline measurements (PNIF, AR, VAS, SNOT-22) simultaneous bilateral nasal airflow measurements were obtained using hot-wire anemometry. Subjects were instructed to take 5 normal breaths and then to sniff through the pipes containing the hot-wires, this was repeated 5 times for each subject. Subjects were then instructed to take 5 normal breaths and then to smell lemon through the pipes, this again was repeated 5 times for each subject. Finally subjects were instructed to take 5 normal breaths and then smell ammonia through the pipes, this was also repeated 5 times for each subject. For each subject 45 normal breaths, 5 sniffs, 5 lemon smells and 5 ammonia smells were recorded. A metronome was used to guide subject towards a regular pattern of normal breathing, at a rate of 15 breaths per minute[228]. Subjects were not instructed to perform 'maximal' sniffs, and hence the sniffs recorded by the hot-wires cannot be taken as representative of the maximal effort inhalations employed for PNIF measurements (voluntary sniffs were performed in the absence of odorants).

Subjects were then decongested with two sprays of 0.1% xylometazoline topically administered at each nostril and repeated once after 5 minutes with a single spray as per the MRI protocol (section 3.3.1). All measurements (hot-wire, AR and PNIF) were subsequently repeated twenty five minutes after administration, thus allowing time for the decongestant to take effect.

The experimental apparatus for acquiring inspiratory profiles using the hot-wire technique is depicted in figure 3.7. The connection between the nostril and measuring tube is an important consideration to ensure the fidelity of both the hot-wire and acoustic rhinometry measurements[128]. Anatomical nose adaptors and sealing gel were used to increase the reproducibility of measurements[229]. Forehead and chin supports were used to limit the pressure exerted by the nasal adaptors on the nostril, which could alter the morphology of the nasal vestibule[230] and, hence, constrain its motion during inspiration.

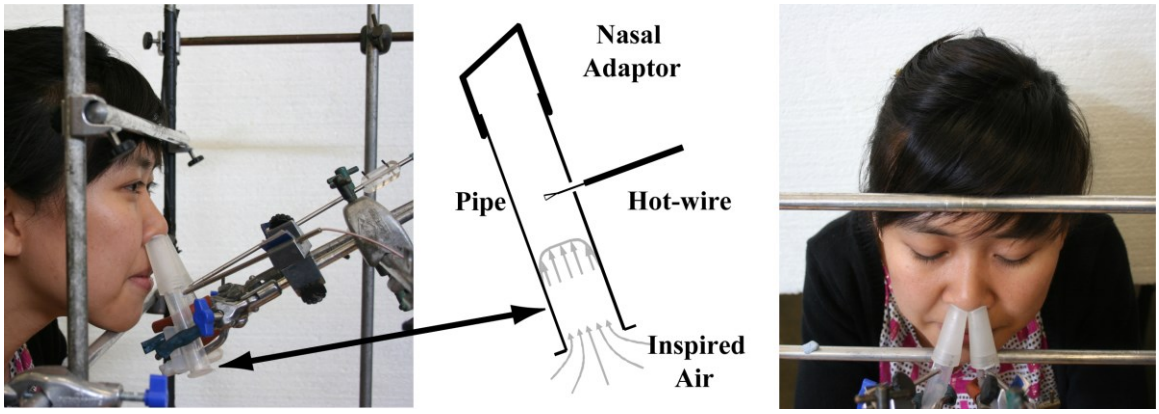

Figure 3.7 The layout of the experimental apparatus is depicted. Forehead and chin supports, anatomical nasal adaptors (with adjustable orientation) are shown with a schematic representation of the hot-wire configuration within the measurement pipe.

3.4.2 Hot wire anemometry

The hot-wire technique provides a means to measure the fluid velocity at a point in a given flow with high temporal resolution. A fine wire (~5 microns), heated by an electrical current, is placed in a flow. The frequency response of the hot wire depends on its thermal inertia, with a small diameter a response of tens of kHz is attainable. Usually the attainable frequency response is limited by the conditioning electronics. For these experiments, sampling at 10kHz provided an excellent dynamic response. Variations in the flow velocity affect the cooling provided by the flow, and thus alter the instantaneous wire temperature. In turn this affects the electrical resistance of the wire, which can be measured directly to enable the flow velocity to be determined (Figure 3.8). For a comprehensive account of this method see Bruun (1995) [231].

This study used a miniature tungsten hot-wire probe connected to an anemometer (two models were used: DISA 55M01 and Dantec mini CTA) and run at an overheat ratio of 1.5. The output was connected to: i) a filter-amplifier unit and then on to an National Instruments 16-bit data acquisition card and ii) directly to the same card hence recording both the raw and conditioned data. The data was sampled at a frequency of 5000 Hz and filtered at 1000 Hz.

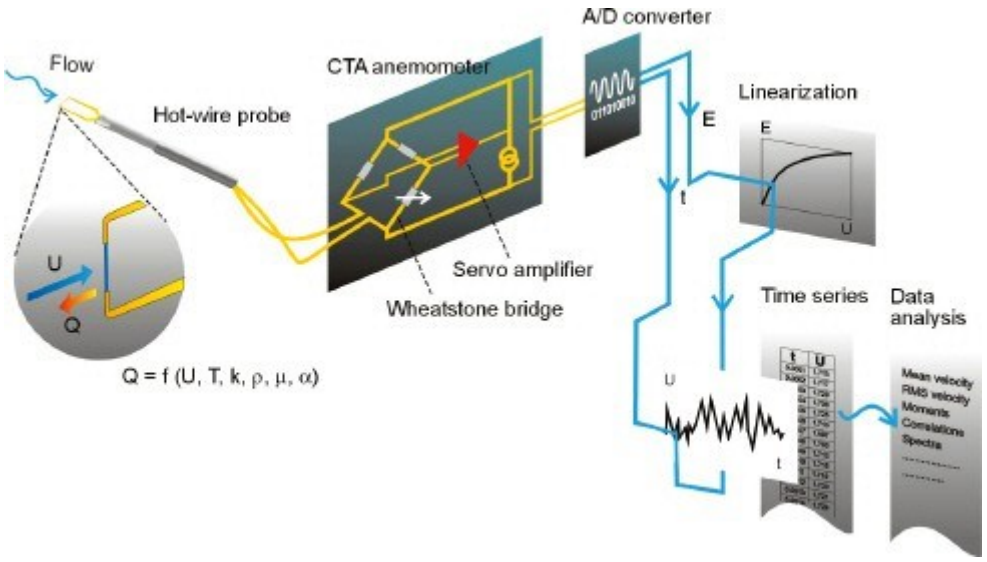

Figure 3.8 Schematic of the hot- wire anemometry technique[232].

To ensure the accuracy of the measurements the hot-wire was calibrated against a known flow in a controlled wind tunnel. The hot-wire and a Pitot-static probe (connected to a Furness micro-manometer FCO510) were positioned in the freestream air-flow of the wind-tunnel. The flow was incrementally adjusted through 12 different speeds spanning the largest range of velocities expected during the experiments. At each velocity, a 10-second long record of the hot-wire anemometer output and the freestream velocity (obtained from the dynamic pressure registered by the micro-manometer) was recorded. A King's power law and a fourth-order polynomial were fitted to the data to obtain the hot-wire calibration relationship.

After calibration, the hot-wires were each positioned at the centre of the short pipes through which the subject breathed. With a distance of approximately 3 diameters between pipe inlet and hot-wire location, theoretical predictions suggested a blunt velocity profile and thus near unity value for the ratio of mean velocity to that measured by the probe. As a fidelity check, an exercise was performed to compare the hotwire measured, integrated flow, with an independent volumetric measurement. In this exercise a subject inhaled via the instrumented pipes and orally exhaled through a pipe connected to a large inverted jar full of water to measure the total exhaled volume over 20 respiratory cycles, this was repeated 5 times. The volume of air inhaled was determined from the hot-wire measurements and compared to the total exhaled volume captured in the tank. The ratio of the velocity, V(probe)/V(mean), was determined to be 0.89 +/- 0.08.

3.5 Methods to assess sinonasal transport

Both physical and numerical modelling were employed to investigate sinus gas exchange. Gamma scintigraphy, theoretical order-of-magnitude estimates and computational fluid dynamics simulations were used to investigate convective and diffusive transport between the nose and the sinus in a range of idealised geometries.

3.5.1 Definition of Anatomy

A simplified Perspex model was constructed, based on detailed measurements of sinonasal anatomy made with image segmentation software (Amira 4.1) (as previous see section 3.3.3) and a 3D Computer Aided Design (CAD) programme (Rhinoceros, McNeel Europe), from pre-existing computed tomography (CT) scans of a patient with no known sinus pathology [92].

The idealised model was based on retrospective CT data from a 53 year old female subject. The scans were performed using a standard sinus protocol with axial acquisition and the patient in a supine position. The acquisition boundaries were from the inferior border of the maxillary sinus to the superior border of the frontal sinuses. The entire nasal cavity was included. The data was acquired using a with a Philips MX800 4-slice helical scanner with a slice thickness of 1.3 mm and a 0.7 mm increment. The scanner settings were a peak kilo voltage of 120 and a tube current of 35-85 mA. The data sets had a 512 x 512 matrix and the image stacks were in the region of 150 slices. The scans were reported by a consultant radiologist as showing no signs of sinonasal pathology. Coronal reconstructions were used for segmentation work.

The boundaries to the airway were segmented primarily using threshold-based contour selection as previously described (Section 3.3.3). Considerable user intervention was required however to modify the selected contours and to correct spurious defects in the fine structures due to inadequate resolution and partial volume effects (Figure 3.5). After segmentation of the volume, smoothing was applied to remove digitisation artefacts and the results checked for fidelity with the original image resolution.

The proposed dimensions for the model were as follows: a diameter of 3 mm with a length of 6 mm and for the main ostium, and a diameter of 1.5 mm with length of 2mm with for the accessory ostium, an inter-ostial separation of 14 mm, a width of the middle meatus of 2 mm and a model span width of 50 mm. These are based on the characteristics of the left sinonasal airway on the CT scan (figure 3.9). The diameter of the main ostium is comparable with the mean literature values and although its length approaches the shorter end of the spectrum, it is

still within the normal range (table 1.1). The diameter of the accessory or smaller ostium is small but again within the range found in the literature. The inter-ostial separation is one of the larger described by Blenke (2011)[48] but there is no other comparable data available in the literature.

The advantage of a physical model study is that, if well-designed, it can be adjusted to test different configurations in a regulated manner. With this in mind an idealised model of the sinus and middle meatus was devised. The entire model was made from plastics to avoid imaging artefacts. The model consists of a box with a detachable top lid, through which two ostia pass, with a 20 ml syringe with adjustable plunger attached to it as the sinus. The syringe is attached downstream to ensure a more laminar flow in the middle meatus in the region of the ostia. The ostial configuration can be altered by occluding the ostia with adhesive tape. The box is filled with a spacer to create a middle meatus with a diameter of 2 mm, as based on the narrowest diameter of the middle meatus measured on the CT scan, under the assumption that the narrowest diameter would be the most restricting factor.

The eventual model had the following dimensions: a diameter of 3 mm and a length of 8 mm for the larger main ostium, similar to mean literature values (table 1.1), and a diameter of 1.7 mm and a length of 3.5 mm for the smaller accessory ostium. The diameter for the small ostium is at the small end of the spectrum according to the literature. The length of the small ostium is larger than the mean 0.6 mm reported by Blenke (2011)[48]; however there are no other literature reports to compare with. The width of the middle meatus, the span width of the model and the interostial separation remained unchanged.

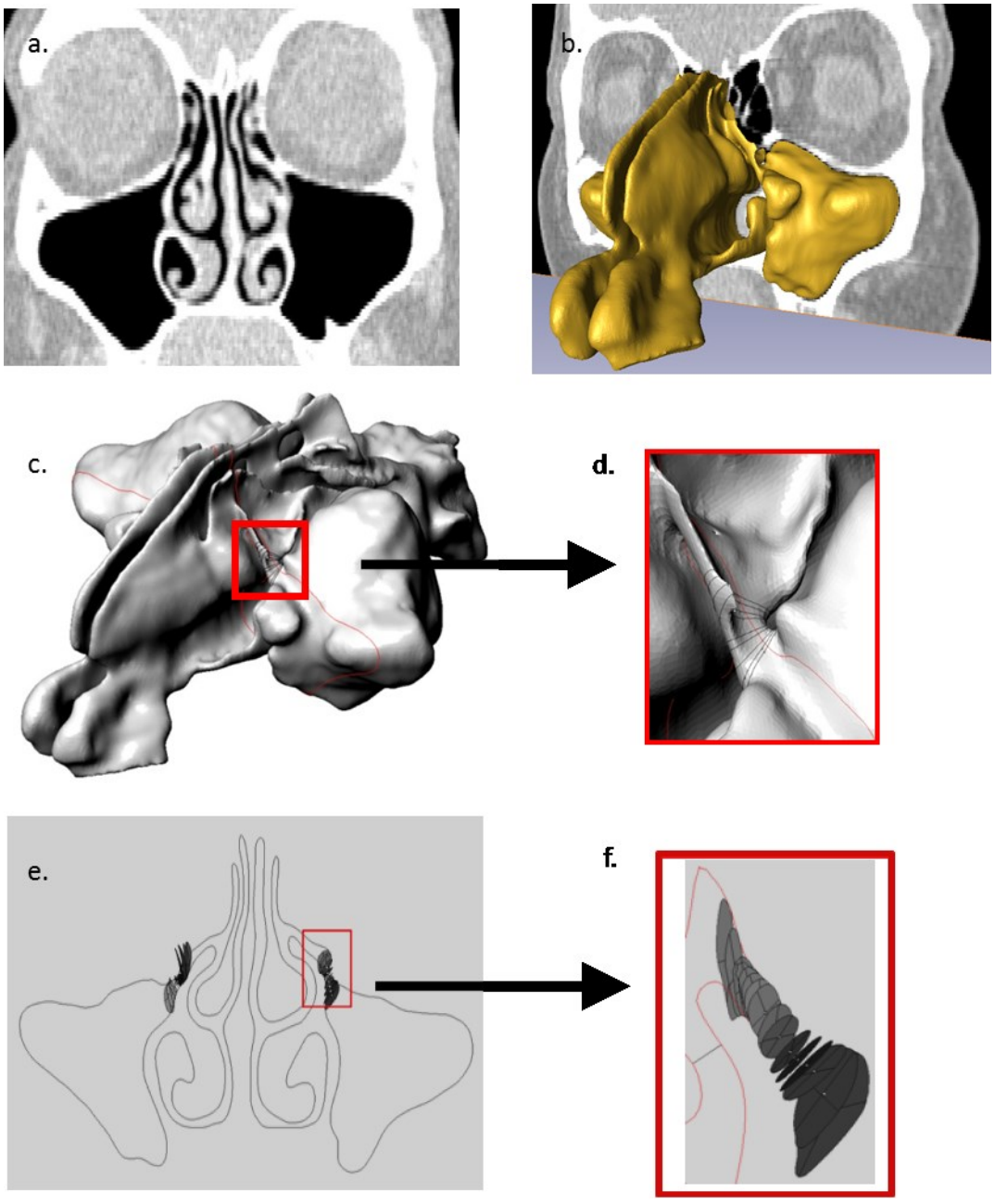

Figure 3.9 Defining the sinus and ostial anatomy[213]

a. Coronal section of CT sinuses

b. Reconstructed surface definition in conjunction with CT image.

c. Reconstructed surface definition with maxillary ostium highlighted. The red line depicts the cross-sectional cut shown in e.

d. Detailed view of the maxillary ostium.

e. Cross-section through c showing multiple cross-sections of the maxillary ostia

f. Detailed picture showing cross-sections through right maxillary ostium.

3.5.2 Creation of Experimental Model

An experiment was designed to analyse gas flow between one side of the nose and a maxillary sinus in the idealised model using Krypton 81m and ɣ-Scintigraphy. The physical model geometry (figure 3.10) represents a human middle meatus, maxillary sinus and two ostia which connect the sinus to the meatus. The top plate of the model was removable to allow the ostium configuration to be changed. Adhesive tape was used to cover each ostium in turn for single-ostium tests, and removed for the double-ostium tests. The sinus volume was adjustable through the use of a syringe plunger. The sinus was attached downstream on the middle meatus to allow a more laminar flow to have developed in the region of the ostia. The use of idealised physical models has allowed the ostium geometry to be varied in a controlled manner. It was constructed in Perspex and other plastics for flexibility with different scanning methods.

a.

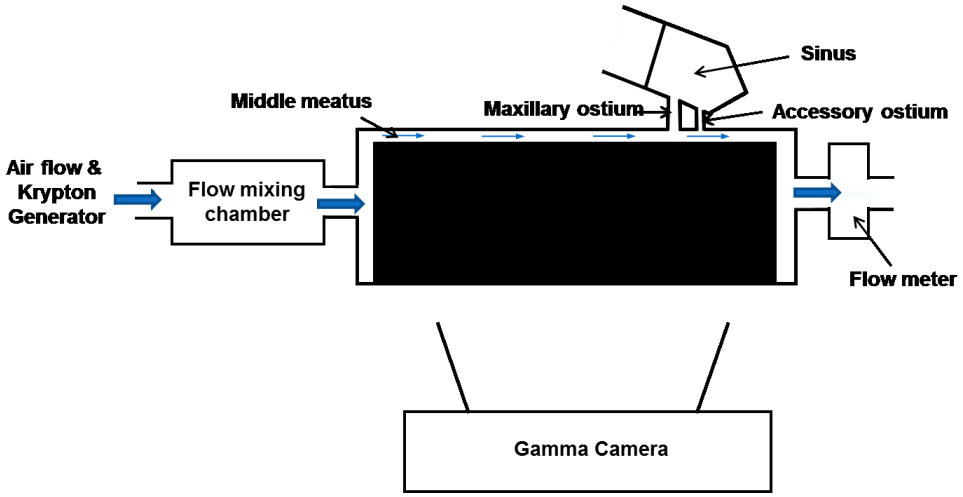

b.

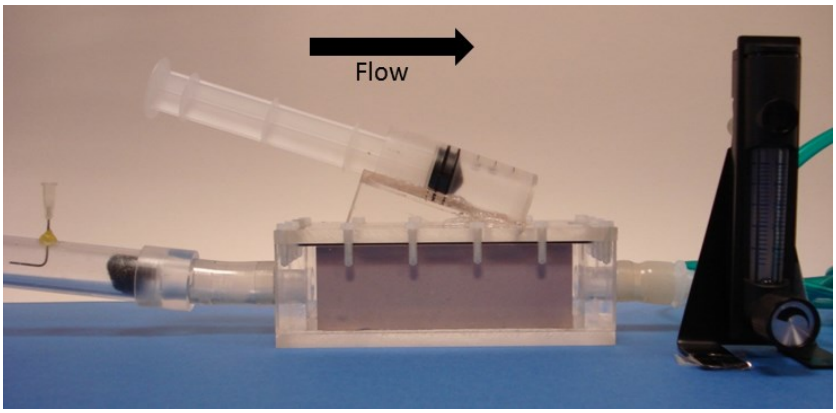

Figure 3.10 a. Diagram of physical model geometry. The sinus volume is adjustable between 5 and 20ml. The channel dimensions are 125 mm long by 2 mm thick and 50 mm wide. The larger maxillary ostium (MO) has a diameter of 3.0 mm and length of 8 mm, and the smaller accessory ostium (AO) has a diameter of 1.7 mm and length of 3.4 mm. The interostial distance is 14 mm. b. Photograph of the idealised model.

3.5.2.1 Experimental Apparatus

The idealised model described above was connected upstream to a mixing chamber, in which krypton 81m was injected into the stream of compressed air and then passed through a tightly packed ball of wire wool (see figure 3.11). Downstream of the model a rotameter was connected to ensure the correct flow rates were obtained.

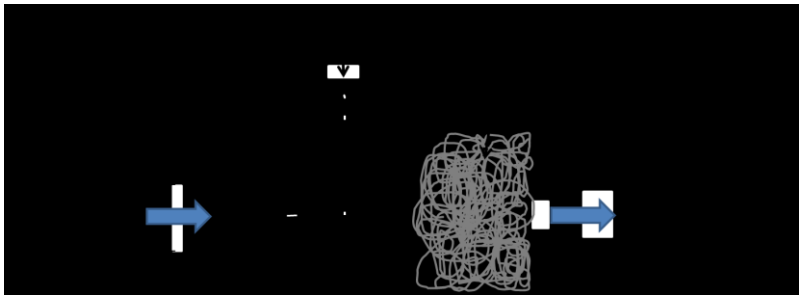

Figure 3.11 Krypton mixing chamber.

^{81m}Kr was obtained from a Rubidium generator, as used for clinical tests[214]. The flow rate from the generator was 1L/min, with compressed air added to increase the flow rate. The model was viewed through parallel γ cameras, which detected the γ decays emitted by the model. Images of cumulative count number were recorded for times ranging from two to ten minutes. Dynamic imaging sequences, with 2s collection times, were used to assess the time taken for the counts to reach steady state. Three different ostial configurations (double ostia, large single ostium (MO) and small single ostium (AO)) were investigated at two different flow rates (2.5L/min and 5L/min). The experiments were run five times for each different ostial configuration and flow rate to ensure repeatability of results. Please see appendix for the experimental protocol.

The known volume of the model sinus also allows the effective volume flow rate to be calculated from the images, whereas for real sinuses with unknown volume only ventilation per unit volume can be found. The flow rate used is based on model studies of nasal airflow[92] where the peak flow velocity in the middle meatus for quiet breathing was found to be 1.2m/s.

The experiments used steady flow through the nose to drive gas transport in the sinus. Bi-directional flow in breathing has two possible flow effects for the sinus, both of which have previously been shown to be minor. During the breathing cycle there is a pressure variation in the nose and sinuses of around 10mm water (100 Pa), and it has been suggested based on unpublished results that this pressure variation could drive flow to the sinuses Möller *et al*.

(2009) also asserted that pressure gradients had been found to drive flow to the sinuses [208-210,212]. However, earlier publications found the pressure in the sinuses to follow exactly the pressure in the nasal cavity during normal breathing, implying that there is no pressure gradient and no flow is driven[194,233]. There will be a small movement of air due to the volume change associated with the pressure change, but the volume moved is very small relative to the volume of the sinus, as initially calculated by Proetz[193] to take around an hour to replace all the air in a typical sinus. There may also be some additional mixing caused by the reversal of flow between each half-cycle. Aust and Drettner (1974)[56] used bi-directional flow in their experiments, whose results were well matched by computational simulations in comparable simplified sinus geometries with steady flow through the nose[151], suggesting that the effect of flow reversal mixing is small.

3.5.2.2 Gamma scintigraphy

Gamma scintigraphy is a technique in which a gamma camera is used to image gamma radiation emitting isotopes. The most common indication for ɣ scintigraphy is to diagnose pulmonary embolism with a lung ventilation/perfusion scan. In the ventilation phase of a ventilation/perfusion scan, a gaseous radionuclide, usually krypton 81m in the UK, is inhaled by the patient through a mouthpiece. The perfusion phase of the test involves the intravenous injection of radioactive technetium macro aggregated albumin (Tc99m-MAA). A gamma camera acquires the images for both phases of the study. These images are then examined for any ventilation perfusion mismatch.

Gamma scintigraph involves a crystal inside the head of a gamma camera scintillating in response to radioactive particles and producing a burst of light that is picked up by sensors (photomultipliers) located behind the crystal. The camera constructs an image based on this information. A collimator is attached to the head of the gamma camera to help focus the gamma photons and give spatial information about the subject. It consists of a thick lead sheet with thousands of holes through the detector. Only gamma photons travelling perpendicularly to the crystal manage to hit it. All the other photons are absorbed by the collimator. However, the collimator is also one of the sources of blurring within the image; lead does not totally attenuate incident gamma photons, there can be some crosstalk between holes[234].

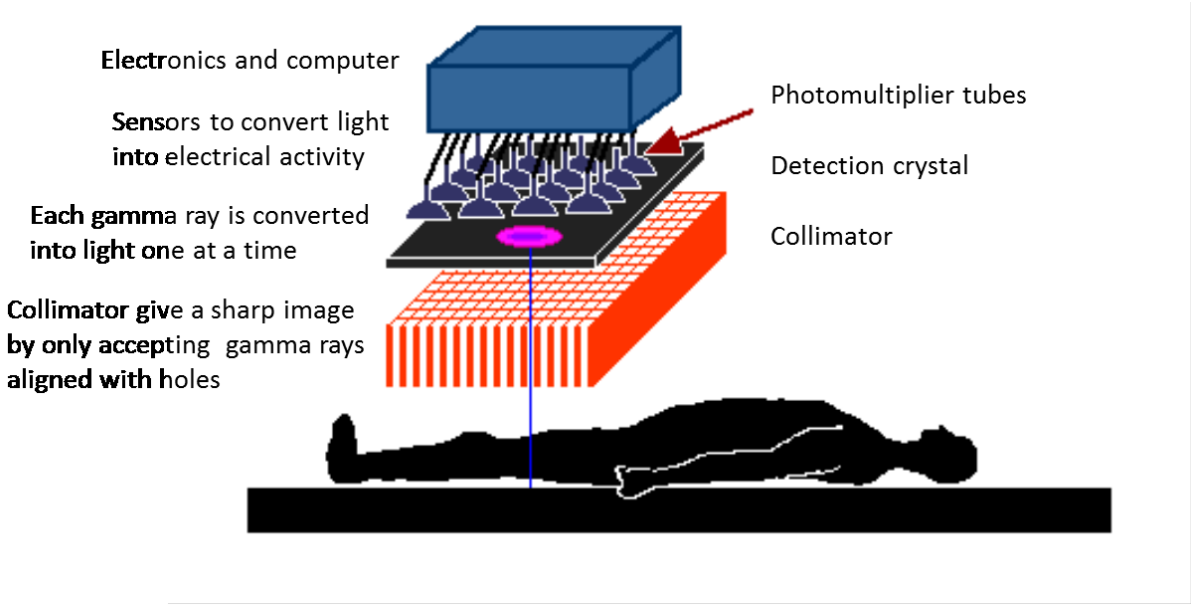

Figure 3.12 Gamma Camera Components[235].

3.5.2.3 Image Processing

The γ images were processed by identifying two regions of interest, containing the sinus and channel respectively, and assessing the number of counts in each region. Further analysis follows Amis and Jones[236] who considered the steady state balance between the transport and decay of krypton to find relationships between activity and ventilation per unit volume in lung images. The effective ventilation flow rate through the sinus can thus be found according to the following equation:

$$Q_{eff} = \beta Q_c \lambda / (Q_c/V_c + \lambda - \beta Q_c/V_s)$$

Equation 3.2

where Q_{eff} is the effective volume flow rate of gas replacement in the sinus, β is the ratio of counts found in the sinus to those in the channel at steady state, Q_c is the flow rate through the channel representing the middle meatus (converted from l/min into m^3/s), λ is the decay constant for ^{81m}Kr (0.0533/second), V_c is the volume of the region of interest in the channel and V_s is the volume of the sinus (converted from ml into m^3). Q_{eff} is thus the only unknown variable in the equation and its value can be found.

The placement of the measurement region of interest (ROI) could have a significant influence on the prediction of transport from the channel to the sinus. To address these concerns a sensitivity analysis was performed to assess the influence of the measurement

region location on the predicted transport between the channel and sinus. This identified that a non-subjective method of determining the measurement region locations was required to obtain reliable transport predictions.

This ambiguity arises as the exact location of the physical model boundaries cannot be adequately identified from the gamma camera images. For instance, both partial volume effects and the fact that for gamma camera imaging the signal reaching the detector array can bleed to neighbouring pixels complicates precise discrimination between the signal originating from the channel and the signal from the adjacent sinus. The channel sections appear much wider on the image than in the physical model. This 'spreading' effect is due to the gamma rays not all following horizontal paths to reach the camera plates. This was tested by placing a 1 mm wide solid source in the field of view of the cameras at the same distance as the krypton model would be placed and measuring its width on the image, which was 9 mm. The real width of the model channel to which the sinus is attached is 2 mm, but this broadens significantly in the image, leading to counts originating in the channel being detected in the sinus and vice versa. The resulting meeting and overlap of the sinus and channel regions prevents the ostia being visible on the images and effectively reduces the resolution of the images. The number of counts detected in the sinus and channel regions were corrected for this interference by defining additional regions of interest.

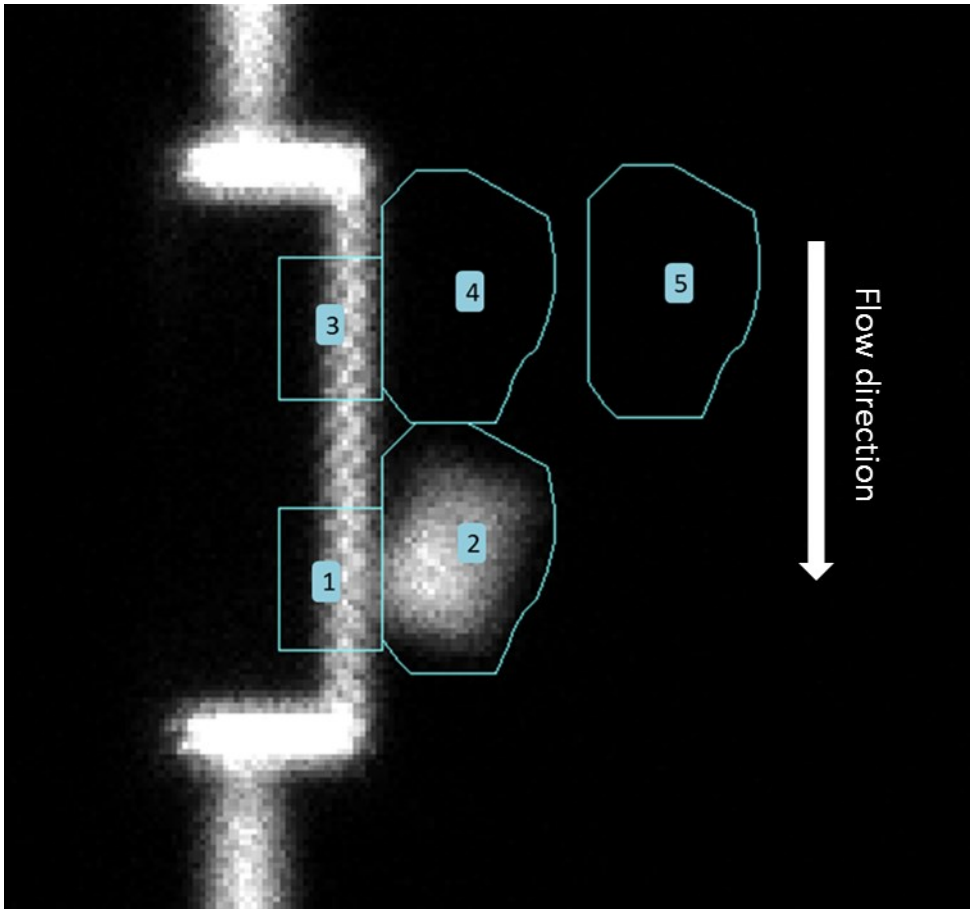

Figure 3.13 Determining optimal region of interest position.

In Figure 3.13 one would expect the total count number in ROI 1 to be less than or equal to ROI 3. The krypton is flowing from 3 to 1 and decaying over time but the rate of decay is slower than the flow rate. However the results show a higher total count number in ROI 1 than 3. This is due to counts from the sinus (ROI 2), contributing to the count number in ROI 1. Therefore ROI 3 (the proximal channel region of interest) and ROI 2 have been used to calculate flow rates (as opposed to 1 and 2) as there is no sinus adjacent to position 3 and therefore no additional source of counts. Determining the exact location of the ROI on the image requires careful consideration as small changes in positioning by just 2 or 3 pixels could alter the flow rate by up to 30%.

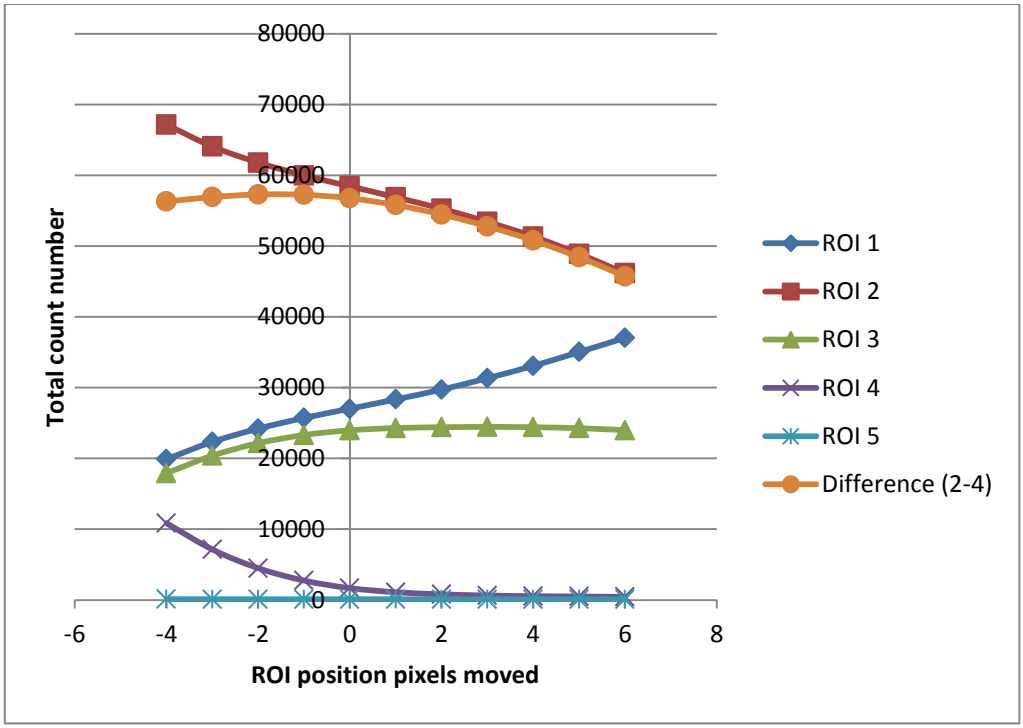

Figure 3.14 The change in total count number of each ROI identified in Figure 3.13 associated with moving the ROI to the left or right on the image (figure 3.13), corresponding to the left and right of the vertical axis.

To determine the optimal ROI location the orange and green lines in figure 3.14 were studied. The optimal location needed to capture all the counts from the sinus and all the counts from the channel with minimum cross over. Figure 3.14 illustrates that moving the ROI 2 one pixel to the right leads to loss of some of the counts from the sinus (orange line) and by moving the ROI's one pixel to the left there is a loss of counts from the channel (green line). This is illustrated in figures showing the detail of ROI 3 and ROI 2-4 in the appendix.

To determine the optimal location the channel ROI 3 was placed as far to the left as possible but still within 2% of the maximal value to ensure minimal loss of true channel count signal whilst minimising contribution of spurious channel counts to the sinus.

3.5.2.4 Acoustic Excitation

Acoustic modelling was carried out in collaboration with Christina Hood PhD student in the department of bioengineering to assess the responses of the sinuses to vocal frequency sounds. The voiced speech of a typical adult male will have a fundamental frequency from 85 to 180 Hz, and that of a typical adult female from 165 to 255 Hz[237,238]. Simple acoustic experiments were

performed with the physical model and Dr Hood performed one dimensional acoustic modelling to explore the physical basis for the increase of NO transport found during humming.

The experimental set up for the acoustic experiments is depicted in Figure 3.15 below. It consisted of a small speaker connected downstream of the physical model (representing the nasopharynx) and two 8 mm diameter condenser microphones (RS 242-8905), used to measure sound levels (one microphone close to the speaker and the other in the sinus). The microphones were modified to use an external power source which gave a more consistent output voltage than the original batteries. Only one microphone could be connected to the filter at a time, so consecutive frequency sweeps were carried out for the sinus and speaker microphone positions for each ostium-sinus geometry combination.

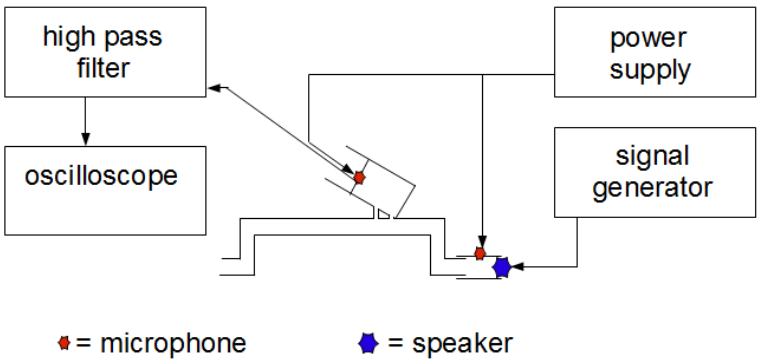

Figure 3.15 Schematic representation of the experiment apparatus used for acoustic experiments.

To ensure that the microphone responses were consistent simple calibrations tests were performed using a short length of straight pipe, with a speaker at one end and a microphone at the other. The matching responses of both microphones are illustrated in the graph (Figure3. 16).

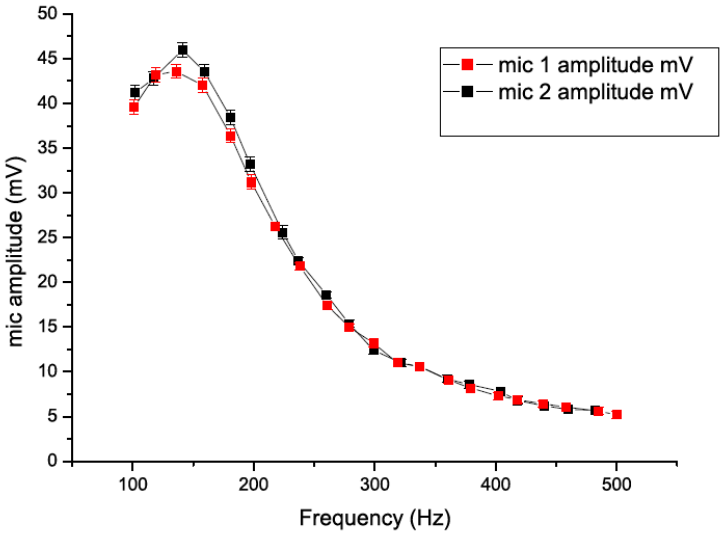

Figure 3.16 Calibration results for the two microphones in a straight tube. Speaker frequency was varied between 100 and 500 Hz with constant output from the signal generator.

For the acoustic experiments the setup was modified to incorporate a “sinus” microphone in an alternative syringe plunger and the additional speaker with nearby microphone was mounted in a short length of tubing which could easily be attached and detached from the main model thus, maintaining the integrity of the model. A signal generator was used to drive the speaker at frequencies between 100 and 700 Hz, at intervals of approximately 10 Hz. A high-pass filter was required for the removal of mains frequency (50 Hz) noise from the microphone signals, which was introduced by the microphone power supplies. The filtered microphone signals were examined on an oscilloscope and the frequency and amplitude near the speaker and in the sinus recorded. The ratio of the sinus amplitude to the speaker amplitude (‘gain’) was plotted against frequency in order to identify the resonant frequency and calculate the Q-factor. The Q factor is a dimensionless parameter that characterizes a resonator's bandwidth relative to its centre frequency illustrated in figure 3.17.

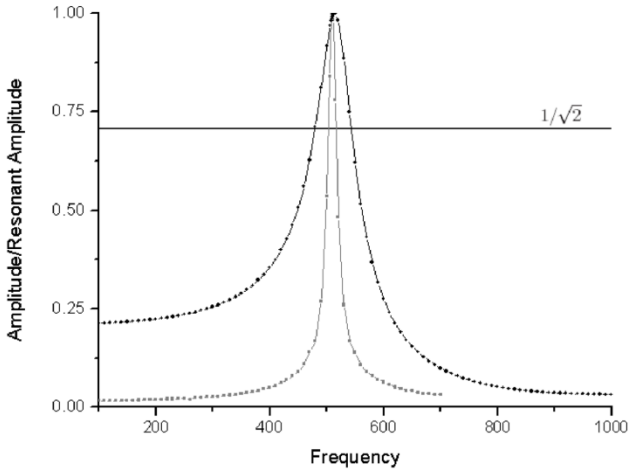

Figure 3.17 Resonances with high and low Q-factor. The grey acoustic response has a higher value of Q-factor than the black response[239].

3.5.3 Predicting Sinus Ventilation

First order estimates and computational simulations have been used to provide a valuable cross checking of results with the physical experiments. Once matching has been established with a few sets of variables with results from both methods, there is increased confidence in results from each method alone.

3.5.3.1 Péclet Number

The Péclet (Pe) number is a dimensionless number used to compare the significance of convective and diffusive transport.

$$Pe = \frac{UL}{D}$$

Equation 3.3

Where U is a typical velocity (m/s); L is a typical linear dimension (m); and D is the diffusivity of the species of interest (m^2/s). Péclet numbers of much less than 1 indicate diffusion dominated transport, values around one indicate convection and diffusion are of similar importance and values much greater than 1 signify convection dominated transport. The Péclet numbers for the single ostium geometries were calculated using the peak x-velocity on the ostium-sinus interface as U and the ostial diameter as L.

3.5.3.2 Diffusive Transport

Studies have shown that ventilation of sinuses with a single ostium <4mm in diameter is through diffusion. Therefore for geometries with a single ostium gas exchange was modelled using Fick's first law of diffusion. If the concentration in the sinus is C_s, while that in the nasal cavity is C_N, diffusive flux through the ostium will be given by;

$$\frac{DA\ (C_S - C_N)}{L}$$

Equation 3.4

where D is the diffusivity of the species of interest (m^2/s) in air,
A is the cross-sectional area of the ostium (m^2) and
L is the length of the ostium (m).

3.5.3.3 Convective Exchange

Estimates of convective exchange times were obtained from ostial volume flow rates. It was assumed that the sinus is a well-mixed vessel with a uniform concentration and any gas leaving the sinus has the same composition as the gas in the sinus. To obtain the estimates, mixing in the vessel was considered to be fast compared to the transport through the vessel. Coulson & Richardson[240] gave the following expression for the time taken to achieve 90% exchange in a well-mixed vessel:

$$T_{90} = -\frac{Vs}{Q} \ln 0.1$$

Equation 3.5

where T_{90} is the time for 90% exchange (s), VS is the volume of the sinus (m^3) and Q is the flow rate into or through the sinus (m^3/s).

3.5.3.4 Flow Rate through a double-ostium sinus

The addition of a second or accessory ostium to the maxillary sinus results in a net flow through the sinus. The pressure differential that would drive this flow was investigated using the intranasal pressure drop predictions of Croce *et al.*[241] and Taylor *et al.*[191]. Croce *et al.* measured the intranasal pressure at various points along the nose in a plastinated cadaveric model of the human nose at 3 different flow rates, namely 109 ml/s, 231 ml/s and 353ml/s (figure 3.18). The position of the main and accessory ostia of the geometry described earlier and verified by computer aided design measurements are plotted onto the graph (figure 3.18). Taylor (2008)[242] used computational fluid dynamics to investigate nasal pressure drop in the same nasal geometry as that on which the idealised model is based (Figure 3.19).

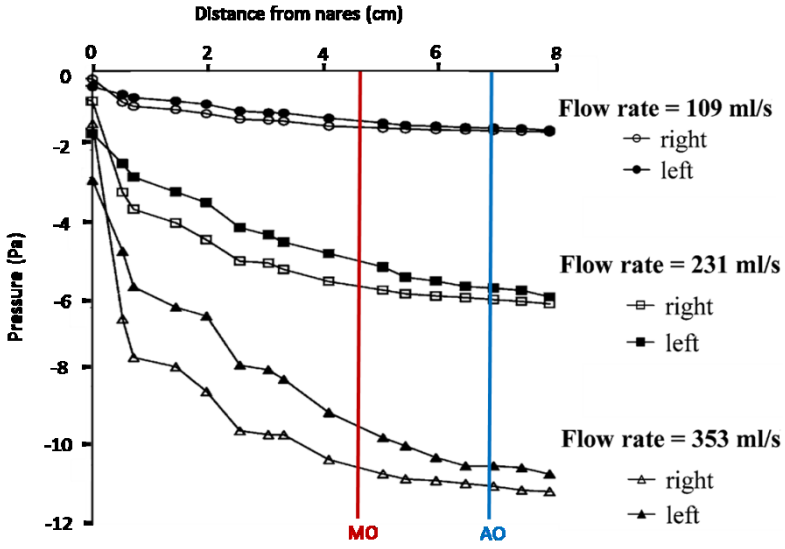

Figure 3.18 Pressure drop curves along the nasal cavity for flow rates of 109 ml/s, 231 ml/s and 353 ml/s. MO refers to the maxillary ostium and AO refers to the accessory ostium. Adapted from Croce *et al.*[241].

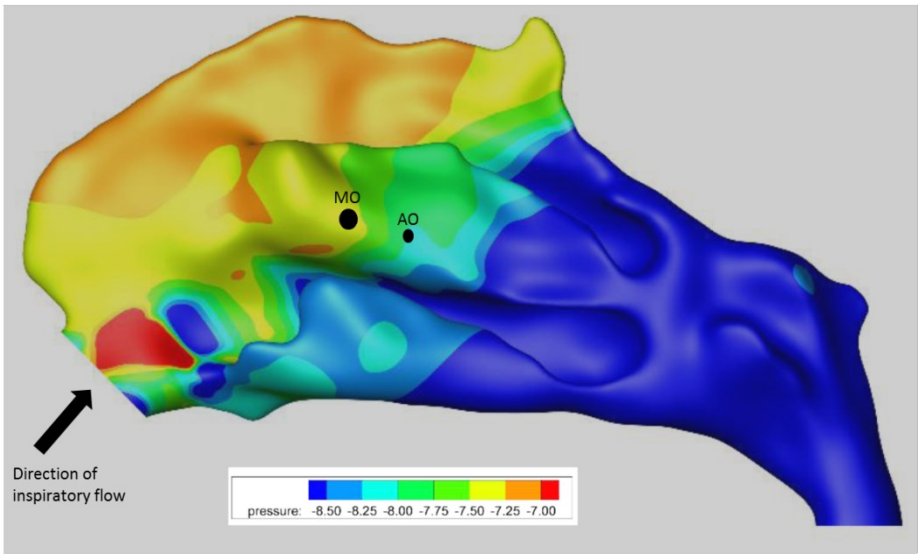

Figure 3.19 The pressure drop in the left nasal cavity based on the same CT scan data as the idealised sinus model. The airway boundary is colour-coded to indicate the local static pressure for a flow rate of 5 l/min. The nasal vestibule is not shown and the external reference pressure is set to zero. The large black spot indicates the position of the maxillary ostium. The smaller black spot AO indicates the position of the accessory ostium. Pressure scale in Pa. Figure provided by Dr D. J. Taylor, Imperial College London.

The volume flow rate can be estimated using Poiseuille's law as described by Hood[239]. An important consideration in estimating the volume flow rates is the ostial entry flow effects. If the ostial Reynolds' number (Re) is below 30, as then entry flow effects can be neglected[243]. However, when the value is greater than 30 as in this case, entry flow effects will be significant and must be taken into account. Loudon and McCullogh (1999)[244] developed an empirical correction for this which was utilised to estimate the effects of entry flow in the ostia on the flow rate through a double ostium sinus. For the Poiseuille flow estimate, the unknown pressure in the sinus, P_s is assumed to be uniform and constant, while the pressures at the nasal end of the upstream and downstream ostia, P_u and P_d respectively, are assumed constant and known. Thus the volume flow rate through the upstream ostium (positive into the sinus) is given by

$$Q_u = \frac{\pi r_u^4}{8\mu L_u} (P_u - P_s)$$

Equation 3.6

and similarly for the downstream ostium

$$Q_d = \frac{\pi r_d^4}{8\mu L_d} (P_d - P_s)$$

Equation 3.7

where Q is the volume flow rate into the sinus (m^3/s), r is the ostium radius (m), μ is the dynamic viscosity of air (1.79x10−5 m^2/s at T=36^{0}C), L is the ostium length (m) and subscripts u and d refer to the upstream and downstream ostia respectively. By conservation of mass, the flow into the sinus through the upstream ostium must be equal to that out of the sinus through the downstream ostium,

$$Q_u = -Q_d = Q_o$$

Equation 3.8

Hence where the ostia have unrelated geometry,

$$Q_o = \frac{\pi}{8\mu} \frac{1}{\frac{L_u}{r_u^4} + \frac{L_d}{r_d^4}} (P_u - P_d)$$

Equation 3.9

Loudon and McCullogh (1999)[244] used the following expression for entry length, the pipe length required for flow to reach 99% of its Poiseuille flow profile:

$$\frac{L_E}{D} = 0.58Re = 0.058\frac{U_d}{v}$$

Equation 3.10

where L_E is the entry length (m); d is the pipe (ostium) diameter (m); Re is the pipe Reynolds' number (dimensionless); U is the average velocity in the pipe (m/s); and is the kinematic viscosity of air (1.46x10−5 m^2/s at T=360C). Their correction to Poiseuille flow rates in the entrance region is given by

$$\frac{Q_E}{Q_P} = \frac{L/L_E}{L/L_E + 0.52}$$

Equation 3.11

where Q_E is the corrected flow rate (m^3/s); Q_P is the Poiseuille flow rate (m^3/s); L is the total length of the ostium (m); and L_E is the entry length calculated earlier. This expression tends to under-estimate Q_E, as the entry length is calculated based on the Reynolds number derived from

the Poiseuille flow estimate, which tends to be too large. Consequently the correction was used iteratively, with a new Reynolds number calculated from the corrected flow rate and used to find an updated entry length and improved flow rate estimate. Hence, using $Q = \frac{\pi d^2 U}{4}$

$$Q_{E(i+1)} = \frac{1}{1 + 2630 Q_{E(i)}/L} Q_P$$

Equation 3.12

where $Q_{E(i+1)}$ is the updated entry flow estimate and $Q_{E(i)}$ is the previous estimate. The first value of the series, $Q_{E(0)}$ is the Poiseuille flow rate. The convergence of this series is shown in the appendix . The flow rates vary by less than 3% beyond the 10th iteration, so 10 iterations were used to find a converged solution[47].

3.5.3.5 Computational Fluid Dynamics

A computational geometry and mesh were created in Gambit 2.4.6 (Fluent Inc., NH, USA) by Dr C Hood to match each physical model configuration. In order to reduce computational expense, the vertical sections at each end of the physical model channel were not included in the computational geometry, as they did not affect the flow profile approaching the ostia. Different volume cell geometries were used in different regions of the model in order to improve computational efficiency. Hence anisotropic hexahedral cells were used in the channel, with the highest mesh density across the thickness of the channel where the gradients of flow variables are expected to be steepest, and increased mesh density close to the ostia. The irregular shapes of the ostia and sinus did not allow for hexahedral meshing, so tetrahedral cells were used in these components. Non-conformal surface meshes at the interface of the different types of volume mesh were avoided by using triangular prism cells in the projections of the ostia across the channel. The quality and density of the computational mesh used is critical for the accuracy of any CFD solution. The mesh independence of the solution was tested by comparing the x-velocities in the maxillary ostium of the idealised model for three meshes of different densities. A graph of these velocities is given in figure 3.20, where the velocities found for the 3.0 and 6.1 million cell meshes are almost indistinguishable, indicating that the 3.0 million cell mesh is adequately resolved.

Flow simulations were run in Fluent 6.3.26, initially only modelling steady velocity and pressure for convective transport and later adding unsteady transport of an inert species in

order to allow for diffusion. Convective-only volume flow rates for single-ostium sinuses are upper-bound estimates and were determined by finding the integral of positive z-velocities across a surface of constant z (perpendicular to the ostium axis) just below the curved ostium-sinus interface. For the double-ostium sinuses, the volume flow rate through each ostium could be obtained directly from Fluent.

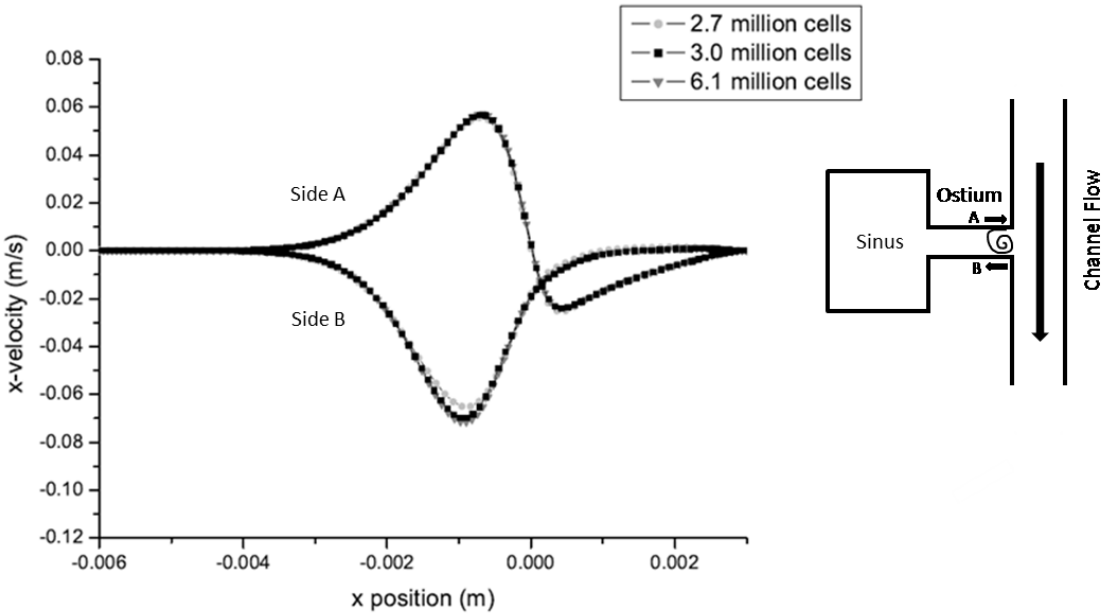

Figure 3.20 Graph of x-velocities in the ostium and channel on lines parallel to but offset from the ostium axis for meshes with 2.7, 3.0 and 6.1 million hexahedral cells. x=0 is the interface between the channel and the ostium while x=-0.006 m is the interface between the ostium and the sinus.). On the right the schematic illustrates the relationship of the graph to the model. Adapted from Dr C.M. Hood[47].

The computational fluid dynamic simulations were performed by Dr C.M. Hood, Department of Bioengineering, Imperial College London.

Effective volume flow rates for combined convection and diffusion simulations were calculated based on the concentration of Kr in the sinus relative to that in the nose (ratio α), based on the assumption that the sinus is a well-mixed cavity so $Q_{eff} = V_s \ln(1-\alpha)/T_\alpha$, where V_s is the volume of the sinus and T_α is the time at which the ratio of concentration in the sinus to that in the nose is α. For the single-ostium geometries, where transport is expected to be dominated by diffusion, first-order estimates of Q_{eff}, based on Fick's Law of one-dimensional diffusion, were also made as $Q_{Deff} = DA/L$, where D is the diffusion coefficient of Kr in air (1.578×10^{-5} m^2/s), A is the cross-sectional area of the ostium and L is the ostium length.

3.5.3.6 Estimating NO transport

High concentrations of nitric oxide (NO) have previously been measured in human maxillary sinuses, but the transport rates between the sinus and the nose during normal breathing have not been quantified. In this study, NO transport is investigated using published NO concentrations and production rates, first-order modelling and computational fluid dynamics (CFD) in idealised physiological, pathological and post-surgical geometries. The diffusive transport of NO through the ostium is given by

$$\frac{DA\,(C_S - C_N)}{L}$$

Equation 3.13

where D is the diffusivity of NO in air (2.4x10-5 m^2/s), A is the cross-sectional area of the ostium (m^2), C_s is the concentration of NO in the sinus (mol/m^3), C_N is the concentration of NO in the nasal cavity (mol/m^3) and L is the ostium length (m). The corresponding convective flux of NO is given by

$$QC_S$$

Equation 3.14

where Q is the convective volume flow rate (m^3/s) and C_S is the sinus concentration as before. Balancing NO production (P, mol/s) and transport gives the following expression for the steady-state sinus NO concentration:

$$C_S = \frac{P + \frac{DA}{L}C_N}{Q + \frac{DA}{L}}$$

Equation 3.15

Sinus and nasal NO concentrations in the literature are typically quoted in parts per billion (ppb), equivalent to nl/l. For calculations it is however more consistent to use the SI units mol/m^3. Conversion between these units was carried out using the perfect gas law, where 1mol of gas is known to occupy $22.4x10^{-3}$ m^3 at atmospheric pressure and 0◦C, or $25.4x10^{-3}$ m^3 at atmospheric pressure and 37◦C. Hence 1ppb is equivalent to $39.3x10^{-9}$ mol/m^3. Production rates were converted similarly from nl/min to mol/s.

Chapter 4

Nasal Anatomy in the congested and decongested states

4.1 Introduction

This chapter presents the results of a pilot study on the capability of MR imaging to reveal the regional changes in nasal anatomy associated with decongestion. Procedures to map the changes in geometry are outlined and, within the limitations of a preliminary investigation, to consider the implications for nasal airflow and transport.

The geometry of the nasal airway plays an important functional role in maintaining a healthy upper respiratory tract. The large surface area of nasal cavity covered with respiratory epithelium and a mucociliary blanket provides a surface over which heat and moisture exchange can take place. Warming inspired air to core temperatures protects the delicate lung alveolar membrane from thermal injury, while saturating it with water keeps the membrane wet, facilitating rapid absorption of oxygen and excretion of carbon dioxide. Although all parts of the respiratory tract are capable of temperature and moisture modification, the vast majority of heating and humidification of inspired air during nasal breathing occurs in the internal nasal passages[68,245,246]. Upon inspiration, ambient air comes in contact with the warm, moist respiratory mucosa where thermal and water vapour pressure gradients promote changes in the temperature and moisture content of the inspired air. Heat is transferred from the nasal mucosa to the inspired air primarily via convection, and since the ability of air to hold water

vapour increases with temperature, raising the temperature of the inspired air results in the concurrent transfer of moisture via evaporation. [68,71,74,245,247]

However the complex three dimensional anatomy of the nasal cavity is not static, given that the erectile tissue in the nasal turbinates (especially the inferior turbinate), fluctuates greatly in size depending on physiological changes (e.g. nasal cycle, body temperature, posture and exercise) and response to inflammation. To date there has been little investigation of the normal intra-individual variations in nasal anatomy due to congestion and decongestion. These changes could lead to alterations in the transport of inhaled substances and the processes of heat and water exchange at the nasal mucosal surface. The nasal anatomy varies in a time dependent manner in around 40% of the population[36,248]. This 'nasal cycle' results in alternating patent and congested passages for periods ranging from 1 to 7 hours [249]. The nasal cycle usually goes unnoticed since the total nasal airflow resistance remains unaffected[2,250]. There is currently little available data to detail the anatomical changes during the nasal cycle or with decongestion.

Recent improvements in imaging techniques, such as computed axial tomography (CT) and magnetic resonance imaging (MRI), have enabled the capture of accurate in vivo nasal geometric information, which goes beyond that previously obtained by acoustic rhinometry (AR) and cadaveric dissection (which is complicated by the drying out and loss of tissue volume in specimens). Earlier investigations comparing CT and AR cross-sectional data show a good correlation between measurements within the relatively open anterior spaces of the nose[120,251]. However, AR tends to overestimate cross-sectional area (CSA) beyond the complex and sometimes obstructed turbinate region[121]. Post-processing of CT or MRI data also provides additional morphological information unavailable through AR techniques, such as airway perimeter and total airway volume. MRI scans have previously been used for assessing nasal morphology[93,97], with the advantage of MRI being that there is no associated dose of ionising radiation and hence scans can be repeated. However, many of the MRI studies were performed on early MRI scanners and required long scan times and as a result suffered significant movement artefact. The introduction of 3T MRI into clinical practice has dramatically reduced scanning times. High resolution 3T MRI scans are fast, non-invasive and provide a detailed 3D geometry. The MRI sequence used for the data reported here is a new isotropic three-dimensional (3D) fast spin-echo (FSE) pulse sequence called 3D cube. Recent 3D FSE MRI imaging has proven very efficient in imaging soft tissues in joints such as the knee, ankle and has also been used in imaging the brain[252-254].

For this study, the effect of decongestion on nasal airway dimensions was investigated in seven normal subjects using high resolution 3T MRI scanning. Subject ages ranged from 21-38 years (mean=28). The SNOT-22 scores ranged from 1-7 (mean=3.8). The study protocol is given in appendix and outlined in section 3.3.1 pg 51.

The results are presented in the sections as follows. (4.2) shows sample image slices at three representative locations for two subjects to illustrate the scale of changes observed with decongestion; (4.3) illustrates of the procedure to quantify change in nasal passage cross-sectional area; (4.4) shows mean change in turbinate volume associated with decongestion; (4.5) offers a comparison between 6-slice sample of MR data and AR measurements of mean cross-sectional area (4.6) describes metrics related to exchange function of the nose: SAVR (surface area to volume ratio) and PA (perimeter to area). Finally (4.7) summarises the findings.

4.2 Images of Geometry Changes with Decongestion

Figures 4.2 and 4.3 illustrate the dramatic scale of changes in nasal airway geometry associated with decongestion, in the anterior, mid-turbinate and posterior turbinate zones, as indicated in fig. 4.1.

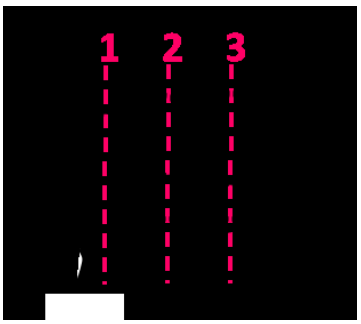

Figure 4.1 Sagittal sections through the nose showing the location of slices.

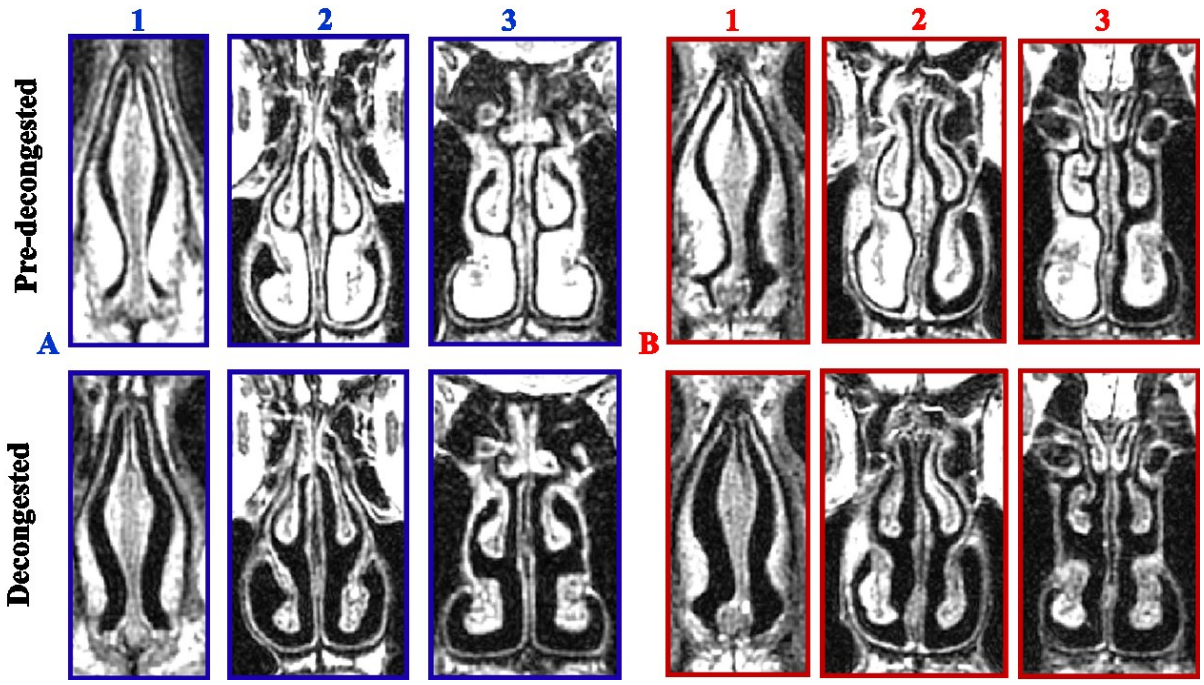

Figure 4.2 MRI images of nasal anatomy pre- (top) and post- (bottom) decongestion, for Subject A left and B right

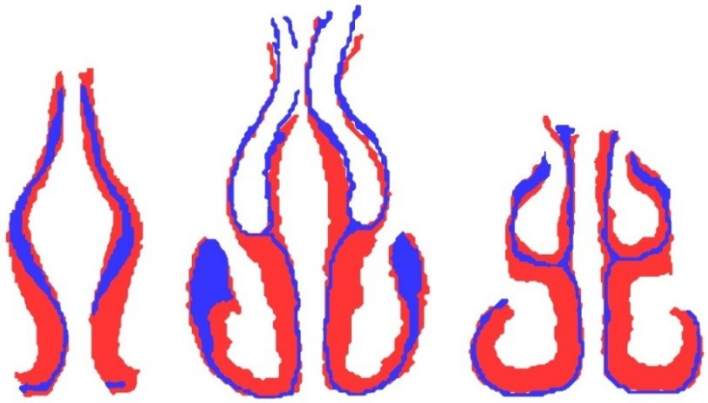

Figure 4.3 Coronal sections through subject A's nose with the pre-decongested and decongested nasal airspace shown in blue and red, respectively

After image registration (using MatLab[255])the segmented airways are overlapped for comparison of the pre- (labelled blue) and post (labelled red) decongestion airway anatomy (figure 4.3). Pronounced shrinkage of the inferior turbinate is evident, the middle turbinate and septum also demonstrate shrinkage with decongestion but to a far lesser extent. The calibre of the inferior part of the nasal cavity is significantly larger following decongestion.

4.3 Quantifying Regional Patterns of Change

A series of six coronal slices at 15mm spacing through the nasal anatomy, from nares to nasopharynx, were examined for comparison (Figure 4.4). Slice 1 is just anterior to the head of the inferior turbinate, slice 2 in through the anterior part of the inferior turbinate, slice 3 in through the anterior part of the middle turbinate, slice 4 posterior end of the middle turbinate, slice 5 posterior end of the inferior turbinate and slice 6 the nasopharynx. Cross sectional areas calculated using the CAD package Rhino from the 2D segmentations which automatically calculates area within a defined boundary. The maximum change in cross sectional area was seen in the turbinate region slices 2-4 figure 4.4. The areas least effected by decongestion were the region of the nasal vestibule slice 1 and the nasopharynx slice 6.

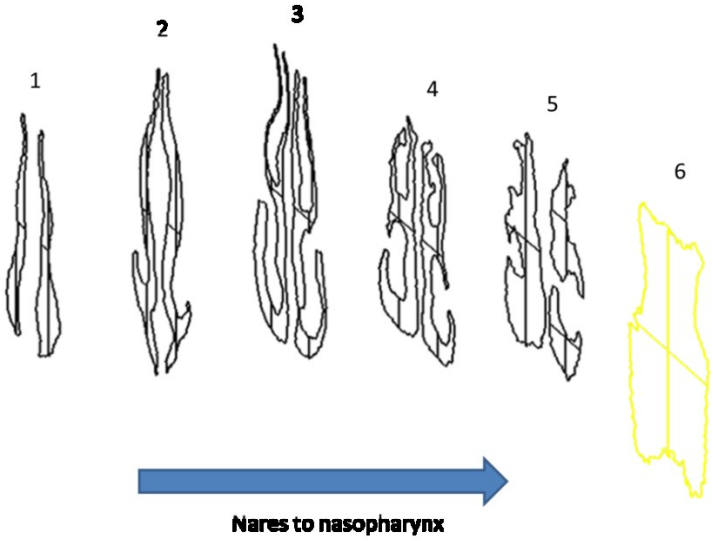

Figure 4.4 6 representative slices through the nasal anatomy for comparison from just anterior to the head of the inferior tubinate to the nasaopharynx. The slice spacing is 15mm.

Cross sectional area in mm^2						
	Congested		Decongested		% Area Change	
#Slice	Right	Left	Right	Left	Right	Left
1	84.4 (+/-2%)	79.3 (+/-1%)	128.6 (+/-4%)	89.4 (+/-3%)	52.5	12.8
2	36.3 (+/-4%)	92.2 (+/-1%)	170.8 (+/-2%)	131.7 (+/-1%)	370.2	42.8
3	52.8 (+/-6%)	128.8 (+/-4%)	177.6 (+/-1%)	184 (+/-1%)	236	42.9
4	35.1 (+/-7%)	144.1 (+/-5%)	166 (+/-2%)	197.2 (+/-2%)	372.8	36.9
5	288.4 (+/-3%)		469.6 (+/-4%)		62.8	
6	856.7 (+/-1%)		871.3 (+/-2%)		1.7	

Table 4.1 Cross sectional area at each of the 6 slices in subject B. A much larger change in area is demonstrated on the right side however when the MRI scans are studied (figure 4.2) it can be seen that the left nostril was in a decongested state prior to the application of the nasal decongestant.

The narrowest point of the nasal passage determines the nasal resistance to airflow and this area is referred to as the ‘‘nasal valve’’ [256]. The anatomical and physiological evidence indicates that the nasal valve occurs at the entrance of the piriform aperture. The nasal valve region, formed by the junction of the upper lateral cartilages, the nasal septum and the inferior turbinate, is typically the narrowest point in the nasal cavity and accounts for up to 50% of total airway resistance in quiet breathing conditions[2]. The nasal valve is not a fixed anatomical constriction of the airway but a dynamic valve. The nasal airway resistance is determined by swelling and constriction of the venous sinuses of the inferior turbinate and nasal septum which can cause complete obstruction of the nasal passage[37,257]. Haight and Cole (1983)[258] found that the anterior end of the turbinate could advance by as much as 5 mm after application of histamine. In subject B described above, the minimal cross sectional area on the right side moves anteriorly from slice 2 in the normal congested state to slice 1 in the decongested state due to decongestion of the engorged right inferior turbinate which was obstructing the airway.

4.4 Turbinate volume changes with decongestion

Turbinate volume changes were investigated in collaboration with Raul Cetto PhD student, Imperial College London. To determine the changes in turbinate volume, the MR images were first resampled to reduce the size of each individual pixel, reducing the size of the stepped finishes in the original image of 512 x 512 and producing a better quality image of double the resolution 1024 x 1024. Resampling is a common operation in all signal and image processing applications. Methods available vary in their computational complexity, speed, and quality[259].

Following resampling, image registration between the pre- and post-decongestion images was performed using non-rigid registration algorithms[260,261]. The registration aligns structures such as bone and septum from both scans so one can focus on the soft tissues inside of the nasal cavity of each patient. After going through the process of resampling and non-rigid registration, the nasal geometries were segmented as described in section 3.3.3. The resulting segmentations were then analysed using MATLAB, providing numerical data allowing us to map changes within the nasal cavity including the airway, the inferior turbinate, middle turbinate and the septum.

Decongestion had the greatest effect in three sites: the inferior turbinate, middle turbinate and the septum. Figures 4.5 and 4.6 demonstrate the mean volume changes of erectile tissue in the inferior and middle turbinates for all 7 subjects[262]. The greatest change in erectile tissue volume (ETV) was observed in the inferior turbinate (p value<0.005). Figure 4.4 illustrates the dramatic volume change in the inferior turbinate with decongestion and figure 4.5 demonstrates the much smaller change in the middle turbinate. Changes were also seen in the septal mucosa but to a much lesser extent.

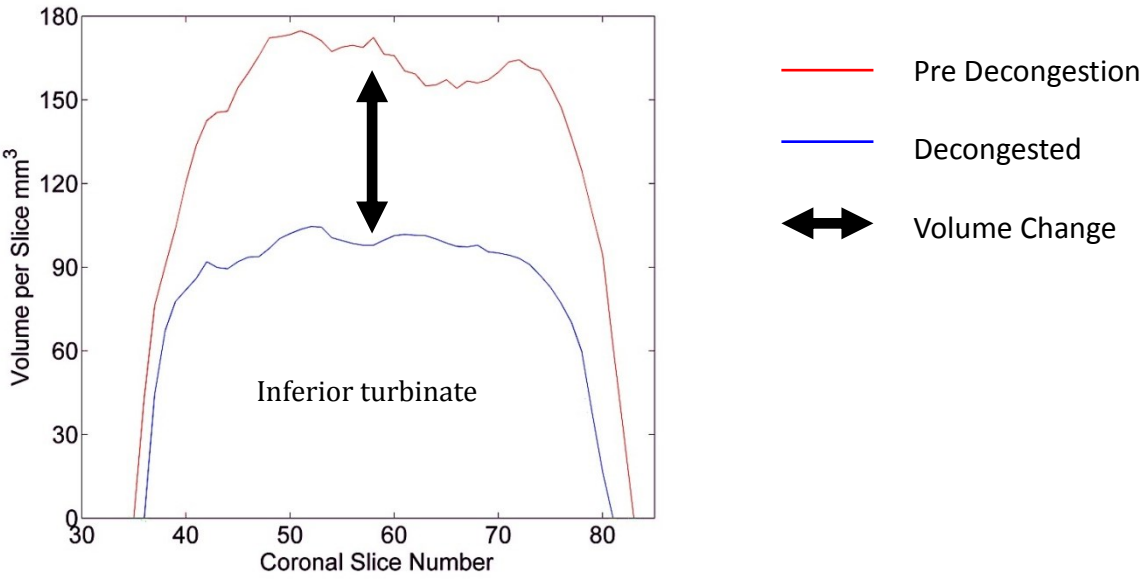

Figure 4.5 Mean volume changes of erectile tissue in inferior turbinate for all seven subjects. The red line represents the volume per coronal slice from anterior to posterior found in the pre decongested nose. And the blue line represents the corresponding coronal section following decongestion. The space between the two lines represents the mean volume change found.[262]

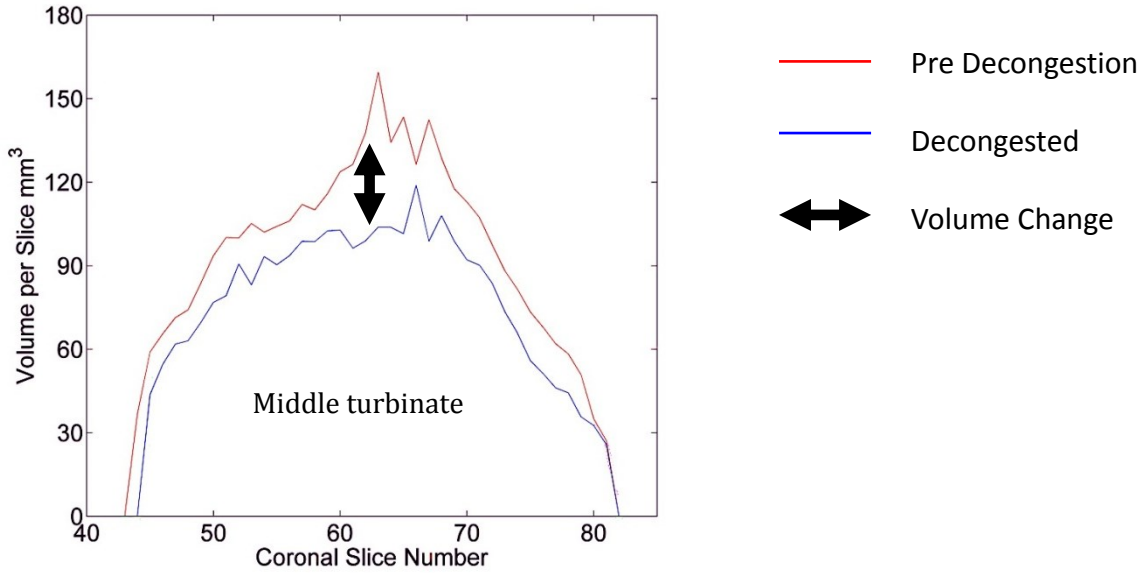

Figure 4.6 Mean volume changes of erectile tissue in middle turbinate for all seven subjects. The red line represents the volume per coronal slice from anterior to posterior found in the pre decongested nose. The blue line represents the corresponding coronal section following decongestion. The space between the two lines represents the mean volume change found.[262]

Acoustic rhinometry was performed pre and post decongestion for comparison with the MRI imaging.

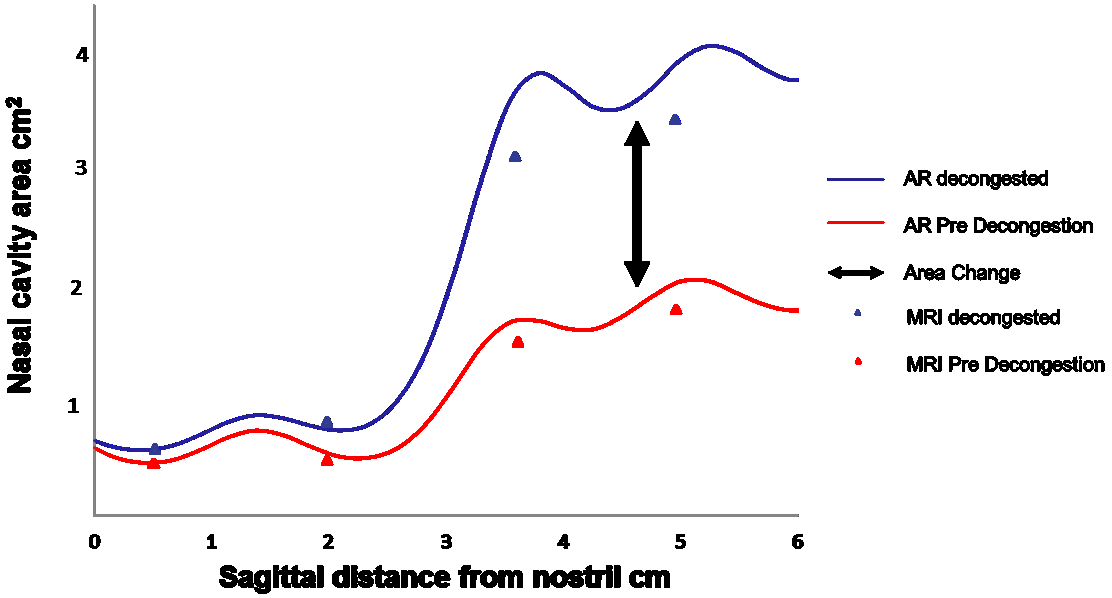

Figure 4.7 Comparison of the mean acoustic rhinometric data and MRI data. The red line is the cross sectional area before decongestion and the blue line is following decongestion. The red triangles are the MRI cross sectional area prior to decongestion and blue post decongestion. The distance between the red and blue line represents the change in area.

The mean acoustic rhinometry and MRI data of all seven patients is represented in the figure 4.7. There is good agreement between the data particularly anteriorly. The differences from 2-6 cm could be accounted for by the difference between the acoustic path and a straight line from nares to nasopharynx. The acoustic path through the nose is curvilinear and not perpendicular to the MRI coronal slices through the nose which have been measured. Terheyden *et al.* (2000)[122] found that it was problematic to correlate area-distance curves derived from other methods with those derived by AR, unless the individual sound path and the individual measuring planes were known. The acoustic rhinometry measuring planes follow the individual propagation of the sound waves on a curved line through the nasal cavity. Hence when comparing the area-distance curve determined by AR with real distances in the nose on a straight line from the nosepiece to the pharynx AR appears to overestimate areas towards the back of the nasal cavity.

4.5 Geometric Measures Related to Exchange: SAVR & PA

Previous studies have found surface area to volume ratio (SAVR) to be a useful measure of nasal patency. Patients with atrophic rhinitis have been shown to have very low SAVR's compared to healthy individuals [3]. The aim in surgery for atrophic rhinitis is to restore the original surface area in order to minimise the water flux per unit area. Calculating the surface area to volume ratio is a time consuming laborious process as it requires segmentation of the entire nasal airway with significant user intervention. However, if a quick approximation was possible this could provide a useful clinical measure. Yokley (2009)[263] in his anthropological study looking the CT scans of 49 patients found that the perimeter to cross sectional area ratio (P/A) of a coronal section just beyond the head of the middle turbinate provided a good approximation of the SAVR. The surface area to volume ratio and perimeter to area ratios for subjects A and B pre and post decongestion are compared in Table 4.2.

	Pre-decongested SAVR (P/A)		Decongested SAVR (P/A)	
	Left	Right	Left	Right
A	1.16 (2.76)	1.65 (2.51)	0.89 (1.10)	1.00 (1.07)
B	1.32 (1.65)	2.15 (4.24)	0.88 (1.09)	0.92 (0.97)

Table 4.2 Comparison of the surface area to volume ratio (SAVR) and perimeter to cross sectional area ratio (P/A) just posterior to head of the middle turbinate pre and post decongestion in Subjects A and B (previously described in Figure 4.2).

Surface area to volume ratios are significantly decreased with decongestion. In the decongested (non physiological) state the perimeter to cross sectional area ratio approximates well to the SAVR. However, in the pre decongested (normal physiological) state this is not the case. The difference between these findings and those of Yokley (2009)[263] could be accounted for by the small sample size in this pilot study.

4.6 Discussion

The effect of decongestion on ETV has been investigated here in-vivo in far greater detail than previously studied, and at higher spatial resolution. High resolution 3T-MRI was found to be an excellent modality as it provides a detailed 3D-geometry ideal for mapping changes in nasal mucosa.

Following analysis of the images from a number of MRI sequences on healthy volunteers a sequence known as a "Cube" sequence was selected for this study. Conventional MR imaging has typically provided discrete slices in one plane only. This requires repeating the acquisition for every additional plane or evaluating images without the benefit of data provided from different angles. However, the Cube sequence replaces several slice-by-slice, plane-after-plane 2D acquisitions with a single 3D volume scan. The scan time is short hence minimising movement artefact and the high definition, high contrast images with a slice thickness of only 1.2mm, permit detailed segmentation work. Therefore the Cube sequence provided the best sequence option for this study.

The sequence used proved to be efficient in mapping changes within the nasal mucosa using a fast spin Echo to provide contrast and does not rely on the much lower soft tissue contrast produced by gradient Echo sequences which can also carry out isotropic 3-D volumes. This sequence allows data to be obtained in a single scan plane but the data can then be reconstructed into multiple other planes because of the isotropic nature of the Voxel acquisition. The sequence has been employed in a variety of areas to provide fine detail in a single sequence which can then be manipulated into multiple planes[264].

These results demonstrate the significant effect of decongestion on ETV, with the greatest result seen in the inferior turbinate. Decongestion was found to have a significant impact on surface area to volume ratio. Variations in SAVR have implications for the transport of inhaled substances and the processes of heat and water exchange at the nasal mucosal surface. Further work using this MRI sequence will enable mapping of the normal nasal cycle and could be used to study the response to allergen challenges as well as detailing post surgical changes and the healing process.

Chapter 5

Characterising nasal inspiratory flow patterns

5.1 Introduction

Air flow through the nose is cyclic, though with significant breath to breath variability. This in turn leads to variability in function (olfaction, heat and water exchange) and the mechanics of absorption or deposition of inhaled species. However the modelling of nasal airflow to date has ignored inter- and intra-breath flow variability; indeed as the mean time required for inspired air to transit the nasal airways is relatively small compared to the course of a single breath, the flow is often assumed quasi-steady. This chapter presents the results of an investigation of the time-varying flow rate during inspiration at rest, in smelling and in sniffing, both pre- and post-decongestion. It aims to provide a better understanding of nasal airflow mechanics, both to improve the physiological modelling of respiratory airflow and for potential applications such as the delivery of aerosolized therapeutic drugs and to improve clinical knowledge.

Although breathing is generally treated as a rhythmic process, the variability in cycle-by-cycle measurements of respiratory period and breath amplitude is, in fact, considerable in healthy adults, where no two breaths are identical. It is scarcely possible to attempt to quantify every possible breath, given that the extent of conscious control is large, particularly in comparison with the cardiac cycle. For this investigation, subjects were guided by metronome in order to establish some form of rhythmic breathing, in a restful state. This permits investigation of flow characteristics in a mode that should be common to the cohort of subjects, as well as enabling the inherent degree of variability that exists within a particular regime to be examined

The temporal profile of inspiration through each nostril during normal breathing, sniffing and smelling (in 14 healthy subjects) was measured using high speed simultaneous bilateral sampling of hot wires mounted in the centre of short tubes connected to each nostril.

This enabled many features to be determined, including the rapidity of flow establishment during inspiration, the time course of inspiration, the degree of bias between the flow in the left and right passages, the range of peak amplitude and the constancy of flow during inspiration. Moreover all the above could be compared pre- and post-decongestion. Averaging and normalisation of the measurements allowed comparison of mean inspiratory profiles for the various conditions. The results reveal significant and distinct unsteady dynamic attributes of the various modes of inspiration, as will be described.

5.2 Processing methodology for Hot-wire measurements

At low flow velocities the hot-wire technique can be unreliable due to natural convection effects becoming significant. Therefore, the data acquired at the start and end of each inspiration were truncated below a voltage corresponding to a flow rate in the 10 cm diameter tubes attached to the nostrils of approximately 55 $ml.s^{-1}$. A data fitting procedure was applied to reconstruct the initial portion of the profile (where flow rate rapidly increases) and the terminating portion of inspiration (where flow rate decays). The steps of this process are illustrated in figure 5.1, where a least squares fit approach was applied to extrapolate for both the initial and terminating phases. The intervals over which fitting was applied were defined respectively as: a) the data between the truncation location at the start of inspiration and a point at ⅔ of the initial maximum flow rate, Q_{max1} (determined as the first peak in flow rate); and b) the data between one third of the maximum flow rate (⅓ Q_{max1}) attained in the particular inspiration and the end truncation point.

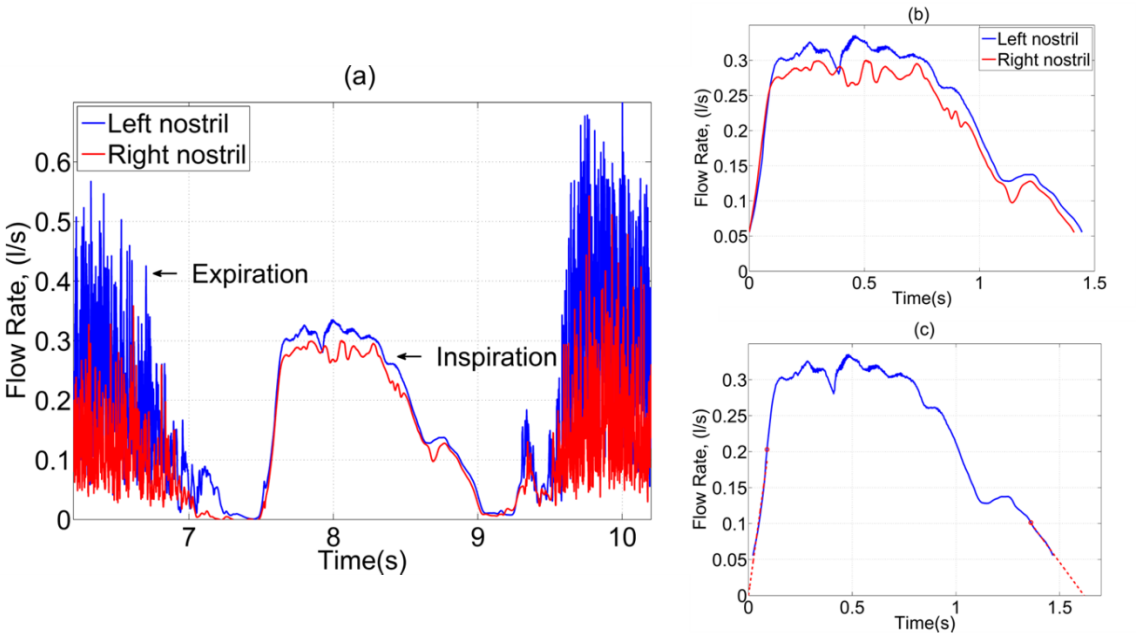

Figure 5.1 Left: A typical measurement of inspiration at rest for the right and left nostril. The flow in expiration is highly disturbed, and therefore was not considered further at present. The truncation process is illustrated (upper-right) along with the corresponding reconstruction of the initial and terminating portions of inspiration (dashed lines – lower-right).

To analyse the temporal profile, each inspiration was divided into its three constituent phases, namely:

1) flow initiation – where the flow rate rapidly increases;

2) a 'plateau' region – where a high flow rate is sustained; and

3) flow decay – where inspiratory flow rate decreases up to the end of inspiration, as shown in figure 5.2 (a).

The portion of the inspiration in which flow is above the mean is taken as defining the plateau phase; the corresponding plateau flow rate is the average flow over this phase. Given the variability of breathing profiles, care must be exercised when fitting data. This is illustrated in figure 5.2 where three measured profiles are compared, yielding respectively a good overall fit (a), a poor fit to the initial (b) and a poor fit to the terminating (c) phases.

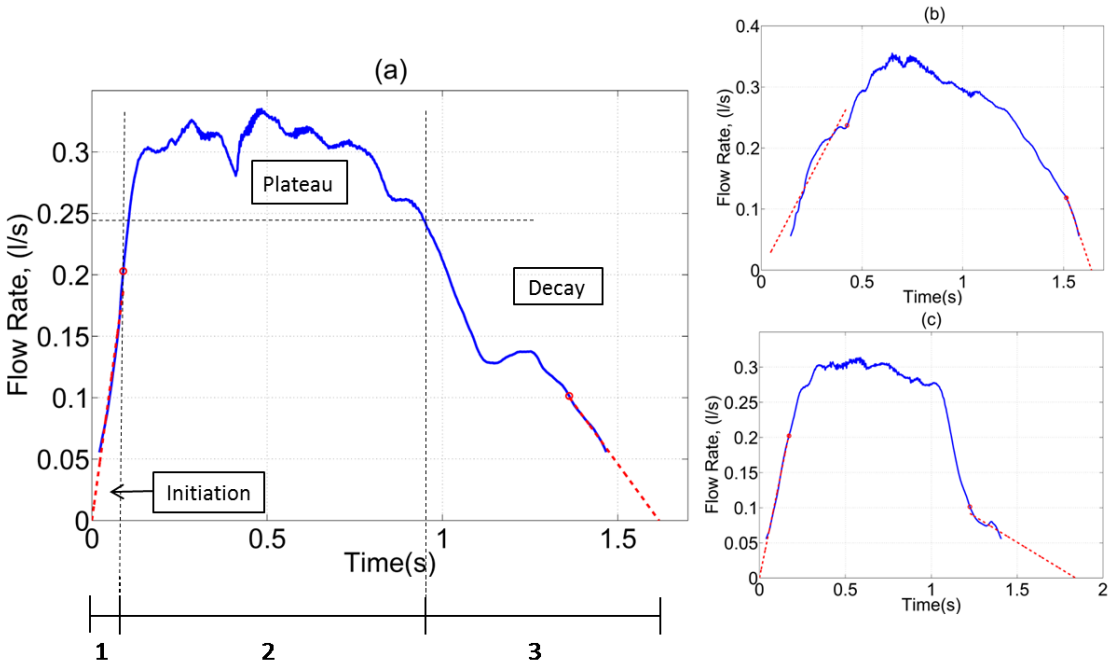

Figure 5.2 A typical inspiration at rest is shown for a good fit at both the initiation and termination of the inspiratory profile. The three phases of inspiration are indicated: 1) initiation; 2) plateau and 3) decay. An example of a poor fit for the initial and terminating portions of the profile are shown (upper-right and lower-right, respectively).

In order to test whether the above fitting process exerted any bias, a comparison was performed of the time taken for the flow rate to increase from 55 to 150 ml.s^{-1} by the above procedure namely:

(a) deriving the interval from a linear fit applied to the corresponding inspiratory profiles, with a simple measure,

(b) subtraction of the times at which flow first attained these values in each inspiration.

The results are shown in figure 5.3. For inspiration at rest the slope of the linear regression line for the data (solid line) was determined to be 1.001 (with 95% confidence bounds of 0.983 and 1.020) indicating that there are no artifactual effects or significant bias in the determined rise-times introduced by the fitting process. Similarly, for the sniffing measurements, a slope of 1.268 (with 95% confidence bounds of 1.161 and 1.375) indicates that fitting may result in a bias of the rise-time estimate of ~25%. Overall, the fitting procedure is preferred as it prevents experimental noise from introducing unfeasibly low values for rise-times. The plots indicate that some of the outliers represent points where the data may have been too poor to provide a good fit.

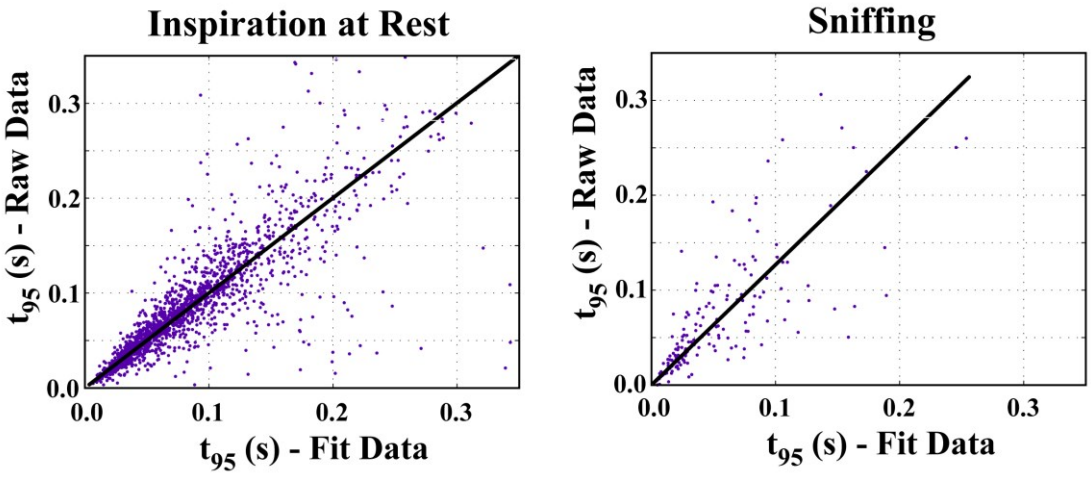

Figure 5.3 The correlation between the raw and fitted data is shown for time taken for flow rate to increase from 55ml.s^{-1} to 150ml.s^{-1}. The time determined from the raw data is plotted against that obtained by the least squares fit, together with the respective linear regression line, during inspiration at rest and sniffing, shown left and right, respectively.

To investigate the reliability of the fitting process, and to provide a criterion to exclude poor data, the error in the fitting process (R^2, i.e., coefficient of determination) and the additional time added as a result of the fitting (Δt) were analysed. A scatter plot of these variables, shown in figure 5.4, illustrates a clustering of points (representing ~2,000 individual measurements) at the top-left of each plot for fits to the initial phase (left) and terminating phase (right). The dashed-line boxes delineate the data points which were deemed reliable and, hence, were included for further analysis. This included 97% of the original measurement data for the initiation phase and 98% for the decay phase.

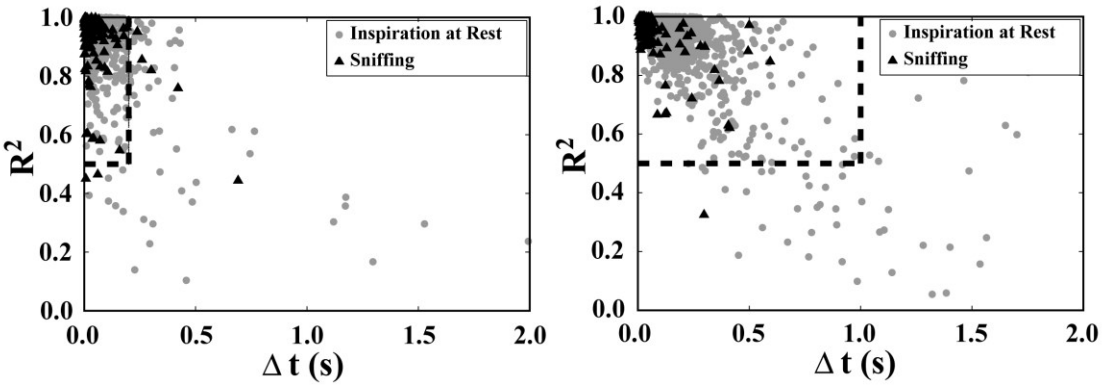

Figure 5.4 The error in the fitting process (R^2 - coefficient of determination) was determined for each inspiration and is plotted against the additional time added as a result of the fitting process, for the initiation (left) and termination (right) portions of inspiration. Inspirations at rest are shown as grey circular symbols and sniffs as black triangles. Data points outside the dashed lines have not been considered in further analysis.

To eliminate concerns that the pipes and their connection to the nose might affect the measured inspiratory profiles, measurements were made with and without (figure 5.5) the pipe in position. As demonstrated in figure 5.6 no discernible difference was seen in the characteristics of typical flow profile whilst breathing at rest or sniffing, whilst naturally the amplitude of the measured velocity is much reduced when the flow is not constrained to enter and exit via a tube. The unsteadiness of the expiratory flow is also demonstrated in both cases. It would be of interest to fully explore the flow field without the use of a tube attachment, but in order to derive a measurement of instantaneous flow, this would require simultaneous velocity sampling at multiple locations, which is not currently practical.

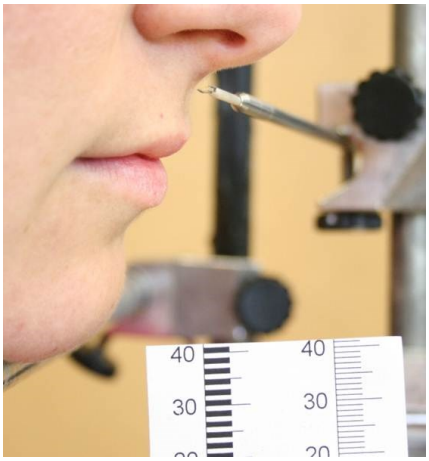

Figure 5.5 Experimental set up without the pipe attachments**.** (See figure 3.7 for comparison)

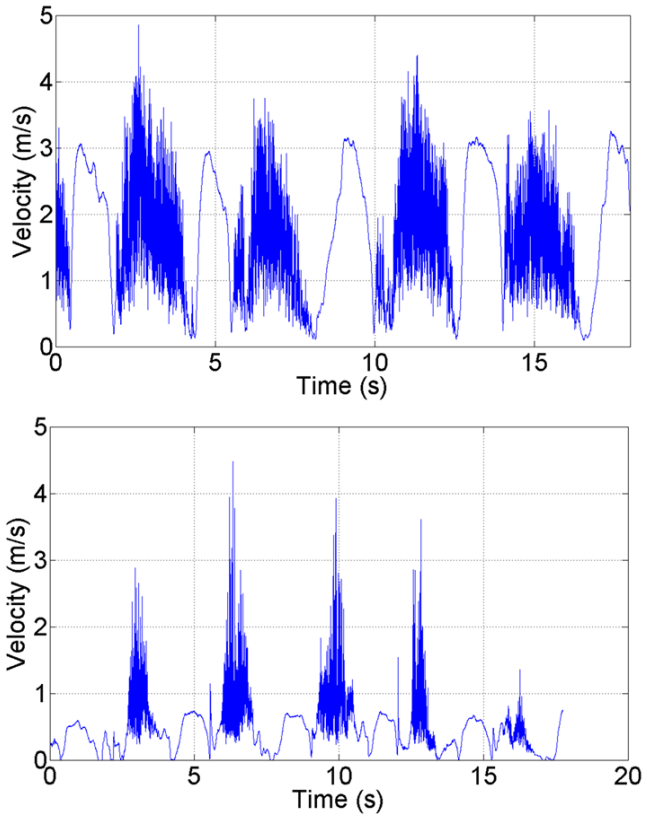

Figure 5.6 Comparison of the inspiratory profiles of a single subject with (top) and without (bottom) the pipe. The measured inspiratory profile has a much greater velocity within the pipe, as it corresponds to a midline peak velocity, whereas without the pipe it corresponds to a single point in the flow field close to the nose so does not capture the same inspiratory flow.

The Poiseuille pressure drop through the pipe was calculated to determine if the increased resistance could significantly impact the subject's inspiration.

$$\Delta P = \frac{8\mu LQ}{\pi R^4}$$

Equation 5.1[83]

In the above expression, ΔP is the pressure drop, μ is the dynamic viscosity of air, (taken to be 17.9 x 10^{-6} kg/m.s), L is the length of the pipe, Q is the volume flow rate and R is the radius. At a flow rate of 200 ml/s consistent with breathing at rest the pressure drop is 0.23 Pascals and at 1000 ml/s more consistent with sniffing the pressure drop is 1.46 Pascals. A typical ΔP for quiet inspiratory breathing is of the order of 8 Pascals in experimental and CFD models, according to Taylor *et al.* 2010 and Croce *et al.* 2006. In vivo measurements with rhinomanometry suggest values of order 20 Pa. Therefore the contribution of the pipe to transnasal resistance is minimal and is likely to have had negligible impact on the mechanics of inspiration.

Many experiments dealing with respiratory flow have been confounded by the fact that the breathing pattern of subjects changes once instructed to breathe and they become aware of what is generally an unconscious act[265-267]. Western and Pack [268] found that focusing attention on breathing resulted in an increase in the inspiratory and expiratory times by 0.4 seconds on average, and also an increase in tidal volume by an average of 75 mL. Experiments applying face masks to patients have found that with the mask on, subjects tend to increase their breathing rate and minute volume[266,267,269-271]. These changes in ventilation have been attributed to: 1) the influence of the additional dead space; 2) stimulation of the nasal and oral mucosa by the nose clip and mouthpiece; 3) shift of respiratory route from unrestricted nose to mouth; 4) focusing a subject's attention on their breathing may influence ventilation.

The use of any recording technique, even a non-invasive one can modify the spontaneous breathing pattern as the subject is aware that their breathing is being recorded [265]. To determine the degree of influence imposed by these experiments on the subjects breathing, the minute volumes for all subjects was compared with typical literature values. The data obtained in these tests correspond to an average minute volume of 11.1 L/min with standard deviation of 2.12 L/min. This would indicate an elevated breathing rate, but not hyperventilation, and lies within typical values in the literature. McGregor[272] reported typical minute volumes of 8.0 +/- 1.27, Baydur [273] reported 10.11 +/-2.69 L/min and Burki[274] obtained values of 8.4+/- 1.3 L/min. McGregor[272] further demonstrated that the ventilatory volume in the sitting position both during rest and exercise was significantly higher than recumbent. At rest the minute volume was found to be 8.0 L/min when recumbent and 9.27 L/min when sitting, during exercise the minute volume was 25.07 L/min when recumbent and 35.23 L/min when sitting. Since the subjects in this experiment were all sitting this could account for the elevated minute volume found.

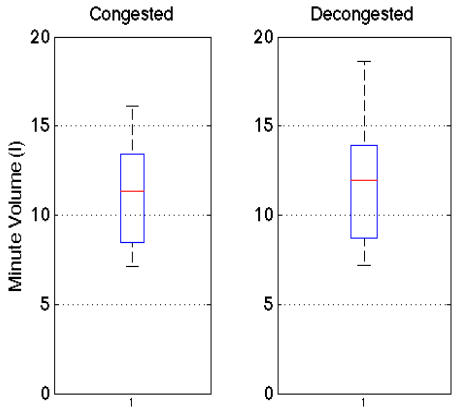

Figure 5.7 Boxplot of minute volumes showing no significant difference between the congested and decongested states.

5.3 Measures to describe the temporal profile of inspiration

The time-dependent profiles of inspiration have been compared over three phases identified in figure 5.2: 1) flow initiation – represented by an initial rapid increase in flow rate; 2) plateau region – represented by a nominally constant flow rate during the mid-portion of the inspiration; and 3) the period – the total time of inspiration. Results are compared pre- and post-decongestion.

5.3.1 Rise times

The rapid initiation of flow was characterised using the time for the inspiratory flow rate to rise to 150ml.s^{-1}, (T_{150}) as shown in figure 5.8.

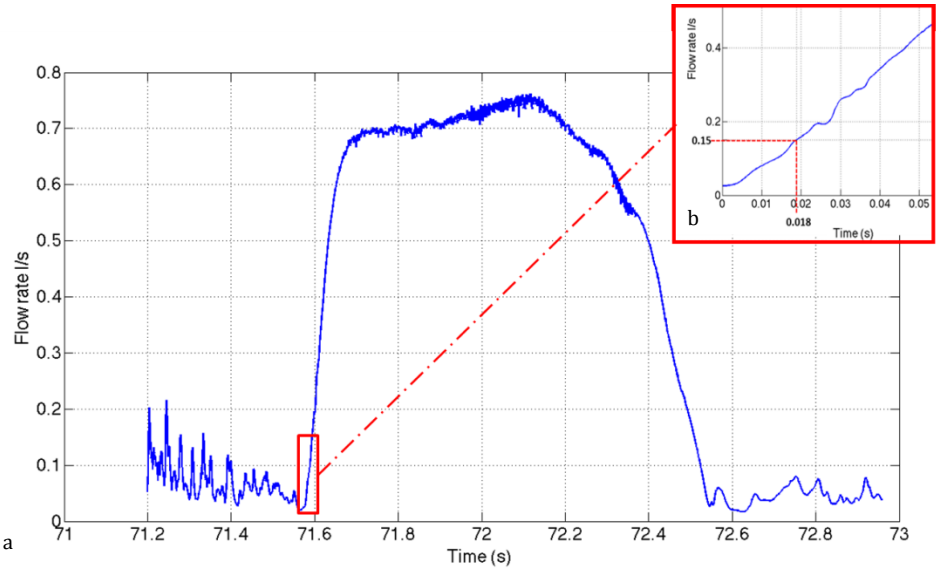

Figure 5.8a Rapid rise times in a single subject's sniff b Detail of extremely rapid sniff

Mean T_{150} rise-times of 129 ms and 136 ms were found in inspiration at rest for the right and left nostrils, respectively, in the pre-decongested state. Sniffing was found to reduce equivalent mean rise-times to 85 ms and 105 ms, respectively, (Fig 5.9), whilst the fastest sniffs showed a T_{150} of only 20 ms (Fig 5.8). These results were not significantly affected by decongestion, either in inspiration at rest or sniffing (Mann Whitney U test, $p < 0.05$). However, there was a significant difference in the rise-time when comparing inspiration at rest to sniffing, both pre- and post-decongestion. To check the finding that overall the results did not show a significant change with decongestion, the paired data for each individual's fastest rise-times before and

after decongestion were compared. However, no significant differences were found. The smelling of both ammonia and lemon showed a trend towards slower rise times than inspiration at rest but this was not significant.

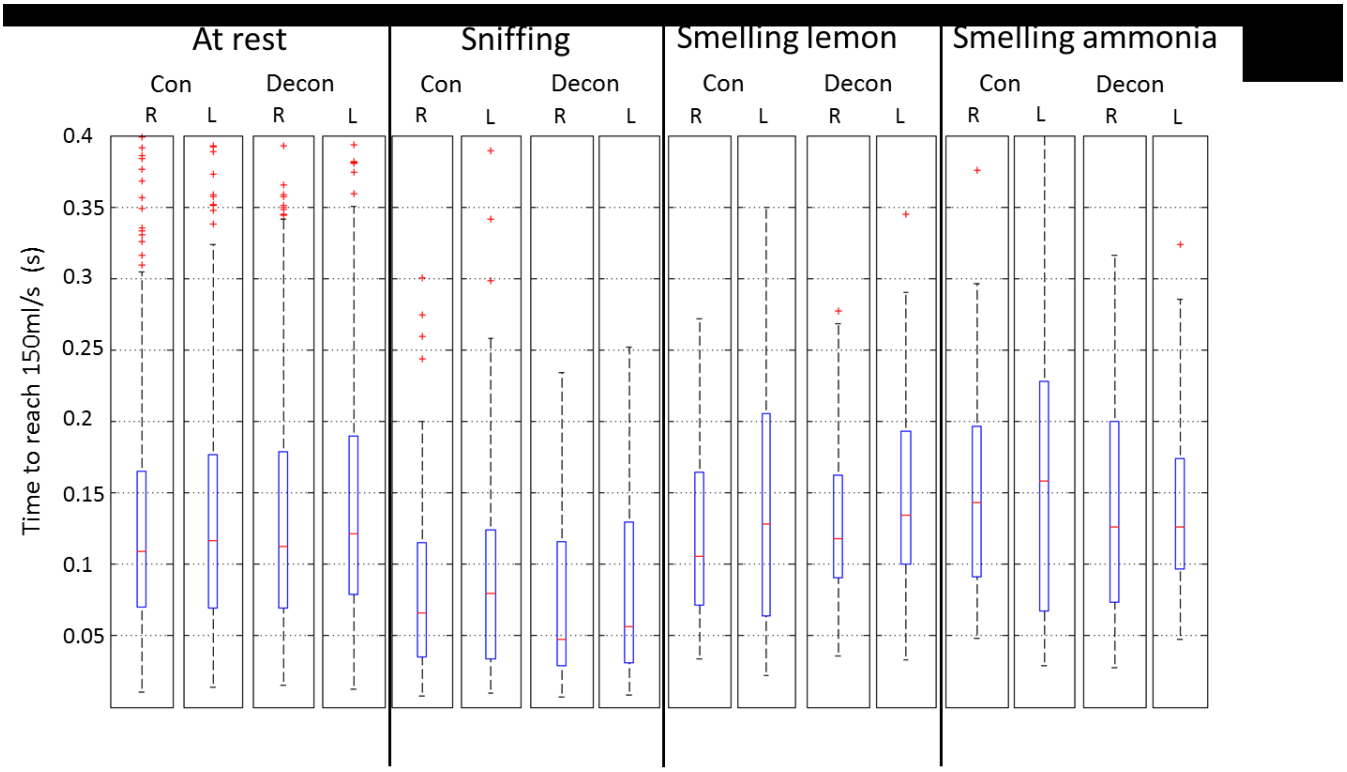

Figure 5.9 The time taken for flow rate to reach 150ml.s^{-1} (t_{150}) is depicted using boxplots, where the median is represented with a thick horizontal line. The whiskers extend to 1.5 times the inter-quartile range (represented by a box) and data points outside this (outliers) are depicted using crosses.

5.3.2 Magnitude of established flow

In the plateau phase, there was a significant difference (Mann Whitney U test, $p < 0.05$) between the flow rate for normal inspiration (median rate ~0.3 L.s^{-1}), compared with sniffing (median ~0.6 L.s^{-1}), as shown in fig. 5.10. Overall, decongestion had no significant effect on this measure. There was no significant difference between smelling lemon and ammonia, or between smelling and normal inspiration.

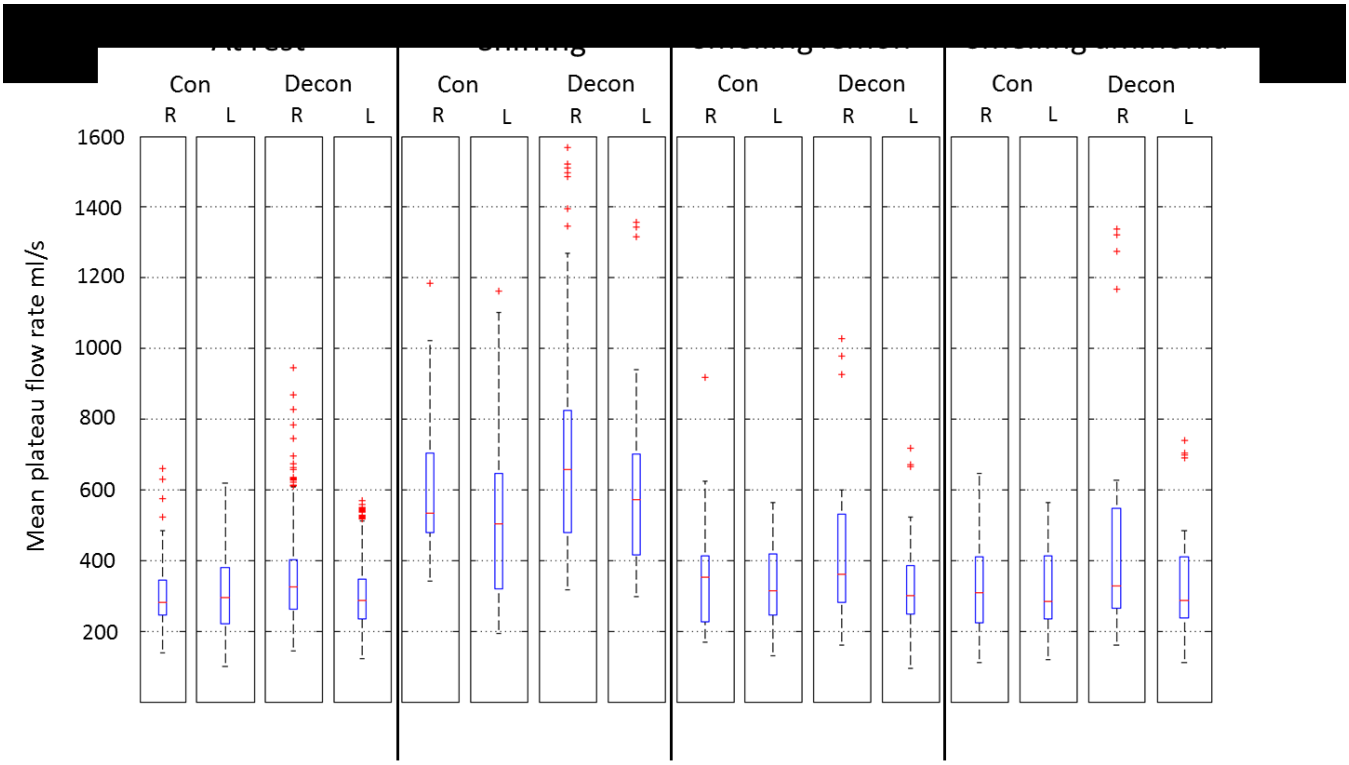

Figure 5.10 The mean plateau flow rate (Q_{MP} – $ml.s^{-1}$), calculated as the mean amplitude in the plateau phase, is depicted using boxplots, where the median is represented with a thick horizontal line. The whiskers extend to 1.5 times the inter-quartile range (represented by a box) and data points outside this (outliers) are depicted using crosses.

5.3.3 Duration

Results for measurements of the period (duration) for inspiration at rest and for sniffing are shown in figure 5.11. The use of the metronome as a guide is expected to have reduced the degree of variability of inspirations at rest and the results are included for completeness. However in spite of the use of the metronome there is still a wide variation in the duration of inspirations and no two inspirations are the same. Sniffing, even though intentional, may be expected to be less responsive to guidance. The results indicated a shorter period associated with sniffing (160ms at rest and 135ms sniffing). In both cases, decongestion did not significantly affect the results. Smelling in contrast had a significantly longer duration than both sniffing and inspiration at rest.

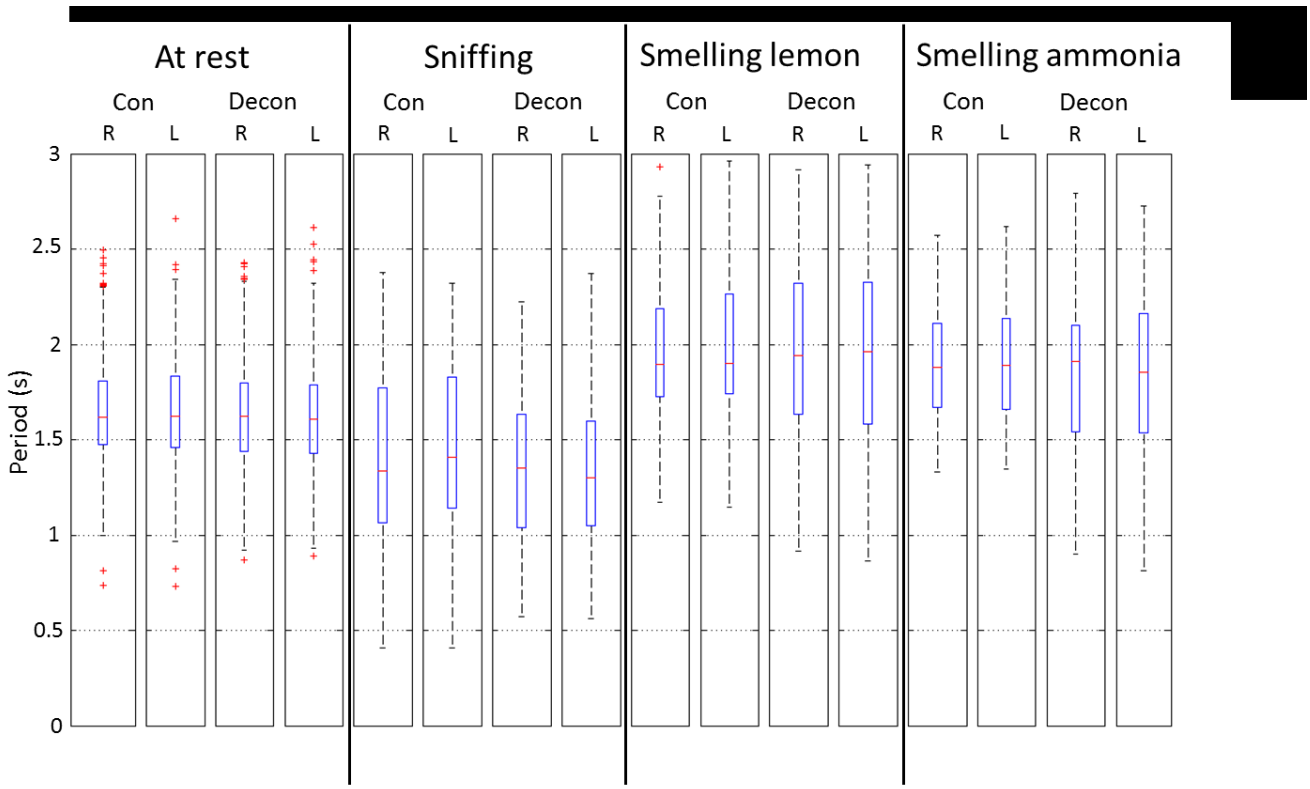

Figure 5.11 The total inspiratory period (T) is depicted using boxplots, where the median is represented with a thick horizontal line. The whiskers extend to 1.5 times the inter-quartile range (represented by a box) and data points outside this (outliers) are depicted using crosses.

5.3.4 Morphological changes on decongestion

The lack of significant changes with decongestion prompted a morphological investigation. The degree of morphological change in nasal anatomy, due to decongestion, was quantified in terms of percentage increase in minimal cross sectional area (MCA) and anterior nasal cavity volume (NCV) using acoustic rhinometry, in order to better understand its lack of significant impact on all of the acquired measures (rise-times, plateau flow rates and inspiratory period).

Measurements of MCA and NCV are shown in figure 5.12, and indicate that decongestion clearly was effective, with results showing a significant increase in nasal volume (Wilcoxon Signed Rank test, $p < 0.05$). However, the increase in minimal cross-sectional area proved less pronounced. Interestingly, despite strong regional variations with decongestion, the MCA does not change significantly, and therefore decongestion might not be expected to reduce nasal resistance significantly. The percentage increase in volume and cross-sectional area between right and left sides proved not to be significant.

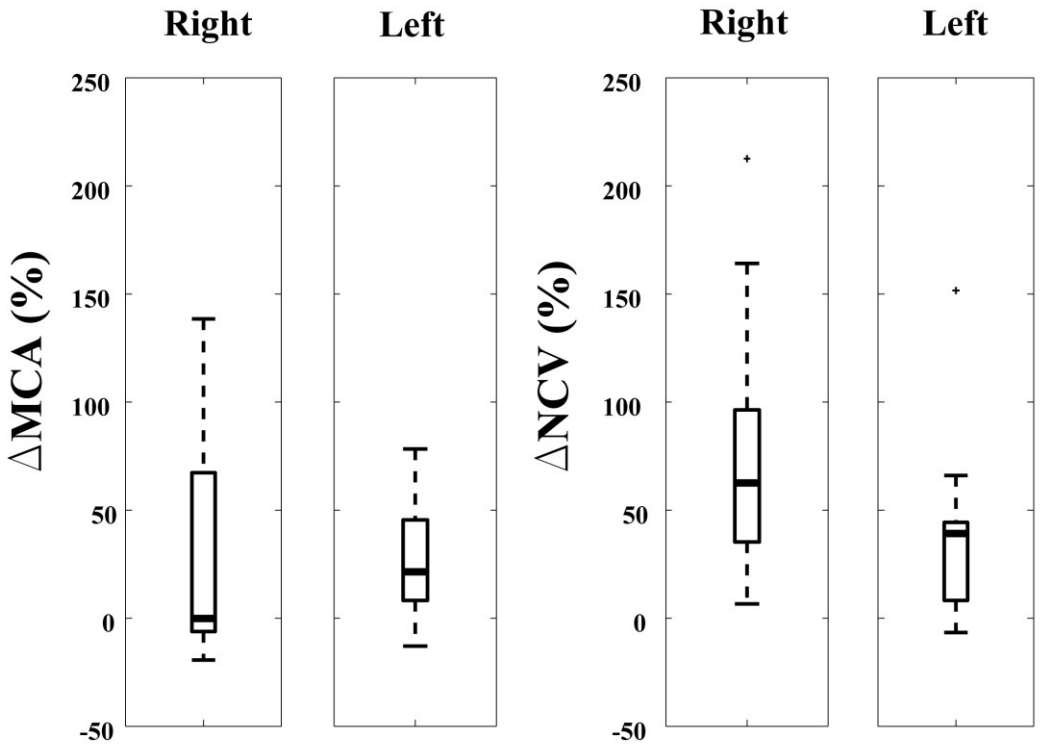

Figure 5.12 The percentage increase in the minimum cross-sectional area (MCA) and nasal cavity volume (NCV) with decongestion are shown to the left and right, respectively. The median levels of the data are represented with a thick horizontal line. The whiskers extend to 1.5 times the inter-quartile range (represented by a box) and data points outside this (outliers) are depicted using crosses.

The limiting effect of nasal resistance, related to congestion, on flow rate should be most pronounced at the highest flow rates. Considering only the maximal plateau flow rate achieved for each individual in a sniff, further processing of the data suggested a weak association between the NCV and sniff maximal plateau flow rate in the pre-decongested state (coefficient of determination 0.34). However, the data did not show a correlation between change in maximal plateau flow rate and increase in either NCV or in MCA resulting from decongestion, even where nasal volume above the median in the pre-decongested state were excluded.

Despite any clear association with the above geometric measures, the sniff maximal plateau flow rate was found to increase with decongestion, (Wilcoxon signed rank test, $p < 0.05$). However although the increase may be statistically significant, the degree of change was found to be slight: the median increase was less than 0.1 $L.s^{-1}$ corresponding to no more than a 10% increase in sniff maximal plateau flow.

By comparison the PNIF measurements showed a 25% mean increase with decongestion. This suggests that PNIF measurements do not necessarily reflect normal or 'non-extreme' sniff inspiratory behavior, which is not unsurprising in a group of normal subjects.

It seems a reasonable conjecture that applying a decongestant should abolish or at least diminish the normal physiological bias of nasal airflow between the nostrils (due to congestion of the turbinates). To test this, the mean plateau flow rate in the dominant nostril, right or left according to the particular subject, was divided by the corresponding flow rate in the non-dominant nostril to derive a measure of inspiratory flow bias, expressed as a simple ratio. The flow bias ratio so defined is compared pre- and post-decongestion for normal breathing and sniffing in Figure 5.13.

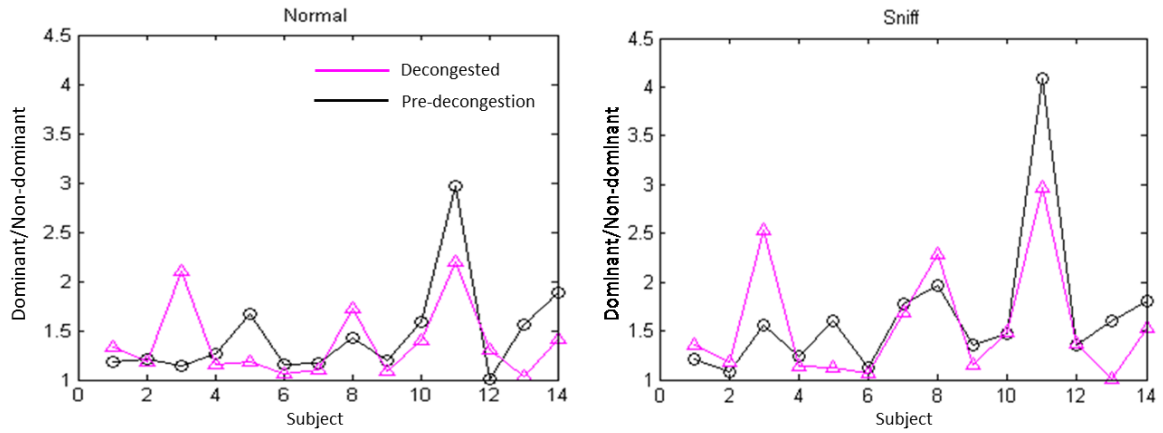

Figure 5.13 The flow bias between the dominant and non-dominant nostrils, pre and post decongestion during normal breathing and sniffing. The mean plateau flow rate in dominant nostril has been divided by the non-dominant nostril for each subject in each instance.

In all but 4 subjects (1,3, 8 and 12) the flow bias approached 1 following decongestion during normal breathing. This suggests that the air flow is more evenly distributed between the nostrils following decongestion. However the data also indicates there are exceptions, as found for subjects 3 and 11. A possible reason is pronounced asymmetry in cavities, which may either remain on decongestion, or could indeed be magnified; for example where decongestion of the inferior turbinate significantly affects the minimum cross-sectional area.

5.4 Determining characteristic profiles for different modes

As outlined earlier, the variability in cycle-by-cycle measurements of respiratory period and breath amplitude is considerable in healthy adults. Here we seek to determine an 'average' inspiratory profile and the degree of breath to breath variability, particularly to aid appropriate modelling of the appropriate flow dynamics.

It is not possible to average the inspiratory traces simply by time, since each inspiration has a different duration as well as amplitude. This is well illustrated for a single subject in Figure 5.14, where a selection of individual right and left inhalations are compared with the average, created as described next. Note also the small bias between left and right nostrils for this subject.

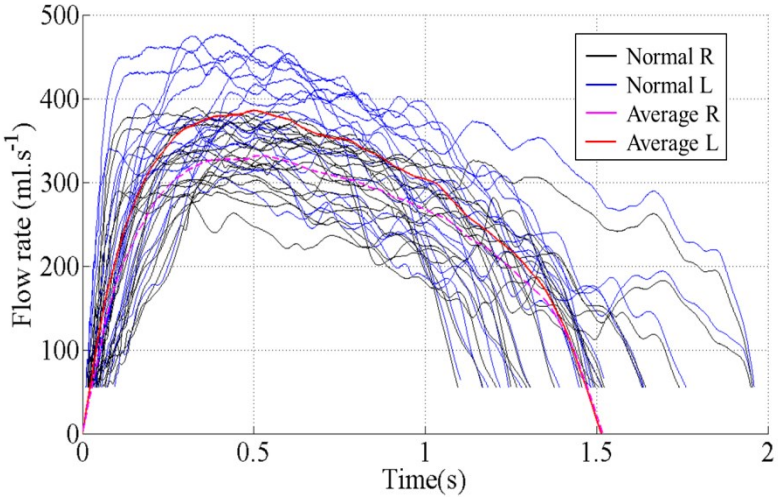

Figure 5.14 Data from 30 normal inhalations of a single subject with the 'average' traces for left and right nostrils superimposed.

Normalisation procedure. For each profile, the period T_1 and mean plateau value A_1 are determined so each trace as plotted consists of a vector of time values and a corresponding vector of amplitude values. The time vector is divided by T_1 and the amplitude vector by A_1; hence the time vector goes between 0 and 1 and the amplitude vector goes between 0 and slightly more than 1, because the peak of the amplitude vector is larger than the mean plateau level. This is then applied to all traces, i.e. every trace is brought to a stencil, of 0 to ~1 in time and in amplitude. Once all traces are normalised the mean trace can be determined. This mean trace is then unnormalised so as to recover real units of time and amplitude. To unnormalise, we find the mean period and mean plateau level of the original data then multiply the mean trace's normalised time and normalised amplitude vectors by these respective means. The resulting trace (in real units) corresponds to an average breath, and is shown superimposed on the normal breaths in figure 5.14.

A comparison of the inspiratory profiles obtained by simple time averaging and normalisation is shown in Figure 5.15. The similarity between the profiles gave increased confidence in the normalisation process. The advantage of normalisation is that the characteristic shape of the inspiratory profile is maintained, whereas simple time averaging flattens the decay phase of inspiration. This is a consequence of the varying period of each inspiration, resulting in the expiratory phase for some profiles contributing to the average during the later part of the decay phase. In turn, the variable breath duration accounts for the progressive deviation between the simple average and normalized mean traces in Figure 5.15.

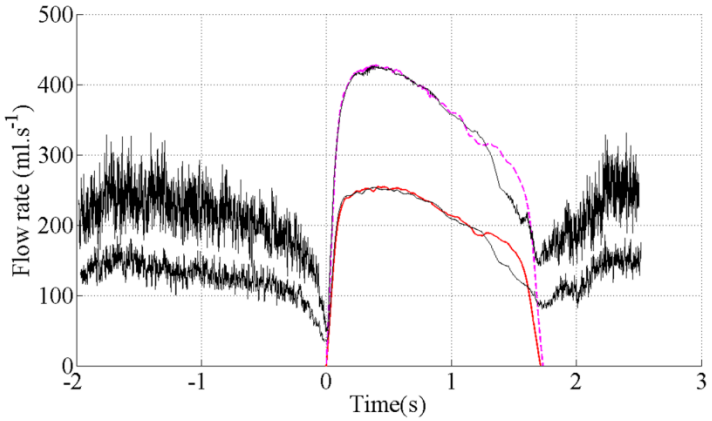

Figure 5.15 Comparison of the inspiratory profiles derived by normalisation (pink and red) and time averaging (black).

The 'average' inspiratory profiles for a single subject, figure 5.16, and across all subjects figure 5.17 may now be compared. It is seen that a normal breath is typified by (i) a rapid ramp to initiate the flow rate, (ii) a plateau phase where a high flow rate is maintained and (iii), a decay phase. The sniff has a similar profile to the normal inspiration but with faster rise times and higher sustained flow rates. The smelling profiles for both lemon and ammonia are observed to be surprisingly similar (subjects were expected to smell the unpleasant ammonia for a much shorter time than the pleasant lemon), the plateau phase is much flatter and longer than a normal inspiration or sniff, and appears to oscillate, which could be important in the mixing of odorants and their transport to the olfactory cleft.

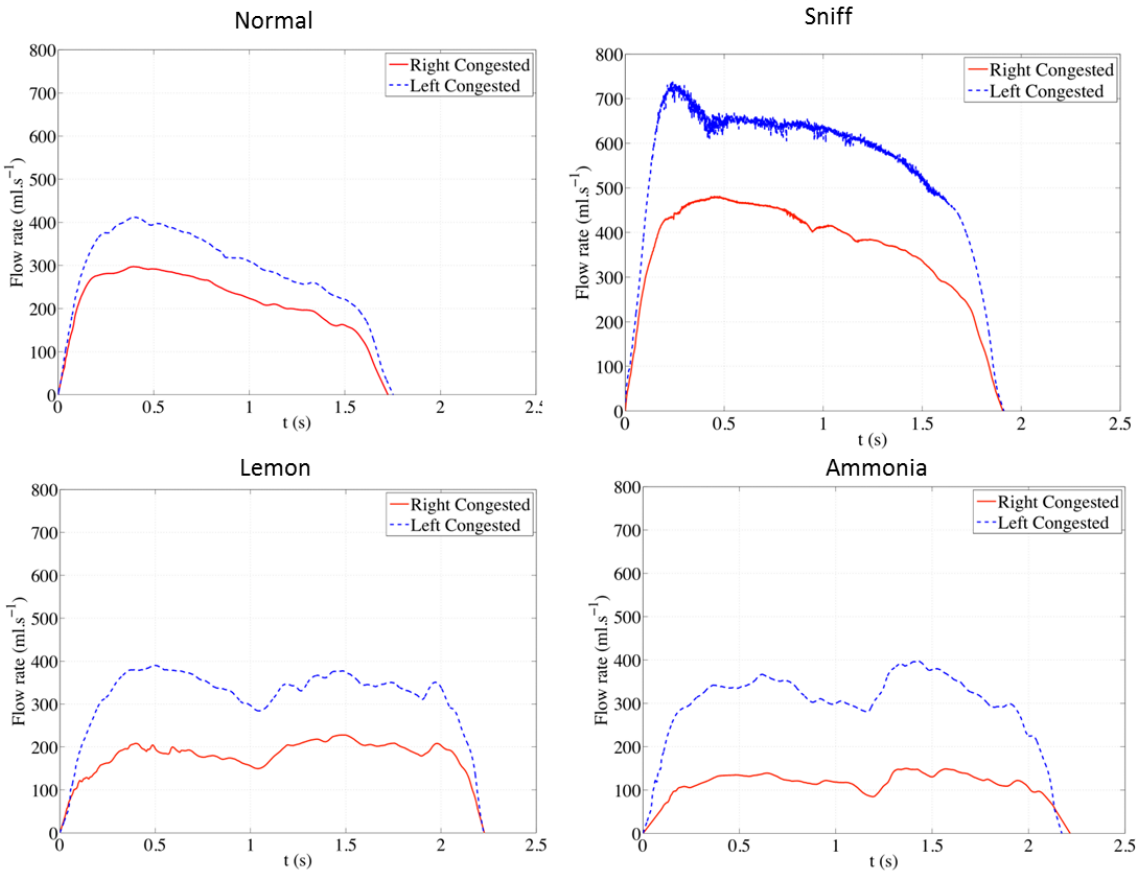

Figure 5.16 The 'average' inspiration traces in a single subject for each mode of inspiration studied.

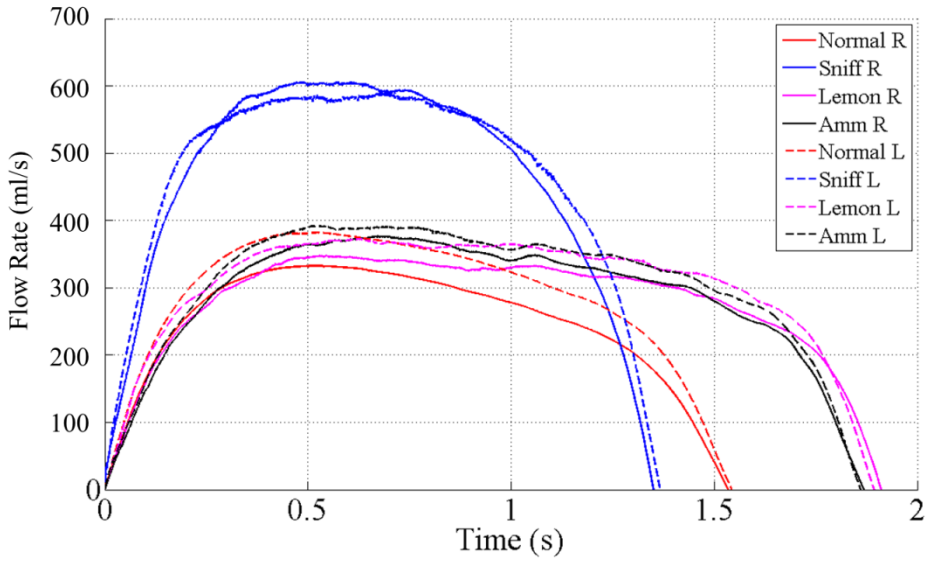

Figure 5.17 The 'average' inspiration traces for all subjects for each mode of inspiration studied.

Within the clinical setting, cycles of inspiration and expiration are typically examined as flow volume loops. Figure 5.18 demonstrates an average flow volume loop for nasal inspiration

and expiration in one subject. This flow volume loop differs from those obtained with spirometry in lung function tests, as spirometry requires the subject to make a maximal inspiratory and expiratory effort, figure 5.18 is a normal inspiration and expiration.

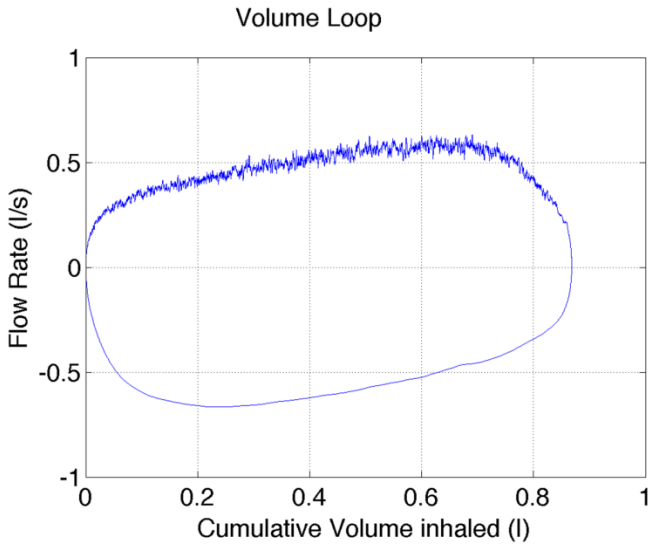

Figure 5.18 Flow-Volume loop for the average normal inspiration in one subject. Positive values represent expiration, negative values represent inspiration. At the start of the test both flow and volume are equal to zero (representing the volume in the spirometer rather than the lung). The trace moves clockwise for expiration followed by inspiration.

5.4.1 Significance of characteristic profiles

Experiments in nasal replica models and computational predictions have been used to investigate nasal air flow mechanics. However these studies have assumed constant volumetric (quasi-steady) inspiration due to its simplicity, or at best have employed simplified waveforms. In figure 5.19 an average nasal inspiratory profile as deduced here is shown compared to a sine wave. These results reveal that the initiation phase represents a very intense acceleration of the flow even in inspiration at rest, which is not captured in the approximation to a sine wave or a constant flow rate. This rapid ramp up in flow rate could impact on accumulative processes such as air conditioning, olfactory sensation, drug delivery, and toxicology. Rapid flow initiation can destabilise flow patterns leading to an alteration from laminar to transitional flow with consequential alterations to the transport of inhaled substances and the processes of heat and water exchange at the nasal mucosal surface. Figure 5.20d demonstrates the enhanced mixing seen with the transient dynamics of a sharp inspiration. [92]

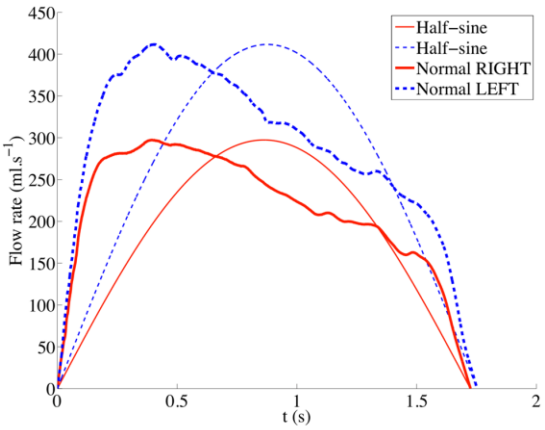

Figure 5.19 Comparison of a normal inspiratory profile with a sine wave.

Future modeling studies should investigate the significance of these phenomena.

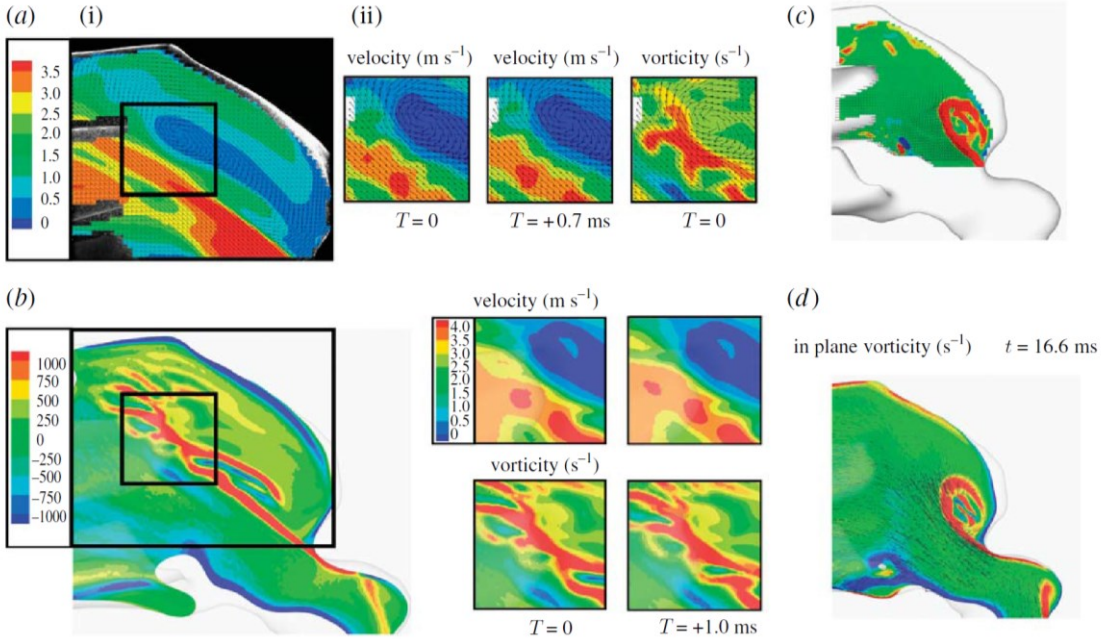

Figure 5.20 Steady-flow instability and sudden inspiration. (a) Experimental: (i) time-averaged PIV measurements at steady inspiratory flow rate of 150 ml s^{-1} through an idealised model, superimposed on a particle image. The inspiratory jet exceeds speeds of 3.5 $m.s^{-1}$ as it is funneled into the main cavity, with weaker recirculating velocities typically 0.5–1 $m.s^{-1}$ indicated by contours and direction indicators in (i). (ii) Instantaneous velocity measurements with a lapse of 0.71 ms (in vivo equivalent interval) are shown with a vorticity map derived from (i), extracted from the region illustrated with a black box in the large flow field image. Regularly shed structures can be observed. (b) Computational: direct numerical simulation shows similar features to experiment. Instantaneous vorticity field indicates unsteadiness of flow in upper and anterior cavity, elsewhere fluctuations not evident. (c) High-speed PIV and (d) direct numerical

simulation, showing the formation of the starting vortex in the idealized model as the flow is impulsed from stationary to 200 ml s^{-1} over a 20 ms interval. The effectiveness of mixing in the nose is greatly enhanced by transient flow dynamics, such as the sharp sniff shown. Figure courtesy of Dr DJ Taylor.

5.5 Discussion

Novel methods were applied to investigate the temporal profiles of nasal inspiration. Inherent features of the profile were identified and found to be significantly different between inspiration at rest and in sniffing. Characteristic temporal profile shapes for the different modes of inspiration were determined. Decongestion was found to have little effect on the temporal profiles for the flow regimes studied.

The initiation phase can be characterised by determining the time required for the flow rate to increase to 150ml.s^{-1}. Intense acceleration was observed in this phase. Typical plateau phase flow rates were found to be of order 350 ml.s^{-1} in inspiration at rest and significantly higher in sniffing.

These results could have significant implications for the understanding of nasal airflow mechanics. Nearly all studies concerned with transport and exchange processes in the nasal airways, such as aerosol deposition, model nasal inspiratory flow as a quasi-steady process, or at best have used grossly simplified approximations (e.g., sinusoidal flow rate variation). However, these results reveal that the initiation phase represents a rapid acceleration of the flow, and moreover that very high flow rates may be sustained in sniffing. It is well recognised that rapid accelerations or decelerations can destabilise laminar flows leading to an alteration from a laminar to a transitional (i.e. incompletely turbulent) state with consequential alterations to the transport of inhaled substances and the processes of heat and water exchange. To accurately predict these accumulative processes within the nasal airways the transient nature of the inspiratory profile should be considered. For instance, the temporal dynamics of the sniff are believed to be central to odorant perception, by affecting odorant intensity and component discrimination.

The use of a bilateral hot wire probe could potentially provide useful information in a clinical setting, enabling for example the degree of nasal flow bias and the response to decongestion to be determined. However means to make the sensors more rugged (perhaps by replacing with a hot film) and providing a calibration means would be required.

Chapter 6

Sinus Ventilation & Transport

6.1 Introduction

Rhinosinusitis is a common condition and accounts for a huge number of medical consultations worldwide[14]. In the United States rhinosinusitis is ranked in the top ten most expensive medical conditions for employers based on combined healthcare and reduced productivity costs[22]. Despite the huge socioeconomic impact, the causes of sinusitis are not well understood. Important factors in the pathogenesis of sinusitis are reduced sinus ventilation and impaired mucociliary transport. Improved sinus ventilation is often a goal of clinical interventions[216,275-277]; however, the links between sinus geometry, ventilation, and clinical outcomes are still poorly understood. Current surgical treatment for chronic rhinosinusitis involves enlarging the natural maxillary sinus ostium creating a middle meatal antrostomy. In the past, surgery involved creating inferior meatal antrostomies as a second ostial opening to improve sinus ventilation however these have largely been abandoned due to disruption of mucociliary clearance pathways and poor long term patency. In this chapter the relationship between sinus ventilation and ostial configuration is elucidated in experimental, computational and numerical models.

6.2 Sinus Ventilation

In the following the effects of

i. ostial diameter,
ii. ostial and sinus geometry,
iii. a second ostium,
iv. nasal flow rate and
v. mucocillary transport

on the mechanics of sinus ventilation are examined.

6.2.1 Effects of ostial diameter on sinus ventilation

An idealised physical model of a human maxillary sinus (Chapter 3 pg 62 fig 3.10) was used in conjunction with gamma scintigraphy employing Krypton-81m to allow measurement of volume flow rates and gas transport. Matching computational simulations enabled investigation of additional variables, which were not possible to examine experimentally, and separation of transport mechanisms. Comparison of geometrical configurations and data on maxillary sinus volumes is summarised in Chapter 3 section 3.5.1 and literature values are given in Chapter 1 table 1.1. The idealised physical model has two ostia connecting the sinus to the middle meatus, the larger the maxillary ostium (MO) has a diameter of 3mm and the smaller or accessory ostium (AO) has a diameter of 1.7mm. Krypton experiments were run occluding each ostium in turn. The results are compared with first order estimates and computational simulations (table 6.1).

Previous studies have shown that when a single ostium is less than 4mm in diameter ventilation is by diffusion[57,151,204]. The qualitative flow characteristics of the idealised physical model geometries were found to follow the predictions obtained either by first order estimates or by accurate computations.

Ostium configuration	Péclet number Pe	Fick's Law V'_{eff}	Computational simulation			Experimental V'_{eff}
			Conv-only	Conv + Diff	T_{90}	
Large single	$3.8x10^{-3}$	1.4×10^{-8}	2.3×10^{-12}	1.4×10^{-8}	2700	1.5×10^{-8}
Small single	$4.5x10^{-5}$	1.1×10^{-8}	2.6×10^{-11}	8.7×10^{-9}	4400	8.5×10^{-9}

Table 6.1 Experimental and computational values for effective volume flow rate and 90% exchange time for krypton transport in physical model geometries with a 10ml sinus and flow rate of 5L/min. Péclet numbers for both geometries <1 indicating diffusion dominated transport. Fick's Law: prediction from Fick's law first-order diffusion; V'_{eff}: effective volume flow rate, m^3/s; Conv-only results are from purely convective simulations; Conv + diff results are from a simulation that combined convective and diffusive effects; T_{90}: 90% exchange time, s.

Increased levels of radioactivity are seen in the sinus when the ostial diameter is increased (figure 6.1). With a single ostium, doubling the ostial diameter doubles the effective volume flow rate of gas exchange. The 90% exchange time for the single large ostia is 45 minutes and for the single small ostium is 73 minutes showing that the natural ventilation rate of a sinus with a single ostium is extremely slow.

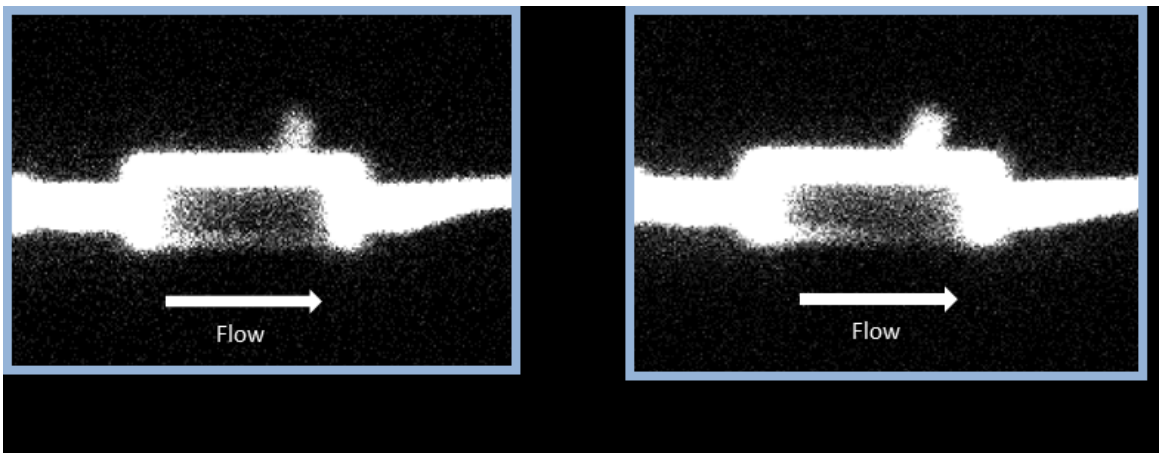

Figure 6.1 Gamma camera images from krypton experiments in the idealised physical model. Left shows a run with a small single ostium and right is a large-ostium only experiment. Sinus volumes are 10ml and the channel flow rate is 5 L/min. The image thresholding and resolution are the same for both images, as can be seen by the identical channel brightness. The channel sections appear much wider on the image than in the physical model. This 'spreading' effect is due to the gamma rays not all following horizontal paths to reach the camera plates see section 3.5.2.3.

The computational results as shown by the streamlines in figure 6.2 clearly demonstrate the flow patterns in the sinus. With a single ostium, there is no net flow across the ostium so exchange is limited to diffusion and is very slow. The channel flow provides a shear driving force at the nasal end of the ostium, which sets up two counter-rotating vortices in the ostium. There is a close match between the pattern of vortices found in this study and theoretical results for shear-driven cavities[278,279], as well as those for a channel side branch with no net flow[280]. The computational simulations also revealed a uniform pressure throughout the ostium and sinus, matching that in the channel outside the ostium. This finding matches earlier experimental evidence that the sinus pressure follows the variation of nasal cavity pressure during breathing [194], and confirms that steady gas movements between the sinus and nose cannot be pressure-driven (figure 6.4).

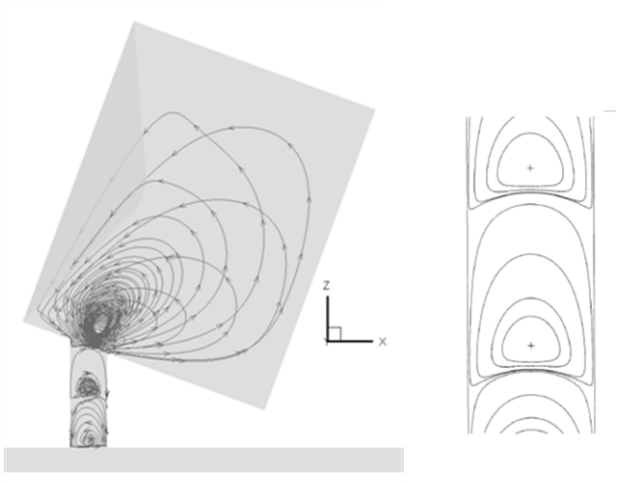

Figure 6.2 Left: Velocity contours for the single large ostium configuration with a 10 mL sinus and flow rate of 5 L/min[215]. Right: Streamlines found analytically for a small side-branch off a larger channel with no net flow along the branch, reproduced from Tutty (1988)[280].

6.2.2 Effect of geometry on ventilatory flow patterns

The design of the idealised physical model permitted the investigation of ventilation in three different sinus volumes 10, 15 and 20ml. Changing the shape of the sinus is expected to affect only the flow in the sinus, not that in the ostium or middle meatus. Table 6.2 demonstrates no change in the effective volume flow rate into the sinuses with increasing volume.

Ostium configuration	V_s (ml)	Fick's law V'_{eff} (m^3/s)	Computational V'_{eff} (m^3/s)		Experimental V'eff (m^3/s)
			Conv-only	Conv + Diff	
Large single	10	1.4×10^{-8}	2.3×10^{-12}	1.5×10^{-8}	1.4×10^{-8}
	15	1.4×10^{-8}	2.3×10^{-12}	1.5×10^{-8}	1.4×10^{-8}
	20	1.4×10^{-8}	2.3×10^{-12}	1.6×10^{-8}	1.4×10^{-8}
Small single	10	1.1×10^{-8}	2.6×10^{-11}	8.5×10^{-9}	1.1×10^{-8}
	15	1.1×10^{-8}	2.6×10^{-11}	9.2×10^{-9}	1.1×10^{-8}
	20	1.1×10^{-8}	2.6×10^{-11}	8.7×10^{-9}	1.1×10^{-8}

Table 6.2 Experimental and computational values of V'_{eff} for all sinus volumes, flow rate 5 L/min, V_s : sinus volume.

Hood 2010[47] was able to further investigate the effects of change in geometry computationally. Ostial length, elliptical cross section area, ostial curvature, channel curvature and taper and sinus shape were studied.

Summarising her results;

- Ostial flow patterns were found to be determined by the relative rather than absolute ostial length. However, the ostium-sinus interface velocities were greater for a larger ostium; therefore the estimated exchange times are affected by both relative and absolute ostial length.
- An elliptical ostium was found to have a similar flow pattern as a cylindrical one of the same length and major diameter. However the ostium-sinus interface velocities and hence the estimated exchange flow rates were much smaller with an elliptical ostium.
- The flow patterns in tapered ostia, with diameter varying along their length, were determined by the maximum diameter.
- Ostial curvature slightly reduced the velocity magnitudes and exchange flow rates, although this could have been due to the slightly larger effective ostium length. Channel curvature of the middle meatus was not found to exert any significant influence on sinus ventilation.
- The effect of sinus shape was studied in a sinus shaped as a truncated sphere. There the peak velocities at the ostium-sinus interface and the estimated exchange flow rate were found to be approximately double the values found for the standard sinus shape. However, this change is very much smaller than the variations found for changing

ostium diameter, length or shape, so the sinus shape does not seem to be a significant factor controlling sinus ventilation.[239]

6.2.3 Implications of a second ostium

An additional ostium can occur due to either a natural accessory ostium or surgical antrostomy, for example, an inferior meatal antrostomy. The proportion of the population who have accessory ostia is controversial, with rates between 5% and 44% reported in the literature [51-53,60]. Measurements of ostial size and the presence of accessory ostia are hampered by the inaccessibility and complex geometry of the sinuses, and as a result many studies have been performed in cadavers, where the thin fontanelle membranes (in which the majority of accessory ostia are found) could easily be damaged when drying out[43]. A relationship between rhinosinusitis and the presence of accessory ostia has been reported in the literature, but the causal link is unclear. It has been proposed that infections may damage the fontanelle membranes and create accessory ostia[28] and that accessory ostia disrupt mucociliary clearance pathways and result in sinusitis[45]. Inferior meatal antrostomies were designed to aerate the maxillary antrum and drain the sinus by gravity; however, it is known that dependent drainage does not occur as the cilia continue to transport secretions to the natural ostium. Inferior meatal antrostomies have now largely been abandoned given the low rate of long-term patency and high rate of failure[281].

The results from the Krypton experiments show increased levels of radioactivity in the sinus with the presence of an additional ostium (figure 6.3). This translates to an approximately 50 fold increase in the effective volume flow rate of gas replacement in the sinus with an additional ostium. The measurements in table 6.3 show the actual increase is from 1.5×10^{-8} m^3/s, (standard deviations of 2.7×10^{-10} m^3/s), to 7.4×10^{-7} m^3/s, (standard deviations of 2.3×10^{-8} m^3/s), hence the rise is more precisely estimated as 49.3 +/- 1.5. The 90% exchange times for the single large ostia is 45 minutes whereas with the 2 ostia is only 36 seconds.

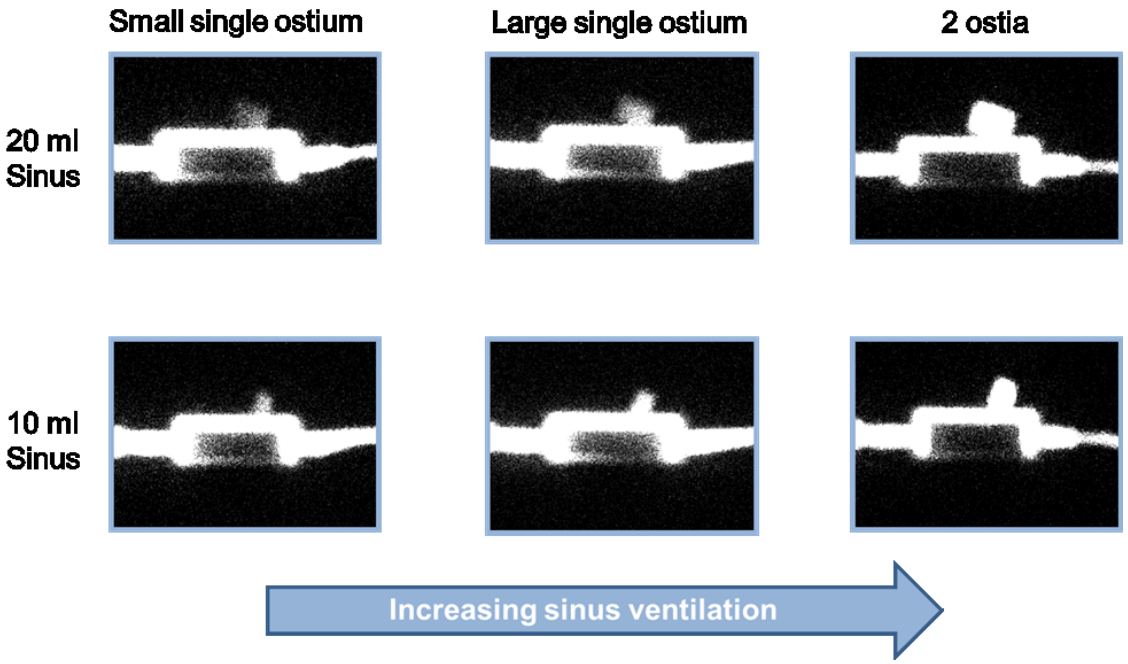

Figure 6.3 Gamma camera images from krypton experiments in the idealised physical model. Left shows a run with a small single ostium, in the centre is the single large ostium and on the right is the double ostium configuration. Sinus volumes are 20ml at the top and 10ml at the bottom and the channel flow rate is 5 L/min. The results for exchange times are given in the following table.

Ostium configuration	V_s (ml)	Experimental V'_{eff} (m^3/s)	Computational V'_{eff} (m^3/s)		T_{90} (s)	Fick's law V'_{eff} (m^3/s)
			Conv-only	Conv+diff		
Double	10	7.4×10^{-7}	7.6×10^{-7}	7.9×10^{-7}	29	-
	15	1.2×10^{-6}	7.6×10^{-7}			-
	20	1.3×10^{-6}	7.6×10^{-7}	8.2×10^{-7}	56	-
Single large	10	1.5×10^{-8}	2.3×10^{-12}	1.4×10^{-8}		1.4×10^{-8}
	15	1.5×10^{-8}	2.4×10^{-12}			1.4×10^{-8}
	20	1.6×10^{-8}	2.3×10^{-12}	1.4×10^{-8}	3300	1.4×10^{-8}
Single small	10	8.5×10^{-9}	2.6×10^{-11}			1.1×10^{-8}
	15	9.2×10^{-9}	2.6×10^{-11}			1.1×10^{-8}
	20	8.7×10^{-9}	2.6×10^{-11}	8.7×10^{-9}	5300	1.1×10^{-8}

Table 6.3 Experimental and computational values of volume flow rate (V'_{eff}) for all geometry configurations, flow rate 5 l/min, V_s : sinus volume, T_{90}: 90% exchange time, s.

The computational results clearly demonstrate the different flow patterns in the sinus for different ostial geometries, as shown by the streamlines in figure 6.4. When there is only a single ostium, there can be no net flow across the ostium so exchange is limited to diffusion and is very slow. In the presence of an additional ostium, there is a net flow through the sinus and convective gas transport is dominant.

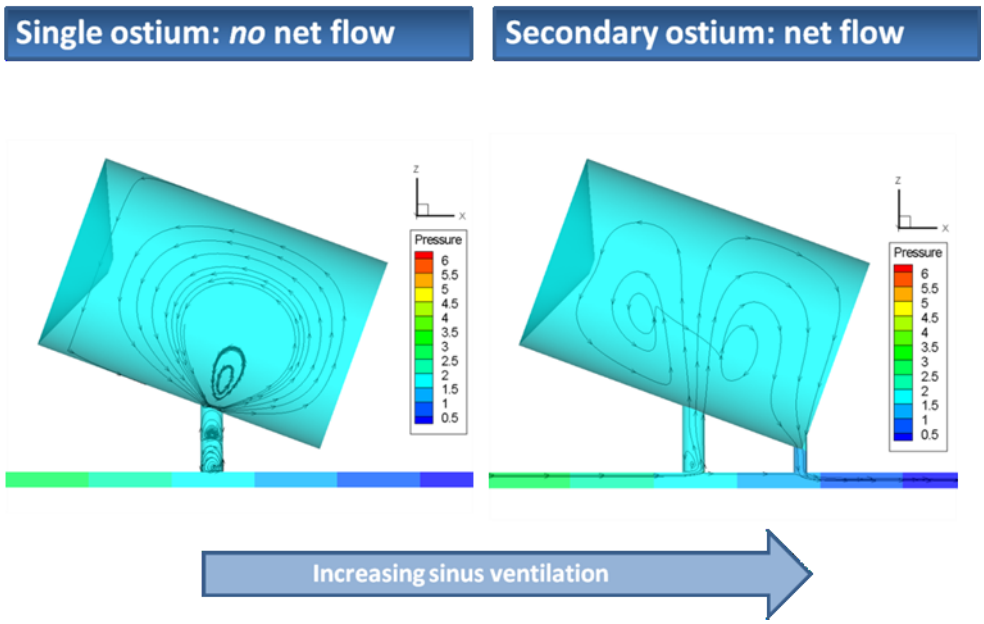

Figure 6.4 Velocity streamlines are superimposed on pressure contours in the physical model geometry with sinus volume 20 ml, single large ostium (left) and double ostium configuration (right). Channel flow rate 5 L/min. Pressure scale in Pa.[47]

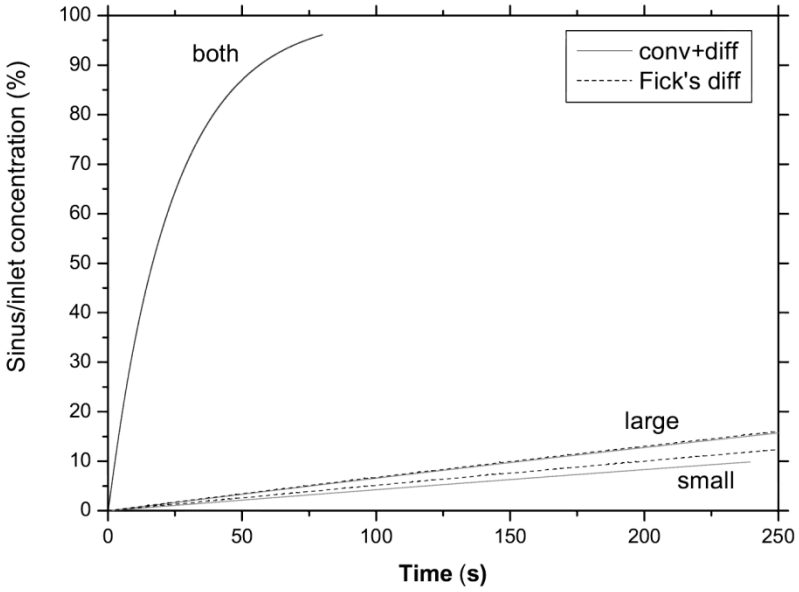

Figure 6.5 Computational results for Krypton concentration against time in the three idealised physical model configurations: all sinus volumes 20 ml, channel flow rate 5 L/min, single small and large ostia and both ostia. Fick's law comparison shown for single ostium geometries[47].

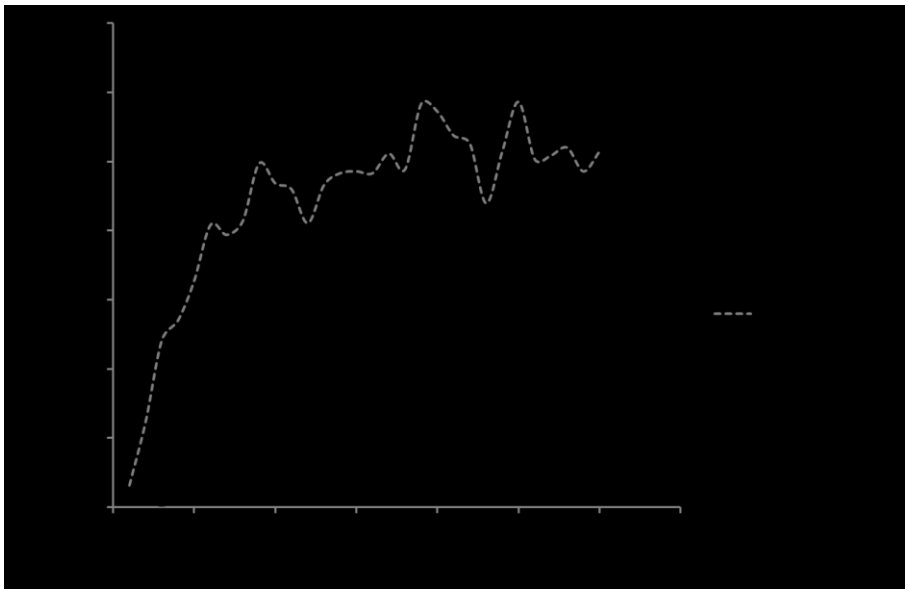

Figure 6.6 Experimental results showing total count numbers against time for the large single and double ostium geometries in the idealised physical model. The rapid wash in for the double ostium case is thus verified experimentally. Direct comparison with fig 6.5 is however complicated by the rapid decay rate of the tracer.

6.2.4 Modelling the effect of nasal flow rate on sinus ventilation

Krypton experiments were run in all ostial configurations of the idealised physical model at two flow rates 2.5L/min and 5L/min and each run was repeated five times. These flow rates correspond to the typical literature values for middle meatal flow rates for a channel calibre of 2mm and spam of 50mm. The increase in the channel flow rate from 2.5L/min to 5L/min increases the pressure difference between the ostial openings and results in an almost doubled volume flow rate through the sinus from 7.6×10^{-7} m^3/s at 2.5L/min to 1.3×10^{-6} m^3/s (compare 20ml sinus with double ostia in tables 6.3 and 6.4). The increase in sinus flow rate is not exactly proportional to the increase in pressure difference along the channel because the ostia-sinus path has higher flow resistance to flow than the parallel channel path, so the flow in this section of the channel will increase more than the flow through the sinus. In vivo the pressure difference between the nasal ends of the ostia can be increased by an elevation in nasal flow rate, as demonstrated above, or (equivalently) by increasing the spacing between the ostia with a constant nasal flow rate and hence pressure gradient.

Ostium configuration	V_s (ml)	Experimental V'_{eff} (m^3/s)	Computational V'_{eff} (m^3/s)		T_{90} (s)	Fick's law V'_{Deff} (m^3/s)
			Conv-only	Conv+diff		
Double	10	5.1×10^{-7}	4.8×10^{-7}			-
	15	7.8×10^{-7}	4.8×10^{-7}			-
	20	7.6×10^{-7}	4.8×10^{-7}	4.9×10^{-7}	94	-
Single large	10	1.6×10^{-8}	1.3×10^{-12}			1.4×10^{-8}
	15	1.6×10^{-8}	1.4×10^{-12}			1.4×10^{-8}
	20	1.6×10^{-8}	1.3×10^{-12}	1.3×10^{-8}	3500	1.4×10^{-8}
Single small	10	8.4×10^{-9}	1.1×10^{-11}			1.1×10^{-8}
	15	8.1×10^{-9}	1.1×10^{-11}			1.1×10^{-8}
	20	8.6×10^{-9}	1.1×10^{-11}	8.3×10^{-9}	5500	1.1×10^{-8}

Table 6.4 Experimental and computational values of the volume flow rate (V'_{eff}) for all geometry configurations, flow rate 2.5 L/min, V_s : sinus volume, T_{90}: 90% exchange time, s.

6.2.5 Estimating the effects of mucociliary transport on ventilation

Previous work has shown that modelling of mucociliary velocities on the mucosal surfaces had no effect on convective or diffusive exchange times[151]. Mucus plugging can prevent gaseous exchange but this has not been modelled in this study. Mucociliary transport is, however, essential in maintaining healthy sinuses as it is required in order to remove pathogens that enter the sinus. Additional ostia are associated with disrupted mucociliary transport[45], possibly leading to delay or prevention of the removal of any pathogens entering the sinus, and to recirculation of mucus, which can introduce pathogens from other parts of the nasal cavity.

6.2.6 Prediction of ventilation rates: comparison of experimental and computational results

Computational predictions of gas exchange rates closely match the experimental findings (tables 6.3 and 6.4), giving increased confidence in both methods. The results show that volume flow rates are independent of sinus volume, indicating that sinus ventilation is influenced by ostial geometry and channel flow rate alone. The results for single ostium geometries are independent of channel flow rate, demonstrating that the gas exchange mechanism is diffusion dominated.

Experimental results and computational predictions for the 15 and 20 ml sinus volumes with double ostia do not agree as closely as the other 14 combinations of ostium geometry, sinus volume and channel flow rate. The processing of the experimental krypton data assumes a uniform concentration in the sinus; hence any variation in sinus concentration may lead to discrepancies between the count ratios and the effective flow rates. Computational plots of krypton concentration normalised by the inlet value are shown in figure 6.7. The single ostium sinuses have a very uniform concentration whereas the double ostium sinuses show a far greater variation in concentration particularly with the largest sinus volume 20ml indicating that the assumptions used to process the experimental data are compromised.

Krypton's very short half-life (13 s) means that the count numbers in each region of the image will reach 90% of their steady state value at or before 43 seconds (3.32 half-lives). This is several orders of magnitude lower than the predicted 90% exchange times for the single ostium geometries. Whereas when compared to the 90% exchange times for the double ostium

geometries, 43 seconds is slighter longer than that for the 10 ml double ostium sinuses, but around half the values predicted for the 15 and 20ml double ostium sinuses.

Therefore, the steady state count numbers for the single ostium geometries reflect a very early state of exchange, whereas the 10 ml double ostium geometries show a completed exchange, and an intermediate stage for both the 15 and 20 ml double ostium sinuses. These differences may be an additional source of error in the experimental results. The use of a tracer gas with a longer half-life, such as xenon-133 (half-life 5.24 days) would prevent these errors. However, xenon also has disadvantages it is lipophilic and would adhere to the model but also the longer half-life means it would need to be captured when leaving the model to prevent exposing the experimenters to excessive radiation doses or the anaesthetic effects of xenon.

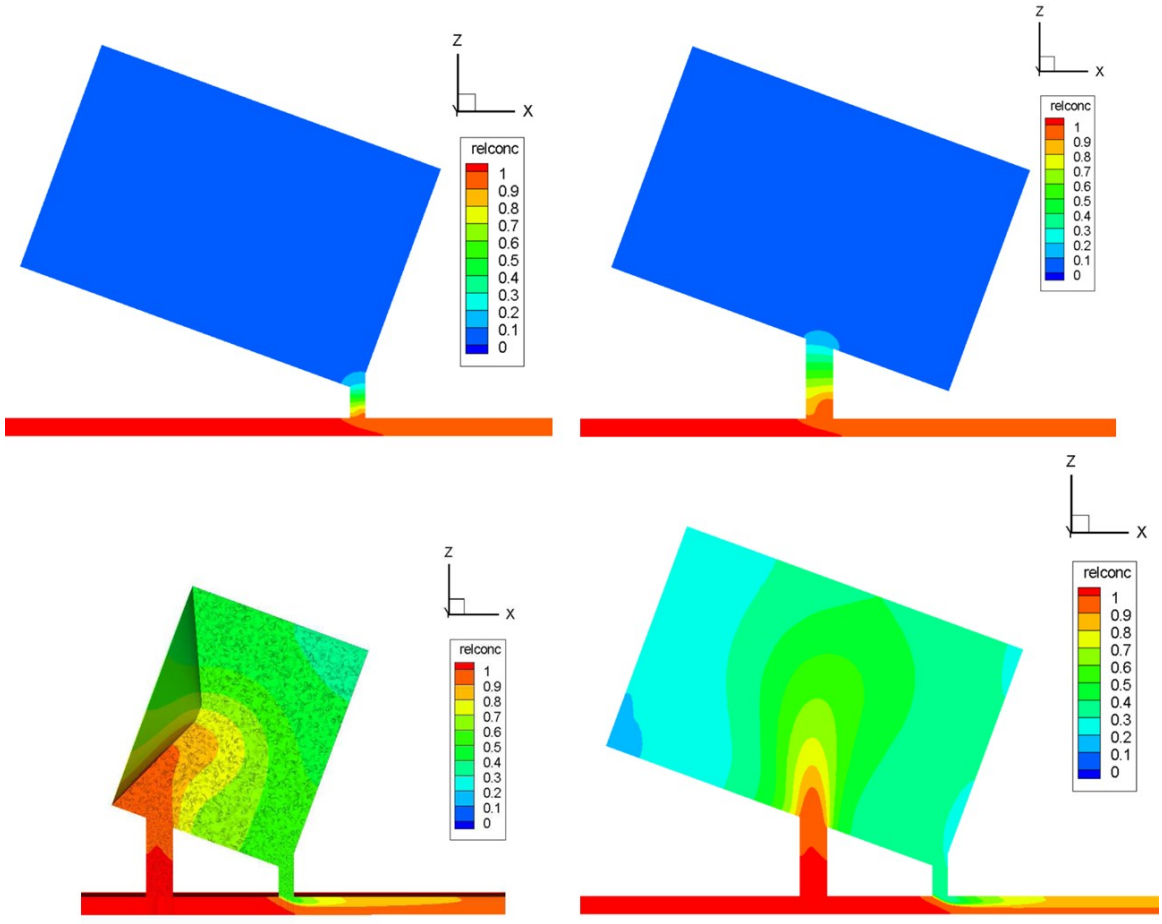

Figure 6.7 Contours of Kr concentration, divided by inlet value, for physical model geometries**.** Channel flow rate 5 L/min for all. Clockwise from top left: single small ostium, 20 ml sinus after 50 s; single large ostium, 20 ml sinus after 50 s; both ostia, 20 ml sinus after 10 s; both ostia, 10 ml sinus after 10 s.[47]

6.3 Sinus transport

The experimental and computational results demonstrated that there is enhanced ventilation associated with an enlarged or accessory ostium. However an excessively augmented ventilation may not be clinically beneficial[151], as it could reduce the normally high Nitric Oxide (NO) concentrations in the maxillary sinus[145], and impair the sterility of the milieu. Since NO has anti-microbial properties and can stimulate ciliary motion, it is therefore thought to be a significant factor in sinus health.

Nitric Oxide is a free radical molecule with many different functions in the body[282]. In the upper airways, NO is particularly noted for its role in immune defence, due to its anti-microbial properties[283,284], and promotion of ciliary activity[285]. NO is formed in vivo from arginine by three isoforms of the enzyme nitric oxide synthase (NOS). Three different types of NOS have been described, two of which have been found in the nose and sinuses. Nasal NO is formed by human endothelial or type 3-NOS[286], with some activity from type 2-NOS, whereas the sinuses contain only type 2-NOS[145]. Type 2-NOS is inducible and can be expressed in response to hypoxia and/or inflammation[287].

Arguments as to what constitutes a desirable level of sinus ventilation are as yet unresolved. On the one hand enlargement of the maxillary ostium is associated with reduced NO levels. Kirihene *et al.* (2002)[288] showed that surgical enlargement of the maxillary sinus ostium produced a significant decrease in both the maxillary sinus and the nasal cavity NO levels and the size of the ostium showed a significant correlation to the sinus NO level. The lowered levels of NO were found irrespective of the technique of measurement of the NO. Qian *et al.* (2000)[289] looked at the NO outputs from each nostril in patients who had undergone unilateral medial maxillectomy compared to normal volunteers and found significantly lower NO levels on the operated side in the post-operative group. NO inhaled from the upper to the lower airways may help with ventilation-perfusion matching in the lungs as it has vasodilative effects.

Conversely, the absence of effective ventilation is associated with decreased NO production[290,291] and diminished mucociliary clearance, may lead to chronic rhinosinusitis[292]. Low nasal NO levels have been reported in cases of acute rhinosinusitis[293], nasal polyposis[294], primary ciliary dyskinesia[179] and cystic fibrosis[295].

6.3.1 Efforts to determine NO production rates and sinus concentrations

Lundberg *et al.* (1995)[145] first identified high concentrations of NO in the paranasal sinuses. They reported a sinus NO production rate of 20 nmol/min ($3.3x10^{-10}$ mol/s), based on the increase in measured sinus NO concentrations when temporarily blocking the ostia for varying durations. Andersson *et al.* (2002)[296] also found a much higher concentration of NO in the maxillary sinus than in the nasal cavity. Unfortunately their measuring technique did not resolve concentrations above 10,000 ppb, which was exceeded in some of the sinuses resulting in artificially low mean sinus concentrations. Menzel *et al.* (2005)[297] investigated the effect of humming on NO concentrations in the sinus, and found a rate constant of $3.7x10^{-3}$ mol/s for sinus NO concentration recovery after washout, indicating a net production rate at the steady state sinus concentration of $3.8x10^{-11}$ mol/s, an order of magnitude lower than the Lundberg value. However, they did not consider gas transport of NO out of the sinus in their model.

The effect of blocking the sinus ostium on nasal NO concentration was studied by Haight *et al.* (1999)[298]. They measured nasal and sinus NO concentrations and production in a single subject with open and then experimentally blocked ostia. They reported a 12% reduction in nasal NO output when the sinuses were blocked, hence concluded that the sinuses contribution to nasal NO was small. They estimated rates of NO production per unit area of epithelium as 6 nL/min/cm^2 ($3.9x10^{-8}$ mol/s/m^2) for the maxillary sinus and 0.5 nL/min/cm^2 ($3.3x10^{-9}$ mol/s/m^2) for the nasal cavity. These values are of a similar order of magnitude to other studies, however their sinus NO production rate was reduced by a much greater proportion than the nasal NO production by the anaesthetic and decongestant used for the study. In view of the significant variations in nasal and sinus NO concentrations between subjects in other studies, these results in a single subject might not be representative of the wider population.

The effect of ambient oxygen concentration on nasal NO output has been investigated by both Haight *et al.* (2000)[291] and Nakano *et al.* (2002)[290]. Haight *et al.* found no change in nasal NO output if the nasal oxygen concentration was increased and a 50% reduction if the concentration was dropped to zero. Nakano *et al.* (2002) found a reduction in NO output of 37% with zero oxygen concentration. These findings suggest that nasal and sinus NO is produced partly with gaseous oxygen and partly with blood oxygen.

DuBois *et al*. (1998)[299] assessed NO production and absorption in the nasal cavities. They estimated a ventilation rate for sinuses based on Xenon washout half-times from Paulsson et al. (1992)[201], and a combined sinus volume of 80 ml, to obtain an equivalent flow rate of 5

ml/min (8.3x10−8 m^3/s). They did not measure sinus concentrations or consider diffusive transport.

6.3.2 Application of the sinus ventilation model to NO transport

Fick's law of first-order diffusion was previously found to give accurate results for sinus diffusive exchange times and thus exchange rates. The diffusive transport of NO through the ostium is given by

$$\frac{DA\ (C_S - C_N)}{L}$$

Equation 6.1

where D is the diffusivity of NO in air (2.4x10-5 m^2/s), A is the cross-sectional area of the ostium (m^2), C_S is the concentration of NO in the sinus (mol/m^3), C_N is the concentration of NO in the nasal cavity (mol/m^3) and L is the ostium length (m).

The corresponding convective flux of NO is given by

$$QC_S$$

Equation 6.2

where Q is the convective volume flow rate (m^3/s) and C_S is the sinus concentration as before. Balancing NO production (P, mol/s) and transport gives the following expression for the steady-state sinus NO concentration:

$$C_S = (P+C_NDA/L)/(Q+DA/L)$$

Equation 6.3

The steady state NO concentration in the sinus can be estimated using the above equation, with published production rates and nasal NO concentrations, along with CFD convective flow rates. Lundberg *et al*. (1995)[145] found that variation in nasal NO concentration had a trivial effect on the sinus concentration.

Ostial diameter (mm)	Steady state sinus NO concentration (ppb)
1.7 mm	300, 000
3 mm	48, 000
10 mm	6, 900
3 mm and 1.7 mm	7, 000

Table 6.5 NO steady state concentrations: Convective flow rates obtained from CFD simulations, diffusive from Fick's law estimates. All values based on Lundberg *et al*. (1995)[145] NO concentration and production rate measurements.

Ostium streamlines for the single large and double ostium configuration are plotted in Figure 6.4, showing that the single ostium geometries have no net flow into or out of the sinus, whereas the double ostium geometries have a net flow through the sinus. Computationally a typical post-surgical geometry has also been created with an ostial diameter of 10mm typical for a middle meatal antrostomy in functional endoscopic surgery. The streamlines for the new geometry are shown in figure 6.12.

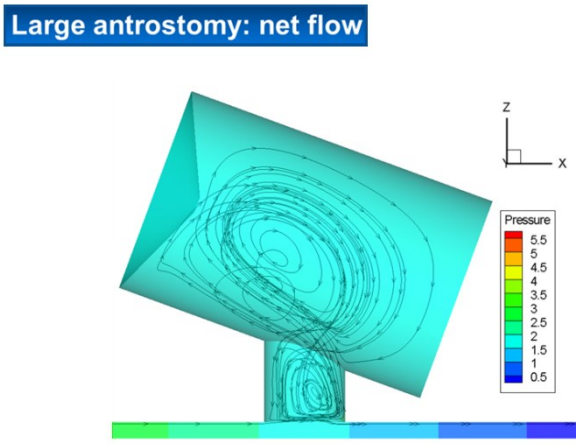

Figure 6.8 Velocity streamlines are superimposed on pressure contours in the physical model geometry with sinus volume 20 ml, single very large ostium with ostial diameter 10mm. Channel flow rate 5 L/min. Pressure scale in Pa. [47].

Values of steady-state NO concentration for each geometry considered are given in Table 6.5. The data shown are based on measurements of NO concentration and production from Lundberg (1995)[145], who found sinus concentrations of 9.1±3.8ppm, nasal concentrations 1.2±0.2ppm and sinus production rate 20nmol/min.

The pathological or post-surgery geometries described have demonstrated significantly higher transport rates and lower steady state sinus NO concentrations than the physiological geometries. There is no significant difference in NO transport or sinus concentration between the two post-surgery geometries considered, representing middle meatal (10mm diameter single ostium) or inferior meatal antrostomy (double ostium). The results suggest that sinuses with a single ositum of 3mm can maintain steady state concentrations similar or higher than published data for maxillary sinuses. In contrast, the pathological or post-surgery geometries described have lower steady state concentration estimates. All of the predicted sinus NO concentrations are above the levels found to have bacteriostatic effects (100-1400 ppb)[283]. The threshold NO concentrations for other anti-microbial effects are less clear, as the primary paper describing anti-viral effects[284] does not determine NO concentrations. Only the pathological or post-surgery geometries described in this study could provide the entire NO found in the nose (205-455nl/min). The physiological geometries described do not allow sufficient transport through the ostium to supply nasal NO levels.

Lindberg *et al*. (1997)[300] defined an abnormally low concentration of NO for the nose as 1.96 standard deviations below the median value, or 100 ppb, and found that nasal NO concentrations below this value were associated with reduced ciliary beat frequency and mucociliary transport rate. A similar threshold can be found for sinus NO concentration using mean and standard deviation values from Lundberg *et al*. (1995)[145], giving a lower threshold of 1652 ppb for the normal range of sinus concentrations. All the steady state NO concentrations predicted using NO production rates from the same Lundberg study are above this level, so the reductions caused by pathological or post-surgery geometries may not be significant. Important caveats are that the assumed NO production rate may be overestimated and placement of accessory ostia affects the flow dependent driving pressure differential. Consequently there is a possibility that the NO levels could be much reduced.

6.3.3 Implications of Transport Estimates

The results demonstrate a significant difference in NO transport rates and steady state concentration values between ostial geometries considered physiological and those which are pathological or post-surgery. Clinically, middle meatal antrosomies have been shown to be more successful than inferior meatal antrostomies[301], in the surgical treatment of chronic rhinosinusitis, but in this example this cannot be attributed to differences in NO transport. The model representing an inferior meatal antrostomy in this study, has an interostial separation of

14mm. An increase in the interostial separation will increase the pressure differential between the ostium ends, resulting in an elevated flow rate through the sinus and thus increased NO transport. The length of the additional ostium in this model is 3.4mm based on CT data for one subject (due to a lack of information about inferior meatus antrostomy lengths). If one ostium was significantly shorter, due to passing through a thinner layer of tissue, the flow resistance would decrease and the sinus exchange flow would increase.

The optimum size for a middle meatal antrostomy is determined by number of factors, not all of which can be addressed by experimental modelling and transport predictions. A balance is required between i) minimising the transport between the sinus and nose in order to maintain a high sinus steady state NO concentration, and ii) allowing sufficient ventilation of the sinus. The final antrostomy size remaining after healing must also be sufficiently large to allow mucociliary transport out of the sinus while extensive scar tissue (which may lack cilia and impede mucous clearance) at the ostium must be avoided. Accessory ostia in the middle meatus are strongly associated with mucous recirculation and surgical failure[302], but including them in a dramatically enlarged natural ostium may cause excessive ventilation. The restricted visibility and confined spaces for instruments during endoscopic surgery will also place limits on antrostomy size and shape, as will the individual patient's anatomy[47].

In conclusion the mechanics of sinus ventilation determine NO transport. Surgical enlargement or creation of an additional ostium can dramatically augment ventilation and the effect of this can be estimated or in principle determined in vivo via imaging. Translation to NO concentration however depends on production rates.

6.4 Effect of acoustic stimulation on sinus transport

Finally we examine whether acoustic stimulation can enhance sinonasal exchange. From the preceding we have demonstrated breathing modes, ostial and interostial flows affect it. Recent experimental results linking humming to increased sinus gas exchange[297,303-305] have raised interesting questions about how sound effects gas transport in the upper airways. Currently there is little understanding of the physical basis of the increase in nasal NO found during humming. It is thought to be due to increased transport from the sinuses. Previous studies have shown that aerosols excited by sound waves deposit in larger quantities in the sinuses than un-excited aerosols[306], and this has been confirmed more recently by Maniscalco *et al.* (2006)[307] and Moller *et al.*[208,209]. Although the sound waves used by the Moller group are not representative of vocal amplitude or frequency.

It has been demonstrated that acoustic excitation can have significant effects on sinus ventilation and particle transport however; the mechanisms involved are not fully understood. Granqvist *et al.* (2006)[308] created an electrical-analogy model of their experimental equipment, including loudspeaker and cabinet, but did not attempt to model a more physiologically relevant geometry. Menzel *et al.* (2005)[297] analysed the increase in transport of NO during humming but did not consider NO transport during normal breathing.

6.4.1 Modelling and Experiments in Physical Model Geometries

The resonant frequencies and Q-factor values were calculated for each of the ostial configurations at the three different sinus volumes in the idealised physical model geometry. The experiments provide validity for the computational methods which can then be extended to investigate further combinations. The computational and experimental results for small ostium configurations in the physical model geometry are shown in (Figure 6.13 pg 130), with a comparison of resonant frequencies for all the modelled geometries in figure 6.14 and table 6.16.

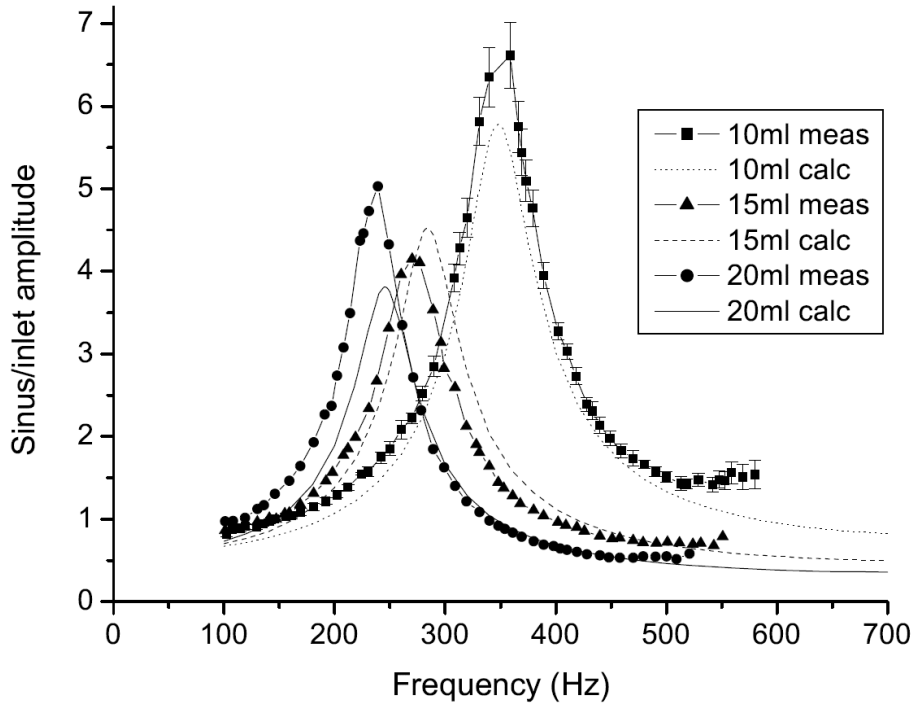

Figure 6.9 Experimental and computational results for small ostium geometries**,** with error bars shown for 10 ml sinus configuration. Figure courtesy of Dr CM Hood.

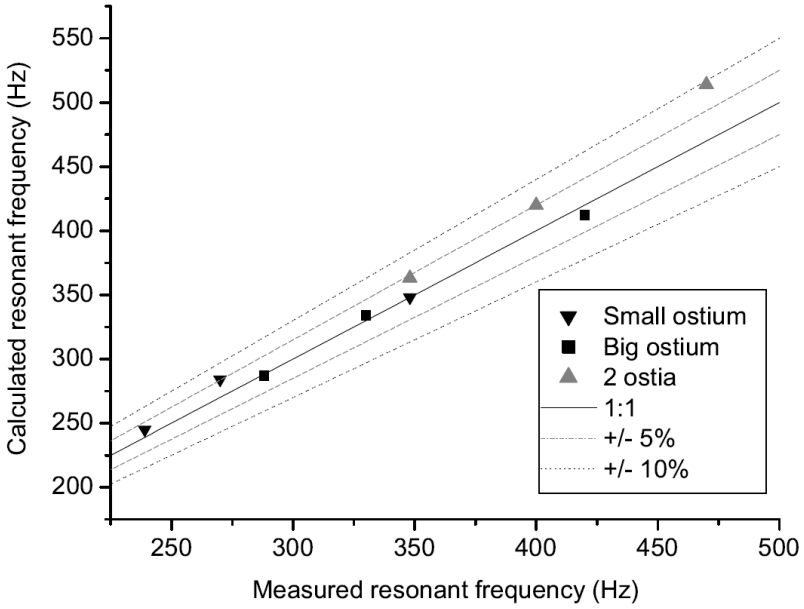

Figure 6.10 Comparison of measured and simulated resonant frequencies for small and large ostium geometries. Figure courtesy of Dr CM Hood.

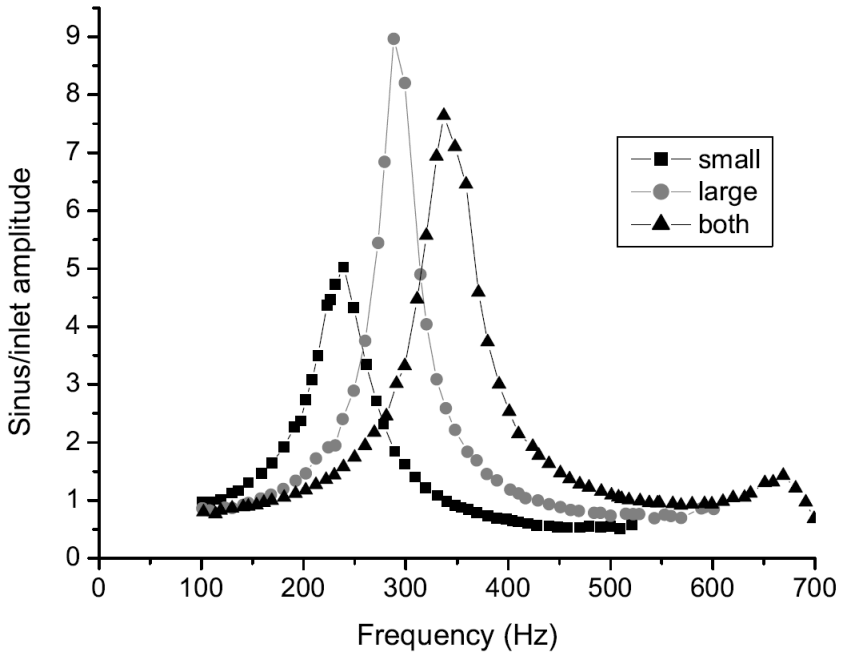

Figure 6.11 Experimental acoustic response results for all physical model ostium configurations with 20 ml sinus.

Ostium Config	Sinus Volume	Resonant Freq (Hz)			Q factor	
		Helmholtz	Expt	Sim	Expt	Sim
small	10	384	348	348	6.0	5.8
	15	313	270	284	4.8	5.2
	20	271	239	245	5.6	4.7
large	10	456	420	412	4.3	4.3
	15	372	330	334	8.1	3.8
	20	322	288	287	9.6	3.5
both	10	587	469	514	5.1	5.6
	15	479	390	420	6.7	5.6
	20	415	337	363	7.2	5.3

Table 6.6 Computational and experimental resonant frequencies and Q-factors from the physical model geometries, compared with first-order Helmholtz resonant frequencies. Table courtesy of Dr CM Hood.

All of the computationally predicted resonant frequencies lie within 10% of the experimental measurements, with most within 5%. Both the experimental and computational resonant frequencies are consistently lower than first-order Helmholtz resonator frequencies. This is likely to be due to the connection through the nasal cavity which is included in both the computations and experiments whereas, the first order Helmholtz predictions are based on a sinus ostium opening to the atmosphere. The computations and experiments follow the trends of Helmholtz resonators with resonant frequency decreasing with increasing sinus volume and ostial diameter.

The peak amplitudes of the computations and experiments match well but the simulations tend to have higher Q-factors. These differences could be a result of simplifications made in the geometry for the computational code. The duct geometry was simplified to the length of the main channel, with reflection coefficients appropriate to the area changes at each end, but this may not be an accurate description of the effects of the real duct geometry [47]. The multiple area changes between the main channel and the open end or the speaker are more likely to affect the magnitude and Q-factor than the resonant frequency. The effect of ostium geometry on the acoustic response of the sinus is shown in the experimental results for the 20 ml sinus in figure 6.15. As predicted the physical model with both ostia open has a similar resonance to the single larger ostium.

The effect of acoustic stimulation on sinus ventilation in krypton model was investigated but no increase in sinus transport was observed. However this could be due to the rigidity of the model whereas parts of the sinus wall are this and could be excited, although if this is the case lower frequencies would be expected to elicit a greater response.

A pilot study of 2 subjects was conducted to determine if the increased in NO transport described when humming was related to particular vocal frequencies. Unfortunately neither of the subjects demonstrated any increase in nasal NO levels when humming although both had normal nasal NO measurements and no evidence of any nasal or sinus disease.

6.4.2 Significance of Acoustic Resonance

The acoustic resonances within the sinuses were found to be in range of human vocal frequencies; however, the significance of this in relation to sinus physiology is unclear. Many studies have demonstrated increased NO transport during humming suggesting that acoustic excitation [297,307] but no physical studies of this phenomenon could be found in the literature. Unfortunately no increase in NO transport was found in the pilot study performed but only 2 subjects were considered.

Menzel *et al*. (2005)[297] modelled their in vivo experimental results of the washout of NO during humming with a rate constant r_H, which they found to have a mean value of 0.216 s^{-1}. If we consider humming to produce gas transport equal to an additional effective volume flow rate QH, then

$$r_H = \frac{Q_H}{V_S}$$

Equation 6.4

where VS is the sinus volume. Re-arranging gives a mean QH value of 6.3×10^{-6} m^3/s [47]. In contrast, the fastest effective volume flow rate from steady convection and diffusion was found in this study to be 1.6×10^{-8} m^3/s, showing that humming could increase transport by at least an order of magnitude.

The experiments performed to date on humming and NO transport, have not determined whether the increased gas transport is frequency dependent. The human voice is generally not a single frequency; this could complicate in vivo investigation of the variation in transport with frequency.

It is possible that geometries with a high Q-factor would have particularly fast transport at the resonant frequency, but less transport at other frequencies. It is not known if the fast clearance of NO associated with humming is beneficial or detrimental so sinus/nasal health. Anecdotally a single case study has reported successfully treating sinusitis through extended humming [309].

6.5 Conclusions

81mKr and γ-camera imaging has been shown to enable a quantitative assessment of effective volume flow rate in physical model sinuses. The effective volume flow rates obtained experimentally for single and double-ostium sinuses match the computational predictions of matching geometries, while velocity fields follow the patterns found in simplified sinus geometries and topologically similar geometries. The combined use of computational simulations and physical experiments provides valuable cross-checking of results. Once matching has been established with a few sets of variables with results from both methods, there is increased confidence in results from each method alone, for example it is not always possible to obtain clear images with very low flow rates but computational simulations are still possible. This demonstration of the use of 81mKr to assess ventilation in model sinuses is seen as a first step to using 81mKr to investigate sinus ventilation in vivo in a clinical setting.

The computational and experimental effective flow rates depend on the ostium geometry. Sinuses with two ostia have much faster transport than sinuses with a single ostium. Sinuses with a single ostium also have diffusion-dominated gas transport, whereas sinuses with two ostia are convection-dominated. In the convection-dominated nature of the two-ostia flow, there is an increase in effective flow rate of 8% when the effect of diffusion is included in the computational model. The differences in both transport mechanism and transport rate between single and double ostium configurations are due to a qualitative difference in flow, as a sinus with a single ostium acts as a reservoir of fluid attached to the nose but a sinus with two ostia forms an alternative flow path to the nose. Increasing the diameter or reducing the length of the ostia is also seen to increase sinus ventilation but not to the extent of an additional ostium unless the ostium is very large (e.g. a middle meatal antrostomy).

The results suggest that the natural single-ostium sinus ventilation is remarkably slow. This limited ventilation may be protective for the sinus, preventing mucosal drying, maintaining sterility with high NO concentrations and minimising entry of pathogens. Whereas ventilation is necessary, excessive ventilation due to an additional ostium or very large ostium may not be clinically beneficial, as it could: 1) increase wash-out of nitric oxide (NO), which is excreted by the mucosa of the paranasal sinuses and is thought to have bacteriostatic and mucociliary regulating properties; 2) increase access of pathogens to the sinus, which could have compound effects with NO reduction; 3) cause mucosal drying, particularly if the upstream ostium is near the nostril and thus exposed to less well-conditioned air.

Rapid sinonasal gas exchange and the resulting reduction in NO levels, could arguably contribute to the development of rhinosinusitis. More research is needed to clarify the role of an additional ostium in sinonasal exchange processes and the effects of changing NO concentrations on sinonasal pathology.

81mKr has recently been used to image sinuses in vivo by Möller *et al.* [208] but they have not made a quantitative assessment of sinus ventilation under normal breathing conditions. This study represents the first step in quantitatively analysing sinus ventilation. The use of krypton imaging for quantitative assessment is successfully demonstrated and corroborated by comparison with computational modelling. Further work should look at the changes of sinus ventilation with variation of flow rate and sinus volume - expanding the verification of computations and testing the flexibility of the experimental method.

The transport of NO between the maxillary sinuses and the nasal cavity has been quantified for a range of physiological, pathological and post-surgical ostium geometries. The pathological and post-surgical geometries show increased NO transport and reduced steady-state sinus NO concentration compared to physiological geometries. Only the pathological geometries could supply the levels of NO output found in the nose. The acoustic resonances of the sinus model were investigated to determine if the sinus could be acting as a Helmholtz resonator. Interestingly the resonances found were all within vocal frequencies however the significance of this in relation to physiological processes remains unknown.

Chapter 7

Conclusions and Further Work

Summary and key findings

The aim of this thesis is to improve our current understanding of airflow and transport in the upper respiratory tract. Major deficiencies in our understanding concern the variability of cavity anatomy, the temporal dynamics of inhalation and the mechanics of sinus ventilation and transport. By performing in-vitro and in-vivo experiments the mucosal changes in the nasal geometry, the time dependent profile of inspiration and sinonasal transport mechanisms have been systematically investigated. The work combined measurement techniques from different fields, including: 3T MRI and image processing (radiology); hot-wire anemometry (aeronautics); acoustic rhinometry (ENT surgery) γ-scintigraphy (nuclear medicine), in a manner that is believed to be hitherto unique.

Prior to summarising the findings with regard to sinonasal airflow and transport the main novelties and improvements in experimental techniques are briefly reviewed as these may benefit future studies.

Firstly, segmentation of high resolution 3T MRI scans allowed the definition of anatomically realistic nasal surface geometries of seven healthy subjects, both pre- and post-decongestion. Localised changes in the nasal mucosa were shown to be well-resolved by the imaging modality, enabling variations in whole nasal cavity morphology to be quantified in a non-invasive manner.

Secondly, nasal inspiratory flow profiles were investigated in high temporal detail using a novel experimental methodology. It was shown that hot-wire anemometry enables simultaneous measurement of the bilateral nasal flow profile at a far higher frequency (5000Hz) than previously accomplished. Hot-wire inspiratory profile measurements were acquired from a cohort of fourteen subjects and complemented by data acquired using clinically available tools (acoustic rhinometry, SNOT-22, VAS and PNIF). Unlike MR imaging, the measurement necessitates a small compromise in geometric fidelity, limited to the external nose. To limit the impact and ensure the fidelity of the hot-wire experiments and acoustic rhinometry, the connection between the measuring tube and the nose was carefully considered to avoid splinting the external nares. Anatomical nasal adaptors and a rim of gel applied to the tip of the nasal adaptors were used to improve the connection, limit deformation of the nasal vestibule and increase the reproducibility of measurements whilst also retaining the normal dynamic resistance characteristics of the external nose. Apart from the most vigorous sniffs, it was concluded that the measurement technique adopted did not significantly affect the inspiratory profile.

Thirdly, 81mKr and γ-scintigraphy has been shown to provide a quantitative assessment of effective volume flow rate within a physical model of the human sinuses. The technique offers a number of advantages for more widespread use in the clinical setting. 81mKr is a γ emitter with a short half-life which is readily available in hospitals as it is used clinically in ventilation-perfusion scanning of the lungs. In contrast to other radionuclides krypton is chemically inert and does not interact with the materials of a physical model or with biological tissues. Having such a short half-life means the counts in the experimental model quickly reduce to typical background levels between experimental runs and minimal radiation protection is required. However, this limits dynamic imaging and the experiment required that ventilation rates be assessed from the count ratios determined from accumulated images.

Key findings

Chapter 4

The nasal geometry and the effects of decongestion on nasal airway morphology were obtained non-invasively in-vivo in greater detail than previously, and at higher spatial resolution. High resolution 3T MRI was found to be an excellent modality to study mucosal changes within the nose as it images the air mucosa interface directly. Regional changes have been quantified throughout the nasal cavity and complemented by anterior acoustic rhinometry. In summary the conclusions drawn were as follows:

(1) Decongestion was found to have greatest effect on the turbinate region where changes of > 300% in the nasal cross sectional area are observed.

(2) Measurements of nasal cross-sectional area by MRI and by acoustic rhinometry displayed a good correlation anteriorly; however the correlation between measurements was markedly reduced beyond the osteomeatal complex.

(3) Decongestion was observed to have a large effect on nasal volume but only a limited effect on the surface area. Surface area to volume ratios are hence significantly decreased with decongestion. These variations in SAVR have implications for the transport of inhaled substances and the processes of heat and water exchange at the nasal mucosal surface.

(4) The ratio of perimeter to cross-sectional area at the head of the middle turbinate provided a good approximation to the SAVR when decongested however this did not apply in the pre decongested state.

Chapter 5

Nasal inspiratory flow patterns at rest, in sniffing and in smelling within a cohort of healthy volunteers have been characterised. Furthermore, both pleasant and unpleasant odours and both pre and post decongested nasal airways were considered. Bilateral inspiratory nasal flow profiles were recorded simultaneously in high definition with hotwire anemometry. It is concluded that significant differences exist between normal inspiration and sniffing. The analysis indicated that the inspiratory profile could be broken down into three constituent phases, namely: 1) flow initiation the phase in which flow rate rapidly increases; 2) a plateau region in which a high flow rate is sustained, representative also of the vigour of inspiration; and 3) flow decay where inspiratory flow rate decreases up to the end of inspiration. A summary of the specific findings is as follows.

(1) The initiation phase can be characterised by determining the time required for the flow rate to increase to 150ml.s-1. Intense acceleration was observed in this phase. An initial rapid ramp up, typically of order ~120 ms, was found in inspiration at rest and became significantly shorter in sniffing (~60 ms), though with rates just below 20 ms in the fastest sniffs. This intense acceleration is likely to induce strong starting vortex type flow, which could dramatically enhance mixing and significantly impact on particle deposition patterns within the nose, odorant perception and heat and water exchange processes.

(2) Typical plateau phase flow rates were found to be of order 350 ml.s-1 in inspiration at rest and significantly higher in sniffing (of order 600 ml.s^{-1}). High flow rates may be maintained in sniffing with the strongest sniffs producing sustained flow rates in excess of 1 L.s^{-1} (per nostril). The mode of sniffing investigated in these studies is generally more representative of gentle to moderate sniffing and does not represent the peak nasal inspiratory flow measurements achieved with maximal exertion.

These new results have significant implications for the understanding of nasal airflow mechanics. Nearly all studies investigating transport and exchange processes in the nasal airways (e.g. aerosol deposition) model nasal inspiratory flow as a quasi-steady process, or at best have used grossly simplified approximations (e.g., sinusoidal flow rate variation). However, these results reveal that the initiation phase represents a rapid acceleration of the flow, and moreover that very high flow rates may be sustained in sniffing. It is well recognised that rapid accelerations or decelerations can destabilise laminar flows leading to an alteration from a laminar to a transitional (i.e. incompletely turbulent) state with consequential alterations to the transport of inhaled substances and the processes of heat and water exchange. To accurately predict these accumulative processes within the nasal airways the transient nature of the inspiratory profile should be considered. For instance, the temporal dynamics of the sniff are believed to be central to odorant perception, by affecting odorant intensity and component discrimination.

Chapter 6

(1) The use of krypton imaging for quantitative assessment of maxillary sinus ventilation has been successfully demonstrated and corroborated by comparison with computational modelling.

(2) The effective flow rates between the nasal cavity and maxillary sinus were found to depend on the ostial geometry. Sinus ventilation through a single natural ostium is remarkably slow. In single ostium geometries diffusion is the dominant transport mechanism as indicated by the Péclet number (Pe O(<1)). In the smallest diameter ostia Fick's Law provides a good first order estimate of diffusive exchange times. However as the diameter of the ostium increases so does the convective influence on transport. Whilst increasing ostial cross sectional area results in a proportional increase in diffusive transport rates, the increases in convective transport are more complex due to changes in flow structures.

Sinuses with two ostia, representative of a pathological accessory ostium or post-surgical inferior meatal antrostomy, provide considerably faster transport than sinuses with a single ostium as gas transport becomes convection dominated. The differences in both the transport mechanism and transport rate, between single and double ostium configurations, are due to a qualitative difference in flow. A sinus with a single ostium acts as a reservoir of fluid attached to the nose but a sinus with two ostia forms an alternative flow path to the nose. These results are in close agreement with the computational findings [47] and are contrary to much of the published otolaryngology literature in which Proetz's conclusions that an accessory ostia would not increase sinus ventilation are cited out of their original context (i.e. unrepresentative of normal breathing).

This study has potentially significant implications for the understanding of sinus ventilation and pathology.

It is hypothesised that the remarkably slow ventilation seen in the case of a natural single ostium may be protective for the sinus, preventing mucosal drying, maintaining sterility with high NO concentrations and minimising entry of pathogens. Mucociliary transport is essential in maintaining healthy sinuses and although previous work has shown it has no effect on convective or diffusive exchange times, mucus plugging would prevent gas transport and this has not been investigated in this study. Furthermore, the presence of additional ostia not only increases sinus ventilation but is also associated with disrupted mucociliary transport [45], which could prevent the removal of pathogens from the sinus.

Ventilation is vital for the healthy function of the maxillary sinus, however, there needs to be a fine balance as both insufficient and excessive ventilation may be clinically detrimental. If the slow natural ventilation of the sinus is reduced there may be a deleterious effect on mucociliary transport as a reduction in oxygen levels within the sinus will inhibit NO production, leading to a reduced concentration of NO in the sinus and a decreased ciliary beat frequency [290]. Similarly excessive ventilation due to an additional ostium or very large ostium may not be clinically beneficial, as it could: 1) increase wash-out of nitric oxide (NO), which is excreted by the mucosa of the paranasal sinuses; 2) increase access of pathogens to the sinus, which could have compound effects with NO reduction; and 3) cause mucosal drying, particularly if the upstream ostium is near the nostril and thus exposed to less well-conditioned air. Rapid sinonasal gas exchange and the resulting reduction in NO levels, could arguably contribute to the development of rhinosinusitis. More research is needed to clarify the role of an

additional ostium in sinonasal exchange processes and the effects of changing NO concentrations on sinonasal pathology.

The findings of this research have potential implications when determining the optimal size of surgical middle meatal antrostomies during Functional Endoscopic Sinus Surgery (FESS). The perfect antrostomy must be large enough to prevent scarring down and closure post operatively but must also permit mucociliary clearance and adequate gas transport. Conversely, it must not be so large as to reduce sinus NO concentrations and increase pathogen entry into the sinus. Hood *et al*. showed that a single ostium with a diameter between 3-6mm (considered physiological) had normal steady state NO concentrations whereas ostial diameters >10mm (representative of post-surgical antrostomies) were associated with reduced NO concentrations. Creating antrostomies within these narrow margins would be technically demanding but could potentially improve surgical outcomes.

Previous work has linked humming to increased sinus ventilation, with many experiments showing a subsequent increased NO transport. To date the effect of acoustics on gas transport in the upper respiratory tract has largely been ignored. Therefore the acoustic resonances of the sinus model were investigated to determine if the sinus could be acting as a Helmholtz resonator. Interestingly the resonances found were all within vocal frequencies however the significance of this in relation to physiological processes remains unknown.

Recommendations for Future Work

Current clinical technology limits the acquisition of detailed patterns of sinonasal airflow and transport in-vivo. Hence, modelling studies are required to further our understanding of these processes. It is therefore important to ensure our modelling processes are based on detailed clinical measurements that can ensure the realism of the results obtained. The dynamic changes in nasal morphology and time varying inspiratory flow rate should be utilised to enhance future models of the sinonasal airways, and hence, improve the understanding of airflow dynamics and transport mechanisms. Future efforts should focus on obtaining detailed clinical measures in order to better define normal and pathological populations.

The investigation of both nasal airway geometry changes with decongestion and the evolution of the time dependent volume flow rate waveform in inspiration has concentrated on small numbers of healthy subjects and therefore may not be applicable to pathological cases. Once parameters have been determined for the normal range, comparison with pathological

cases is essential. This would permit investigations such as determining whether imbalances in the localised burden of transport and exchange may be a manifestation or feature of disease processes. Furthermore, certain parameters could potentially be used as diagnostic criteria in the future.

The characterisation of modes of variation in normal nasal anatomy is highly desirable but requires the segmentation of a large data set and improved geometric analysis techniques. It has been shown that 3T MR imaging provides a means to acquire such measurements, but further progress requires a large increase in the number of available image datasets. This could be accomplished either by new studies or by sharing retrospective data.

Use of the hot wire technique could in principle be migrated to the clinic as a diagnostic tool. Some work would be needed to render the instrumentation more robust and portable.

An ideal model to investigate sinonasal airflow and transport would incorporate the following: consideration of the anatomy during different phases of congestion, realistic inspiratory and expiratory flow dynamics (rather than quasi-steady assumptions), incorporation of a model of the mucociliary blanket (not only for heat and water exchange, but for airborne solute uptake), and finally dynamic airway changes. Air liquid interface cell culture provides a promising technique to bridge model studies and the in-vivo milieu. To render the culture conditions more lifelike, appropriate cyclical airflow should be applied. It is conceivable that rapid prototype techniques, suitably adapted, might even be used to form a more realistic framework. This would offer considerable benefits for pharmacological and toxicological studies.

Gamma scintigraphy of krypton sinus ventilation has shown its potential to accurately determine sinus flow rates in vitro. This work now requires translation to in-vivo, in order to determine its potential as a clinical tool and approval to undertake further studies such be sought.

It has been hypothesised that excessive sinus ventilation may adversely affect sinus health via NO depletion. However, very little is known about sinus NO concentration in vivo, or the effects of NO concentration on sinus health. More research is urgently needed to establish the normal range of NO concentration, the rate of NO production, and hence the ability of the sinus to maintain appropriate levels during a variety of ventilatory regimes. This data would clarify the biological impact of an additional ostium in sinonasal exchange processes and allow the effects of changing NO concentrations to be related to sinonasal pathology. Indeed this would provide a rationale to improve antrostomy procedures.

Finally it would be interesting to further investigate acoustic resonance effects on transport within the upper respiratory tract.

It is hoped that the work presented in this thesis provides a foundation and direction for future studies on sinonasal airflow and transport.

Bibliography

1. Farley RD, Patel KR. Comparison of air warming in the human airway with a thermodynamic model. *Med Biol Eng Comput.* Nov 1988;26(6):628-632.

2. Wolf M, Naftali S, Schroter RC, Elad D. Air-conditioning characteristics of the human nose. *The Journal of Laryngology & Otology.* 2004;118(02):87-92.

3. Garcia GJM, Bailie N, Martins DA, Kimbell JS. Atrophic rhinitis: a CFD study of air conditioning in the nasal cavity. *J Appl Physiol.* September 1, 2007 2007;103(3):1082-1092.

4. Zhao K, Pribitkin EA, Cowart BJ, Rosen D, Scherer PW, Dalton P. Numerical modeling of nasal obstruction and endoscopic surgical intervention: outcome to airflow and olfaction. *Am J Rhinol.* May-Jun 2006;20(3):308-316.

5. Blanton P, L. , Biggs N, L. . Eighteen hundred years of controversy: The paranasal sinuses. *American Journal of Anatomy.* 1969;124(2):135-147.

6. Keir J. Why do we have paranasal sinuses? *Journal of laryngology & otology.* 2009;123(1):4-8.

7. Schaeffer JP. *The nose, paranasal sinuses, nasolachrymal passageways and olfactory organ in man.* Philadelphia: Blakiston Company; 1920.

8. Clark K. *The drawings of Leonardo da Vinci in the collection of Her Majesty the Queen* London: Phaidon; 1968.

9. O'Malley CD, Saunders JB. *Leonardo da Vinci, On the human body: the anatomical physiological and embryological drawings of Leonardo da Vinci.* New York: Schuman, H.; 1952.

10. Márquez S. The Paranasal Sinuses: The Last Frontier in Craniofacial Biology. *The Anatomical Record: Advances in Integrative Anatomy and Evolutionary Biology.* 2008;291(11):1350-1361.

11. Lund VJ. The maxillary sinus in the higher primates. *Acta Otolaryngol.* 1988 1988;105(1-2):163-171.

12. Proetz AW. *Essays on the applied physiology of the nose.* 2nd ed. St Louis: Annals Publishing Company; 1953.

13. Rhys Evans PH. The paranasal sinuses and other enigmas: an aquatic evolutionary theory. *J Laryngol Otol.* Mar 1992;106(3):214-225.

14. Kaliner MA, Osguthorpe JD, Fireman P, et al. Sinusitis: bench to bedside. Current findings, future directions. *J Allergy Clin Immunol.* Jun 1997;99(6 Pt 3):S829-848.

15. Anand VK. Epidemiology and economic impact of rhinosinusitits *Ann Otol Rhinol Laryngol.* 2004;113:3-5.

16. Pleis JR, Lucas JW, Ward BW. Summary health statistics for U.S. adults: National Health Interview Survey, 2008. *Vital Health Stat 10.* Dec 2009(242):1-157.

17. Lund VJ. Impact of chronic rhinosinusitis on quality of life and health care expenditure. *Clin Allergy Immunol.* 2007;20:15-24.

18. Melen I. Chronic sinusitis: clinical and pathophysiological aspects. *Acta Otolaryngol Suppl.* 1994;515:45-48.

19. Fokkens WJ, Lund VJ, Mullol J. European Position Paper on Rhinosinusitis and Nasal Polyps. *Rhinology.* 2007;Supplement 22:1-137.

20. Meltzer EO, Hamilos DL, Hadley JA, et al. Rhinosinusitis: Establishing definitions for clinical research and patient care. *Otolaryngology - Head and Neck Surgery.* 2004;131(6, Supplement 1):S1-S62.

21. Ray NF, Baraniuk JN, Thamer M, et al. Healthcare expenditures for sinusitis in 1996: Contributions of asthma, rhinitis, and other airway disorders. *Journal of Allergy and Clinical Immunology.* 1999;103(3):408-414.

22. Goetzel RZP, Hawkins KP, Ozminkowski RJP, Wang SP. The Health and Productivity Cost Burden of the "Top 10" Physical and Mental Health Conditions Affecting Six Large U.S. Employers in 1999. *Journal of Occupational & Environmental Medicine.* 2003;45(1):5-14.

23. Durr DG, Desrosiers MY, Dassa C. Impact of rhinosinusitis in health care delivery: the Quebec experience. *J Otolaryngol.* Apr 2001;30(2):93-97.

24. Rosenfeld RM. Clinical practice guideline on adult sinusitis. *Otolaryngol Head Neck Surg.* Sep 2007;137(3):365-377.

25. Gliklich RE, Metson R. Economic implications of chronic sinusitis. *Otolaryngology - Head and Neck Surgery.* 1998;118(3):344-349.

26. Gliklich RE, Metson R. The health impact of chronic sinusitis in patients seeking otolaryngologic care. *Otolaryngology - Head and Neck Surgery.* 1995;113(1):104-109.

27. Senior BA, Glaze C, Benninger MS. Use of the Rhinosinusitis Disability Index (RSDI) in rhinologic disease. *Am J Rhinol.* Jan-Feb 2001;15(1):15-20.

28. Lang J. *Clinical anatomy of the nose, nasal cavity and paranasal sinuses.* Georg Thieme Verlag; 1989.

29. Mygind N, Dahl R. Anatomy, physiology and function of the nasal cavities in health and disease. *Adv Drug Deliv Rev.* Jan 5 1998;29(1-2):3-12.

30. Mlynski G, Grutzenmacher S, Plontke S, Mlynski B, Lang C. Correlation of nasal morphology and respiratory function. *Rhinology.* Dec 2001;39(4):197-201.

31. http://www.edoctoronline.com/medical-atlas.asp?c=4&id=21657.

32. Kayser R. Die exacte messung der luftdurchgangigkeit der nase. . *Arch Laryngol Rhinol.* 1895;3:101-120.

33. Eccles R. A role for the nasal cycle in respiratory defence. *Eur Respir J.* February 1, 1996 1996;9(2):371-376.

34. Heetderks DL. Observations on the reaction of normal nasal mucus membrane. *American Journal of Medical Science.* 1927;174.

35. Stoksted P. Rhinometric measurements for determination of the nasal cycle. *Acta Otolaryngol Suppl.* 1953;109:159-175.

36. Hanif J, Jawad SS, Eccles R. The nasal cycle in health and disease. *Clin Otolaryngol Allied Sci.* Dec 2000;25(6):461-467.

37. Eccles R. Nasal airflow in health and disease. *Acta Otolaryngol.* Aug 2000;120(5):580-595.

38. Neskey D, Eloy JA, Casiano RR. Nasal, Septal, and Turbinate Anatomy and Embryology. *Otolaryngologic Clinics of North America.* 2009;42(2):193-205.

39. Jun BC, Song SW, Park CS, Lee DH, Cho KJ, Cho JH. The analysis of maxillary sinus aeration according to aging process; volume assessment by 3-dimensional reconstruction by high-resolutional CT scanning. *Otolaryngol Head Neck Surg.* Mar 2005;132(3):429-434.

40. Wormald PJ. *Endoscopic sinus surgery.* New York: Thieme; 2005.

41. Becker DG, Park SS, eds. *Revision Rhinoplasty.* 1 ed. New York: Thieme Medical Publisher Inc.; 2008.

42. Hosemann W. Surgical treatment of nasal polyposis in patients with aspirin intolerance. *Thorax.* October 1, 2000; 2000;55::S87-S90.

43. Scott-Brown WG. *Scott-Brown's Otolaryngology.* Vol 1: Butterworths; 1987.

44. Genc S, Ozcan M, Titiz A, Unal A. Development of maxillary accessory ostium following sinusitis in rabbits. *Rhinology.* Jun 2008;46(2):121-124.

45. Matthews BL, Burke AJ. Recirculation of mucus via accessory ostia causing chronic maxillary sinus disease. *Otolaryngol Head Neck Surg.* Oct 1997;117(4):422-423.

46. Chung SK, Dhong HJ, Na DG. Mucus circulation between accessory ostium and natural ostium of maxillary sinus. *J Laryngol Otol.* Sep 1999;113(9):865-867.

47. Hood CM. *Modelling the Ventilation of Human Maxillary Sinuses*: Bioengineering, Imperial College London; 2010.

48. Blenke EJSM. *Analysis of Sinonasal Airway Geometry and Exchange Processes*: Aeronautics, Imperial College London; 2011.

49. Van Alyea OE. The ostium maxillare: anatomic study of its surgical accessibility. *Archives of Otolaryngology.* 1936;24(5):555-569.

50. Rantanen T. Clinical function tests of the maxillary sinus ostium. *Acta Otolaryngol Suppl.* 1974;328:1-38.

51. Myerson MC. The natural orifice of the maxillary sinus I : anatomic studies. *Archives of Otolaryngology.* 1932;15:80-91.

52. Myerson MC. The natural orifice of the maxillary sinus II : clinical studies. *Archives of Otolaryngology.* 1932;15:716-733.

53. Simon E. Anatomy of the opening of the maxillary sinus. *Archives of Otolaryngology.* 1939;29:640-649.

54. André RF, Vuyk HD, Ahmed A, Graamans K, Trenité GJN. Correlation between subjective and objective evaluation of the nasal airway. A systematic review of the highest level of evidence. *Clinical Otolaryngology.* 2009;34(6):518-525.

55. Flottes L, Clerk P, Riu R, Devilla F. La physiologic des sinus. *Librairie Arnette, Paris.* 1960. .

56. Aust R, Drettner B. Experimental studies of the gas exchange through the ostium of the maxillary sinus. *Ups J Med Sci.* 1974;79(3):177-186.

57. Aust R, Drettner B. The functional size of the human maxillary ostium in vivo. *Acta Otolaryngol.* Nov-Dec 1974;78(5-6):432-435.

58. May M, Sobol SM, Korzec K. The location of the maxillary os and its importance to the endoscopic sinus surgeon. *Laryngoscope.* Oct 1990;100(10 Pt 1):1037-1042.

59. Earwaker J. Anatomic variants in sinonasal CT. *Radiographics.* Mar 1993;13(2):381-415.

60. Jog M, McGarry GW. How frequent are accessory sinus ostia? *The Journal of Laryngology & Otology.* 2003;117(04):270-272.

61. Eccles R. Nasal airway resistance and nasal sensation of airflow. *Rhinol Suppl.* 1992;14:86-90.

62. Proctor D, F.,. Form and function in the upper airways and larynx. In: Fishman AP, ed. *The Handbook of Physiology Section 3: The Respiratory System Volume III. The Mechanics of Breathing, Part 1*. Maryland: The American Physiological Society; 1986:63-73.

63. Krouse JH. The unified airway--conceptual framework. *Otolaryngol Clin North Am.* Apr 2008;41(2):257-266, v.

64. de Benedictis FM, Bush A. Rhinosinusitis and Asthma*. *Chest.* February 1999 1999;115(2):550-556.

65. Tsao C-H, Chen L-C, Yeh K-W, Huang J-L. Concomitant Chronic Sinusitis Treatment in Children With Mild Asthma*. *Chest.* March 2003 2003;123(3):757-764.

66. Dixon AE, Kaminsky DA, Holbrook JT, Wise RA, Shade DM, Irvin CG. Allergic Rhinitis and Sinusitis in Asthma*. *Chest.* August 2006 2006;130(2):429-435.

67. Naftali S, Schroter RC, Shiner RJ, Elad D. Transport Phenomena in the Human Nasal Cavity: A Computational Model. *Annals of Biomedical Engineering.* 1998;26(5):831-839.

68. Keck T. Temperature Profile in the Nasal Cavity. *The Laryngoscope.* 2000;110(4):651.

69. Elad D, Wolf M, Keck T. Air-conditioning in the human nasal cavity. *Respiratory Physiology & Neurobiology.* 2008;163(1-3):121-127.

70. Williams R, Rankin N, Smith T, Galler D, Seakins P. Relationship between the humidity and temperature of inspired gas and the function of the airway mucosa. *Crit Care Med.* Nov 1996;24(11):1920-1929.

71. Cole P. Temperature and humidity of respiratory air. *J Physiol.* 1953;122(Suppl):51P.

72. Cole P. Biophysics of nasal airflow: a review. *Am J Rhinol.* Jul-Aug 2000;14(4):245-249.

73. Drettner B, Falck B, Simon H. Measurements of the air conditioning capacity of the nose during normal and pathological conditions and pharmacological influence. *Acta Otolaryngol.* Sep-Oct 1977;84(3-4):266-277.

74. Keck T, Leiacker R, Heinrich A, Kuhnemann S, Rettinger G. Humidity and temperature profile in the nasal cavity. *Rhinology.* Dec 2000;38(4):167-171.

75. Quraishi MS, Jones NS, Mason J. The rheology of nasal mucus: a review. *Clin Otolaryngol Allied Sci.* Oct 1998;23(5):403-413.

76. Mall MA. Role of cilia, mucus, and airway surface liquid in mucociliary dysfunction: lessons from mouse models. *Journal of aerosol medicine and pulmonary drug delivery.* Mar 2008;21(1):13-24.

77. Illum L. Nasal drug delivery--possibilities, problems and solutions. *Journal of Controlled Release.* 2003;87(1-3):187-198.

78. Proctor DF. The upper airways. I. Nasal physiology and defense of the lungs. *Am Rev Respir Dis.* Jan 1977;115(1):97-129.

79. Jones N, Rog D. Olfaction: a review. *J Laryngol Otol.* Jan 1998;112(1):11-24.

80. Sundberg J, Birch P, Gumoes B, Stavad H, Prytz S, Karle A. Experimental findings on the nasal tract resonator in singing. *J Voice.* Mar 2007;21(2):127-137.

81. Feng G, Castelli E. Some acoustic features of nasal and nasalized vowels: a target for vowel nasalization. *J Acoust Soc Am.* Jun 1996;99(6):3694-3706.

82. Pruthi T, Espy-Wilson CY, Story BH. Simulation and analysis of nasalized vowels based on magnetic resonance imaging data. *J Acoust Soc Am.* Jun 2007;121(6):3858-3873.

83. White FM. *Fluid Mechanics.* 6th ed: McGraw Hill; 2007.

84. http://www-mdp.eng.cam.ac.uk/web/library/enginfo/aerothermal_dvd_only/aero/fprops/pipeflow.

85. Reynolds O. An Experimental Investigation of the Circumstances Which Determine Whether the Motion of Water Shall Be Direct or Sinuous, and of the Law of Resistance in Parallel Channels. *Philosophical Transactions of the Royal Society of London.* 1883;174:935-982.

86. Schlichting H. *Boundary-Layer Theory. .* 7th ed: McGraw-Hill 1979.

87. Schreck S, Sullivan KJ, Ho CM, Chang HK. Correlations between flow resistance and geometry in a model of the human nose. *J Appl Physiol.* October 1, 1993 1993;75(4):1767-1775.

88. Hahn I, Scherer P, Mozell M. Velocity profiles measured for airflow through a large-scale model of the human nasal cavity. *Journal of applied physiology.* 1993;75(5):2273.

89. Doorly D, Taylor DJ, Franke P, Schroter RC. Experimental investigation of nasal airflow. *Proc Inst Mech Eng [H].* May 2008;222(4):439-453.

90. Doorly DJ, Taylor DJ, Schroter RC. Mechanics of airflow in the human nasal airways. *Respir Physiol Neurobiol.* Nov 30 2008;163(1-3):100-110.

91. Taylor DJ, Doorly DJ, Schroter RC. Inflow boundary profile prescription for numerical simulation of nasal airflow. *Journal of The Royal Society Interface.* March 6, 2010 2010;7(44):515-527.

92. Doorly DJ, Taylor DJ, Gambaruto AM, Schroter RC, Tolley N. Nasal architecture: form and flow. *Philos Transact A Math Phys Eng Sci.* Sep 28 2008;366(1879):3225-3246.

93. Guilmette RA, Wicks JD, Wolff RK. Morphometry of Human Nasal Airways In Vivo Using Magnetic Resonance Imaging. *Journal of Aerosol Medicine.* 1989;2(4):365-377.

94. Saunders MW, Jones NS, Kabala JE. Parameters of nasal airway anatomy on magnetic resonance imaging correlate poorly with subjective symptoms of nasal patency. *Clinical Otolaryngology & Allied Sciences.* 1999;24(5):431-434.

95. Hilberg O, Jensen FT, Pedersen OF. Nasal airway geometry: comparison between acoustic reflections and magnetic resonance scanning. *J Appl Physiol.* 1993 1993;75(6):2811-2819.

96. Caenen M, Hamels K, Deron P, Clement P. Comparison of decongestive capacity of xylometazoline and pseudoephedrine with rhinomanometry and MRI. *Rhinology.* 2005 2005;43(3):205-209.

97. Lindemann J, Tsakiropoulou E, Vital V, et al. Influence of the turbinate volumes as measured by magnetic resonance imaging on nasal air conditioning. *Am J Rhinol Allergy.* May-Jun 2009;23(3):250-254.

98. Naftali S, Rosenfeld M, Wolf M, Elad D. The Air-Conditioning Capacity of the Human Nose. *Annals of Biomedical Engineering.* 2005;33(4):545-553.

99. Shi H, Kleinstreuer C, Zhang Z. Modeling of inertial particle transport and deposition in human nasal cavities with wall roughness. *Journal of Aerosol Science.* 2007;38(4):398-419.

100. Afzelius BA, Mossberg B. Immotile cilia. *Thorax.* Jun 1980;35(6):401-404.

101. Brem MH, Zamani AA, Riva R, et al. Multidetector CT of the paranasal sinus: potential for radiation dose reduction. *Radiology.* Jun 2007;243(3):847-852.

102. Rowe-Jones J, Mackay I, Colquhoun I. Charing Cross CT protocol for endoscopic sinus surgery. *J Laryngol Otol.* Nov 1995;109(11):1057-1060.

103. Lund VJ, Savy L, Lloyd G. Imaging for endoscopic sinus surgery in adults. *J Laryngol Otol.* May 2000;114(5):395-397.

104. Lloyd G, Lund VJ, Howard D, Savy L. Optimum imaging for sinonasal malignancy. *J Laryngol Otol.* Jul 2000;114(7):557-562.

105. Quine SM, Aitken PM, Eccles R. Effect of submucosal diathermy to the inferior turbinates on unilateral and total nasal airflow in patients with rhinitis. *Acta Otolaryngol.* 1999;119(8):911-915.

106. Starling-Schwanz R, Peake HL, Salome CM, et al. Repeatability of peak nasal inspiratory flow measurements and utility for assessing the severity of rhinitis. *Allergy.* Jun 2005;60(6):795-800.

107. Holmstrom M, Scadding GK, Lund VJ, Darby YC. Assessment of nasal obstruction. A comparison between rhinomanometry and nasal inspiratory peak flow. *Rhinology.* 1990 1990;28(3):191-196.

108. Cho SI, Hauser R, Christiani DC. Reproducibility of nasal peak inspiratory flow among healthy adults: assessment of epidemiologic utility. *Chest.* Dec 1997;112(6):1547-1553.

109. Harar RP, Kalan A, Kenyon GS. Assessing the reproducibility of nasal spirometry parameters in the measurement of nasal patency. *Rhinology.* Dec 2001;39(4):211-214.

110. Porter MJ, Williamson IG, Kerridge DH, Maw AR. A comparison of the sensitivity of manometric rhinometry, acoustic rhinometry, rhinomanometry and nasal peak flow to detect the decongestant effect of xylometazoline. *Clinical Otolaryngology & Allied Sciences.* 1996;21(3):218-221.

111. Ottaviano G, Scadding GK, Coles S, Lund VJ. Peak nasal inspiratory flow; normal range in adult population. *Rhinology.* Mar 2006;44(1):32-35.

112. Jones AS, Viani L, Phillips D, Charters P. The objective assessment of nasal patency. *Clin Otolaryngol Allied Sci.* Apr 1991;16(2):206-211.

113. Kjaergaard T, Cvancarova M, Steinsvag SK. Relation of Nasal Air Flow to Nasal Cavity Dimensions. *Arch Otolaryngol Head Neck Surg.* June 1, 2009 2009;135(6):565-570.

114. Day JH, Briscoe MP, Rafeiro E, Ellis AK, Pettersson E, Akerlund A. Onset of action of intranasal budesonide (Rhinocort aqua) in seasonal allergic rhinitis studied in a controlled exposure model. *J Allergy Clin Immunol.* Mar 2000;105(3):489-494.

115. Bende M, Carrillo T, Vona I, da Castel-Branco MG, Arheden L. A randomized comparison of the effects of budesonide and mometasone furoate aqueous nasal sprays on nasal peak flow rate and symptoms in perennial allergic rhinitis. *Annals of allergy, asthma & immunology : official publication of the American College of Allergy, Asthma, & Immunology.* Jun 2002;88(6):617-623.

116. Lund VJ, Flood J, Sykes AP, Richards DH. Effect of fluticasone in severe polyposis. *Arch Otolaryngol Head Neck Surg.* May 1998;124(5):513-518.

117. Marais J, Murray JA, Marshall I, Douglas N, Martin S. Minimal cross-sectional areas, nasal peak flow and patients' satisfaction in septoplasty and inferior turbinectomy. *Rhinology.* Sep 1994;32(3):145-147.

118. Phagoo SB, Watson RA, Pride NB. Use of nasal peak flow to assess nasal patency. *Allergy.* Sep 1997;52(9):901-908.

119. Clarke RW, Jones AS. The limitations of peak nasal flow measurement. *Clin Otolaryngol Allied Sci.* Dec 1994;19(6):502-504.

120. Hilberg O, Jackson AC, Swift DL, Pedersen OF. Acoustic rhinometry: evaluation of nasal cavity geometry by acoustic reflection. *J Appl Physiol.* 1989 1989;66(1):295-303.

121. Tarhan E, Coskun M, Cakmak O, Celik H, Cankurtaran M. Acoustic rhinometry in humans: accuracy of nasal passage area estimates, and ability to quantify paranasal sinus volume and ostium size. *J Appl Physiol.* Aug 2005;99(2):616-623.

122. Terheyden H, Maune S, Mertens J, Hilberg O. Acoustic rhinometry: validation by three-dimensionally reconstructed computer tomographic scans. *J Appl Physiol.* Sep 2000;89(3):1013-1021.

123. Fisher EW, Daly NJ, Morris DP, Lund VJ. Experimental Studies of the Resolution of Acoustic Rhinometry In Vivo. *Acta oto-laryngologica.* 1994;114(4):647-650.

124. Fisher EW, Lund VJ, Scadding GK. Acoustic rhinometry in rhinological practice: discussion paper. *J R Soc Med.* 1994 1994;87(7):411-413.

125. Gilain L, Coste A, Ricolfi F, et al. Nasal cavity geometry measured by acoustic rhinometry and computed tomography. *Arch Otolaryngol Head Neck Surg.* Apr 1997;123(4):401-405.

126. Corey JP, Gungor A, Nelson R, Fredberg J, Lai V. A comparison of the nasal cross-sectional areas and volumes obtained with acoustic rhinometry and magnetic resonance imaging. *Otolaryngology - Head and Neck Surgery.* 1997;117(4):349-354.

127. Corey JP. Acoustic rhinometry: should we be using it? *Current Opinion in Otolaryngology & Head & Neck Surgery.* 2006;14(1):29-34.

128. Hilberg O, Pedersen OF. Acoustic rhinometry: recommendations for technical specifications and standard operating procedures. *Rhinol Suppl.* Dec 2000;16:3-17.

129. Clement PA, Gordts F. Consensus report on acoustic rhinometry and rhinomanometry 169-179 *Rhinology.* 2005;43(3):169-179.

130. Vogt K, Jalowayski AA, Althaus W, et al. 4-Phase-Rhinomanometry (4PR)--basics and practice 2010. *Rhinol Suppl.* 2010(21):1-50.

131. Clement PA, Hirsch C. Rhinomanometry--a review. *ORL.* 1984;46(4):173-191.

132. Clement PA. Committee report on standardization of rhinomanometry. *Rhinology.* Sep 1984;22(3):151-155.

133. Hopkins C, Gillett S, Slack R, Lund VJ, Browne JP. Psychometric validity of the 22-item Sinonasal Outcome Test. *Clinical Otolaryngology.* 2009;34(5):447-454.

134. Piccirillo JF, Merritt MG, Jr., Richards ML. Psychometric and clinimetric validity of the 20-Item Sino-Nasal Outcome Test (SNOT-20). *Otolaryngol Head Neck Surg.* Jan 2002;126(1):41-47.

135. Juniper EF. Measuring health-related quality of life in rhinitis. *J Allergy Clin Immunol.* Feb 1997;99(2):S742-749.

136. Benninger MS, Senior BA. The development of the Rhinosinusitis Disability Index. *Arch Otolaryngol Head Neck Surg.* Nov 1997;123(11):1175-1179.

137. Doty RL, Shaman P, Dann M. Development of the University of Pennsylvania Smell Identification Test: a standardized microencapsulated test of olfactory function. *Physiol Behav.* Mar 1984;32(3):489-502.

138. Doty RL, Shaman P, Kimmelman CP, Dann MS. University of Pennsylvania Smell Identification Test: a rapid quantitative olfactory function test for the clinic. *Laryngoscope.* Feb 1984;94(2 Pt 1):176-178.

139. Doty RL, Shaman P, Applebaum SL, Giberson R, Siksorski L, Rosenberg L. Smell identification ability: changes with age. *Science.* Dec 21 1984;226(4681):1441-1443.

140. Wright HN. Characterization of olfactory dysfunction. *Arch Otolaryngol Head Neck Surg.* Feb 1987;113(2):163-168.

141. Scadding G. Nitric oxide in the airways. *Curr Opin Otolaryngol Head Neck Surg.* Aug 2007;15(4):258-263.

142. Scadding G, Scadding GK. Update on the use of nitric oxide as a noninvasive measure of airways inflammation. *Rhinology.* Jun 2009;47(2):115-120.

143. Phillips PS, Sacks R, Marcells GN, Cohen NA, Harvey RJ. Nasal Nitric Oxide and Sinonasal Disease. *Otolaryngology -- Head and Neck Surgery.* February 1, 2011 2011;144(2):159-169.

144. Wheeler SM, Corey JP. Evaluation of upper airway obstruction--An ENT perspective. *Pulmonary Pharmacology & Therapeutics.* 2008;21(3):433-441.

145. Lundberg JO, Farkas-Szallasi T, Weitzberg E, et al. High nitric oxide production in human paranasal sinuses. *Nat Med.* Apr 1995;1(4):370-373.

146. MacMicking JD, Nathan C, Hom G, et al. Altered responses to bacterial infection and endotoxic shock in mice lacking inducible nitric oxide synthase. *Cell.* May 19 1995;81(4):641-650.

147. Belvisi MG, Stretton CD, Yacoub M, Barnes PJ. Nitric oxide is the endogenous neurotransmitter of bronchodilator nerves in humans. *Eur J Pharmacol.* Jan 14 1992;210(2):221-222.

148. Runer T, Cervin A, Lindberg S, Uddman R. Nitric oxide is a regulator of mucociliary activity in the upper respiratory tract. *Otolaryngol Head Neck Surg.* Sep 1998;119(3):278-287.

149. Deja M, Busch T, Bachmann S, et al. Reduced Nitric Oxide in Sinus Epithelium of Patients with Radiologic Maxillary Sinusitis and Sepsis. *Am. J. Respir. Crit. Care Med.* August 1, 2003 2003;168(3):281-286.

150. Ragab SM, Lund VJ, Saleh HA, Scadding G. Nasal nitric oxide in objective evaluation of chronic rhinosinusitis therapy. *Allergy.* Jun 2006;61(6):717-724.

151. Hood CM, Schroter RC, Doorly DJ, Blenke EJSM, Tolley NS. Computational modeling of flow and gas exchange in models of the human maxillary sinus. *J Appl Physiol.* October 1, 2009 2009;107(4):1195-1203.

152. Ingersoll JM. The function of the accessory cavities of the nose. *Ann Otol Rhinol Laryngol* 1906 15:757–770.

153. Ingersoll JM. Some points in the comparative anatomy of the nose and the accessory sinuses which account for the variations in these structures in man. *Trans Am Laryngol Rhinol Otol Soc.* 1922 28 162–167.

154. Negus V. The function of the paranasal sinuses. *Arch Otolaryngol Head Neck Surg.* 1957(66):430–442.

155. Negus V. *The comparative anatomy and physiology of the nose and paranasal sinuses* London: E & S Livingstone LTD; 1958

156. Takahashi RYO. The formation of the human paranasal sinuses. *Acta Otolaryngol (Stockh.)* 1983 408(Suppl): 2–28.

157. Da Vinci L. *Quaderni d'anatomia. I-VI.*: Vangensten, C. L. Fonahn, A. Hopstock, H. Dybwad, C.F. ; 1489.

158. Braune W, Clasen FE. Die Nebelhohlen der mensclichen Nase in iherer Bedeutung fur den mechanismus des Riechens *Z. Anat Entwicklungsgesch.* 1877;2:1.

159. Strickland GW. Accesssory nasal sinus infections in children. *J M Soc New Jersey* 1932 29:108–111.

160. O'Malley JF. Evolution of the nasal cavities and sinuses in relation to function. *J Laryngol Otol* 1924 39 57–64.

161. Eckert-Mobius A. Comparative study of the nasal sinuses in man and in animals *Arch f OhrenNasen-u Kehlkopfh* 1933;134: 287–307.

162. Sato C. Vergleichende Studien über die Morphologie und den Bau der Schleimhaut der Nasennebenhöhlen bei verschiedenen Tieren (Saugetieren, Vogeln und Amphibien.) *Mitt a.d. Med Akad zu Kioto* 1938 22:227.

163. Proetz AW. Observations upon the formation and function of the accessory nasal sinuses and the mastoid cells *Ann Otol Rhinol Laryngol* 1922 31: 1083–1096.

164. Proetz AW. Nasal physiology and its relation to the surgery of the accessory nasal sinuses. *Proc Roy Soc Med J Laryngol Otol* 1938 31 1408–1416.

165. Proetz AW. *Applied Physiology of the Nose.* St Louis, MO.: Annals Publishing Co; 1941.

166. Gannon PJ, Doyle WJ, Ganjian E, al. e. Maxillary sinus mucosal blood flow during nasal vs tracheal respiration. *Archives of Otolaryngology–Head & Neck Surgery.* 1997;123(12):1336-1340.

167. Cleland J. On the Relations of the Vomer, Ethmoid, and Intermaxillary Bones. *Philosophical Transactions of the Royal Society of London.* January 1, 1862 1862;152:289-321.

168. Bignon F. Contribution a l'étude de la pneumaticité chez les oiseaux. Les cellules aëriennes cervico-céphalique des oiseaux et leurs rapports avec les os de la tête. . *Mémoires de la Société Zoolologique de France.* 1889 2:260–320.

169. Zuckerkandl E. *Normale und Pathologische Anatomie der Nasenhöhlen und ihrer Pneumatischen Anhänge. .* Wien und Leipzig: Wilhelm Braumüller.; 1892.

170. Dieulafé L. Morphology and Embryology of the Nasal Fossae of Vertebrates. (Translated by Loeb HB. St. Louis: St. Louis University). *Reprinted from Ann Otol Rhinol Laryngol.* 1906.

171. Hartz HJ. Remarks on the physiology and development of the nose and accessory sinuses and nasal reflexes, with special reference to the function and importance of the turbinated bodies. . *Ann Otol Rhinol Otolaryngol* 1909;18 709–738.

172. Wegner RN. Die Nebenhöhlen der Nase bei den Krokodilen. . *Wissensch Z Ernst Moritz Arndt Univ Greifswald* 1958 7 1–39.

173. Leakey M, Walker A. Afropithecus—Function and phylogeny In: Begun DR, Ward CV, Rose MD, eds. *Function, phylogeny, and fossils*. New York Plenum Press.; 1997.

174. Coffin LA. The development of the accessory sinuses of nose. . *Am J Med Sci Feb* 1905 129:297–312.

175. Neumayer. Ueber den Luftwechsel in den Nebenhohlen. . *Mon f Ohrenhk* 1901:504.

176. Suarez ADC. Una nueva teoria sobre la posible function de los senos para-nasales y celdas mastoidaas. *Rev Espan Oto-neuro-oftal* 1952 11: 336.

177. Del Canizo A. [Various new concepts on sinusal & mastoid cell physiology]. *Archivio italiano di otologia, rinologia e laringologia.* Jan-Feb 1959;70(1):20-26.

178. Alger LJ. A new theory of physiology of the sinuses. *Lancet* 1943. ;58 511–512.

179. Lundberg JO, Rinder J, Weitzberg E, Lundberg JM, Alving K. Nasally exhaled nitric oxide in humans originates mainly in the paranasal sinuses. *Acta Physiol Scand.* Dec 1994;152(4):431-432.

180. Onodi A. Des rapports entre le nerf optique et le sinus sphénoïdal. La cellule ethmoïdale postérieure en particulier. *Revue hebd de Laryng d'Otol et de Rhino.* 1903;25:721–740.

181. Nemours PR. A comparison of the accessory nasal sinuses of man with those of lower vertebrates. . *Trans Am Laryngol Rhinol Otol Soc.* 1931 195–199.

182. Shea JJ. Morphologic characteristics of the sinuses. *Arch Otolaryngol Head Neck Surg.* 1936 23:484–487.

183. Eckley WT. On the accessory sinuses. . *Chicago Med Recorder.* 1904; 26: 243–253.

184. Blaney SP. An allometric study of the frontal sinus in Gorilla, Pan and Pongo. *Folia primatologica; international journal of primatology.* 1986;47(2-3):81-96.

185. Blaney SP. Why paranasal sinuses? *J Laryngol Otol.* Sep 1990;104(9):690-693.

186. Davis WE, Templer J, Parsons DS. Anatomy of the paranasal sinuses. *Otolaryngologic Clinics of North America.* Feb 1996;29(1):57-&.

187. Witmer LM. Homology of facial structures in extant archosauraurs (birds and crocodiles) with special reference to paranasal pneumaticity and nasal conchae. *J. Morphol.* Sep 1995;225(3):269-327.

188. Witmer LM. *The extant phylogenetic bracket and the importance of reconstructing soft tissues in fossils.* Cambridge: Cambridge Univ Press; 1995.

189. Witmer LM. The evolution of the antorbital cavity of archosaurs: A study in soft-tissue reconstruction in the fossil record with an analysis of the function of pneumaticity. *J. Vertebr. Paleontol.* Apr 1997;17(1):1-73.

190. Rui R, Den L, Gourlaouen L. Contribution à l'étude du rôle des sinus paraassaux. . *Revue de Laryngologie et Oto-Rhinologie* 1960;81 796–839.

191. Kellman RM, Schmidt C. The paranasal sinuses as a protective crumple zone for the orbit. *The Laryngoscope.* 2009;119(9):1682-1690.

192. Bremer JL. The pneumatization of the head of the common fowl. *J. Morphol.* 1940;67(1):143-157.

193. Proetz AW. Some intimate studies of nasal function:their bearing on diagnosis and treatment . *Annals of Otology, Rhinology and Laryngology.* 1932;xli(1):125-139.

194. Drettner B. Measurements of the resistance of the maxillary ostium. *Acta Otolaryngol.* Dec 1965;60(6):499-505.

195. Bachert C. [Experimental studies of the effect of nasal respiratory obstruction on ventilation of the maxillary sinus]. *Laryngologie, Rhinologie, Otologie.* May 1986;65(5):250-255.

196. Tornberg DCF, Marteus H, Schedin U, Alving K, Lundberg JON, Weitzberg E. Nasal and oral contribution to inhaled and exhaled nitric oxide: a study in tracheotomized patients. *Eur Respir J.* May 1, 2002 2002;19(5):859-864.

197. Svanholm H, Falck B, Aust R. Ventilatory effects of the pulse wave in the maxillary sinus. *Rhinology.* Mar 1981;19(1):41-46.

198. Musebeck K, Rosenberg H. Measurement of air flow in the maxillary sinus by hot-film technique. *Rhinology.* Mar 1978;16(1):11-18.

199. Musebeck K, Rosenberg H. [Examination of patency of ostium by measurement of air flow in the maxillary sinus (author's transl)]. *Laryngologie, Rhinologie, Otologie.* May 1978;57(5):383-390.

200. Zippel R, Streckenbach B. 133Xenon washout in the paranasal sinuses--a diagnostic tool for assessing ostial function. *Rhinology.* Mar 1979;17(1):25-29.

201. Paulsson B, Bende M, Larsson I, Ohlin P. Ventilation of the paranasal sinuses studied with dynamic emission computer tomography. *Laryngoscope.* 1992 1992;102(4):451-457.

202. Paulsson B, Dolata J, Larsson I, Ohlin P, Lindberg S. Paranasal sinus ventilation in healthy subjects and in patients with sinus disease evaluated with the 133-xenon washout technique. *The Annals of otology, rhinology & laryngology.* 2001;110(7 Pt 1):667-674.

203. Paulsson B, Lindberg S, Ohlin P. Washout of 133-xenon as an objective assessment of paranasal sinus ventilation in endoscopic sinus surgery. *The Annals of otology, rhinology & laryngology.* 2002;111(8):710-717.

204. Marcucci C, Leopold DA, Cullen M, Zinreich SJ, Simon BA. Dynamic assessment of paranasal sinus ventilation using xenon-enhanced computed tomography. *The Annals of otology, rhinology & laryngology.* 2001;110(10):968-975.

205. Leopold D, Zinreich SJ, Simon BA, Cullen MM, Marcucci C. Xenon-enhanced computed tomography quantifies normal maxillary sinus ventilation. *Otolaryngology--head and neck surgery.* 2000;122(3):422-424.

206. Rizi RR, Dimitrov IE, Thompson A, et al. MRI of hyperpolarized 3He gas in human paranasal sinuses. *Magn Reson Med.* Jun 1998;39(6):865-868.

207. Hanke A, Gast K, Viallon M, et al. [Dynamic imaging of the nasal cavity and the paranasal sinuses with polarized 3helium MRI]. *RoFo : Fortschritte auf dem Gebiete der Rontgenstrahlen und der Nuklearmedizin.* Dec 2001;173(12):1126-1130.

208. Möller W, Schuschnig U, Meyer G, Mentzel H, Keller M. Ventilation and drug delivery to the paranasal sinuses: studies in a nasal cast using pulsating airflow. *Rhinology.* 2008;46(3):213-220.

209. Moller W, Schuschnig U, Meyer G, et al. Ventilation and aerosolized drug delivery to the paranasal sinuses using pulsating airflow – a preliminary study. *Rhinology.* 2009;47(4):405-412.

210. Moller W, Schuschnig U, Khadem Saba G, et al. Pulsating aerosols for drug delivery to the sinuses in healthy volunteers. *Otolaryngol Head Neck Surg.* 2010 2010;142(3):382-388.

211. Moller W, Munzing W, Canis M. Clinical potential of pulsating aerosol for sinus drug delivery. *Expert Opinion on Drug Delivery.* 2010;7(11):1239-1245.

212. Moller W, Saba GK, Haussinger K, Becker S, Keller M, Schuschnig U. Nasally inhaled pulsating aerosols: lung, sinus and nose deposition. *Rhinology.* Aug 2011;49(3):286-291.

213. Blenke E, Rennie CE, Hood CM, et al. Analysis of sinonasal airflow using Krypton81m; a pilot study. *Clinical Otolaryngology.* 2009;34(s1):47-138.

214. Fazio F, Jones T. Assessment Of Regional Ventilation By Continuous Inhalation Of Radioactive Krypton-81m. *The British Medical Journal.* 1975;3(5985):673-676.

215. Rennie CE, Hood CM, Blenke EJSM, et al. Physical and Computational Modeling of Ventilation of the Maxillary Sinus. *Otolaryngology -- Head and Neck Surgery.* February 1, 2011 2011.

216. Fokkens WJ, Lund VJ, Mullol J, et al. EPOS 2012: European position paper on rhinosinusitis and nasal polyps 2012. A summary for otorhinolaryngologists. *Rhinology.* Mar 2012;50(1):1-12.

217. Smith TL, Litvack JR, Hwang PH, et al. Determinants of outcomes of sinus surgery: a multi-institutional prospective cohort study. *Otolaryngol Head Neck Surg.* Jan 2010;142(1):55-63.

218. Hopkins C, Slack R, Lund V, Brown P, Copley L, Browne J. Long-term outcomes from the English national comparative audit of surgery for nasal polyposis and chronic rhinosinusitis. *The Laryngoscope.* 2009;119(12):2459-2465.

219. Gillett S, Hopkins C, Slack R, Browne JP. A pilot study of the SNOT 22 score in adults with no sinonasal disease. *Clinical Otolaryngology.* 2009;34(5):467-469.

220. Scadding G, Hellings P, Alobid I, et al. Diagnostic tools in Rhinology EAACI position paper. *Clin Transl Allergy.* 2011;1(1):2.

221. Djupesland PG, Rotnes JS. Accuracy of acoustic rhinometry. *Rhinology.* Mar 2001;39(1):23-27.

222. Bende M. The effect of topical decongestant on blood flow in normal and infected nasal mucosa. *Acta Otolaryngol.* Nov-Dec 1983;96(5-6):523-527.

223. Bende M, Loth S. Vascular effects of topical oxymetazoline on human nasal mucosa. *J Laryngol Otol.* Mar 1986;100(3):285-288.

224. Falck B, Svanholm H, Aust R. The effect of Xylometazoline on the mucosa of human maxillary sinus. *Rhinology.* Dec 1990;28(4):239-247.

225. Paulsson B, Lindberg S, Ohlin P. Effects of oxymetazoline on the ventilation of paranasal sinuses in healthy subjects. *Am J Rhinol.* Mar-Apr 2002;16(2):125-129.

226. Kindlmann GL, Durkin JW. *Semi-Automatic Generation of Transfer Functions for Direct Volume Rendering.* Cornell University; 1999.

227. Prokop M. Multislice CT: technical principles and future trends. *European radiology.* Dec 2003;13 Suppl 5:M3-13.

228. Bloomfield DM, Magnano A, Bigger JT, Jr., Rivadeneira H, Parides M, Steinman RC. Comparison of spontaneous vs. metronome-guided breathing on assessment of vagal modulation using RR variability. *Am J Physiol Heart Circ Physiol.* Mar 2001;280(3):H1145-1150.

229. Parvez L, Erasala G, Noronha A. Novel techniques, standardization tools to enhance reliability of acoustic rhinometry measurements. *Rhinol Suppl.* Dec 2000;16:18-28.

230. Fisher EW, Morris DP, Biemans JM, Palmer CR, Lund VJ. Practical aspects of acoustic rhinometry: problems and solutions. *Rhinology.* Dec 1995;33(4):219-223.

231. Bruun H. *Hot-Wire Anemometry Principles and Signal Analysis* Oxford: Oxford University Press; 1995.

232. http://www.dantecdynamics.com/Files/Billeder/support_and_download /resarch_and_education/measurement_principles/cta/overveiw[1].jpg.

233. Rantanen T. Ostial Resistance. *Acta oto-laryngologica.* 1977;83(1-6):536-540.

234. Sharp PF, Gemmell HG, Smith FW, eds. *Practical nuclear medicine.* Oxford: IRL Press at Oxford University Press; 1989.

235. http://www.med.harvard.edu/JPNM/physics.

236. Amis TC, Jones T. Krypton-81m as a flow tracer in the lung: theory and quantitation. *Bulletin Europeen de Physiopatholigie Respiratoire.* May-Jun 1980;16(3):245-259.

237. Titze IR. *Principles of Voice Production.* Prentice Hall; 1994.

238. Baken RJ, Orlikoff RF. *Clinical Measurement of Speech and Voice.* 2nd ed. San Diego: Singular Publishing Group; 2000.

239. Hood CM, Schroter RC, Doorly DJ, Rennie CE, Blenke EJ, Tolley NS. Modeling of Human Maxillary Sinus Nitric Oxide Transport *Conference proceedings 6th World Conference of Biomechanics. .* 2010.

240. Coulson JM, Richardson JF. *Chemical Engineering.* Vol 3. Oxford Pergamon Press; 1971.

241. Croce C, Fodil R, Durand M, et al. In Vitro Experiments and Numerical Simulations of Airflow in Realistic Nasal Airway Geometry. *Annals of Biomedical Engineering.* 2006;34(6):997-1007.

242. Taylor DJ. *Experimental and Computational Analysis of Human Nasal Inspiration*: Aeronautics, Imperial College London; 2008.

243. Tritton DJ. *Physical Fluid Dynamics.* Oxford: Oxford University Press; 1988.

244. Loudon C, McCullogh K. Application of the Hagen-Poiseuille equation to fluid feeding through short tubes. *Annals of the Entomological Society of America.* 1999;92:153-158.

245. Inglestedt S. Studies on the conditioning of air in the respiratory tract. *Acta Otolaryngol (Stock)* 1956;131:7.

246. Cole P, Forsyth R, Haight JS. Respiratory resistance of the oral airway. *Am Rev Respir Dis.* Mar 1982;125(3):363-365.

247. Cole P. Some aspects of temperature, moisture and heat relationships in the upper respiratory tract. *J Laryngol Otol.* Aug 1953;67(8):449-456.

248. Davis SS, Eccles R. Nasal congestion: mechanisms, measurement and medications. Core information for the clinician. *Clin Otolaryngol Allied Sci.* Dec 2004;29(6):659-666.

249. Kennedy DW, Zinreich SJ, Kumar AJ, Rosenbaum AE, Johns ME. Physiologic mucosal changes within the nose and ethmoid sinus: imaging of the nasal cycle by MRI. *Laryngoscope.* Sep 1988;98(9):928-933.

250. Eccles KS, Eccles R. Nasal vasodilation induced by electrical stimulation of the vagus nerve. *Rhinology.* Jun 1982;20(2):89-92.

251. Cakmak O, Celik H, Cankurtaran M, Buyuklu F, Ozgirgin N, Ozluoglu LN. Effects of paranasal sinus ostia and volume on acoustic rhinometry measurements: a model study. *J Appl Physiol.* Apr 2003;94(4):1527-1535.

252. Gold GE, Busse RF, Beehler C, et al. Isotropic MRI of the knee with 3D fast spin-echo extended echo-train acquisition (XETA): initial experience. *AJR Am J Roentgenol.* May 2007;188(5):1287-1293.

253. Lefevre N, Naouri JF, Bohu Y, Klouche S, Herman S. Partial tears of the anterior cruciate ligament: diagnostic performance of isotropic three-dimensional fast spin echo (3D-FSE-Cube) MRI. *European journal of orthopaedic surgery & traumatology : orthopedie traumatologie.* Nov 21 2012.

254. Ai T, Zhang W, Priddy NK, Li X. Diagnostic performance of CUBE MRI sequences of the knee compared with conventional MRI. *Clinical radiology.* Dec 2012;67(12):e58-63.

255. http://www.mathworks.co.uk/help/images/registering-multimodal-mri-images.html.

256. Haight JS, Cole P. The site and function of the nasal valve. *Laryngoscope.* Jan 1983;93(1):49-55.

257. Cole P, Haight JS, Cooper PW, Kassel EE. A computed tomographic study of nasal mucosa: effects of vasoactive substances. *J Otolaryngol.* Feb 1983;12(1):58-60.

258. Haight JJ, Cole P. Reciprocating nasal airflow resistances. *Acta Otolaryngol.* Jan-Feb 1984;97(1-2):93-98.

259. Seppa M. High-quality two-stage resampling for 3-D volumes in medical imaging. *Medical image analysis.* Aug 2007;11(4):346-360.

260. Schnabel JA, Rueckert D, Quist M, et al. A generic framework for non-rigid registration based on non-uniform multi-level free-form deformations. *Fourth Int. Conf. on Medical Image Computing and Computer-Assisted Intervention* 2001:573-581.

261. http://www.doc.ic.ac.uk/~dr/software/.

262. Cetto R, Rennie CE, Bates AJ, Schroter RC, Doorly DJ, Tolley NS. Regional Patterns of Nasal Decongestion. *Otolaryngology -- Head and Neck Surgery* 2012 147 116.

263. Yokley TR. Ecogeographic variation in human nasal passages. *American Journal of Physical Anthropology.* 2009;138(1):11-22.

264. Mugler JP, 3rd, Bao S, Mulkern RV, et al. Optimized single-slab three-dimensional spin-echo MR imaging of the brain. *Radiology.* Sep 2000;216(3):891-899.

265. Gilbert R, Auchincloss JH, Jr., Brodsky J, Boden W. Changes in tidal volume, frequency, and ventilation induced by their measurement. *J Appl Physiol.* Aug 1972;33(2):252-254.

266. Perez W, Tobin MJ. Separation of factors responsible for change in breathing pattern induced by instrumentation. *J Appl Physiol.* Nov 1985;59(5):1515-1520.

267. Han J, Stegen K, Cauberghs M, Van de Woestijne K. Influence of awareness of the recording of breathing on respiratory pattern in healthy humans. *European Respiratory Journal.* January 1, 1997 1997;10(1):161-166.

268. Western PJ, Patrick JM. Effects of focusing attention on breathing with and without apparatus on the face. *Respiration physiology.* Apr 1988;72(1):123-130.

269. Hirsch JA, Bishop B. Human breathing patterns on mouthpiece or face mask during air, CO2, or low O2. *J Appl Physiol.* Nov 1982;53(5):1281-1290.

270. Weissman C, Askanazi J, Milic-Emili J, Kinney JM. Effect of respiratory apparatus on respiration. *J Appl Physiol.* Aug 1984;57(2):475-480.

271. Askanazi J, Silverberg PA, Foster RJ, Hyman AI, Milic-Emili J, Kinney JM. Effects of respiratory apparatus on breathing pattern. *J Appl Physiol.* Apr 1980;48(4):577-580.

272. McGregor M, Adam W, Sekelj P. Influence of Posture on Cardiac Output and Minute Ventilation During Exercise. *Circulation Research.* 1961;9:1089-1092.

273. Baydur A, Behrakis PK, Zin WA, Jaeger MJ, Weiner JM, Milic-Emili J. Effect of posture on ventilation and breathing pattern during room air breathing at rest. *Lung.* 1987;165(6):341-351.

274. Burki NK. The effects of changes in functional residual capacity with posture on mouth occlusion pressure and ventilatory pattern. *Am Rev Respir Dis.* Nov 1977;116(5):895-900.

275. Stammberger H. Nasal and Paranasal Sinus Endoscopy A Diagnostic and Surgical Approach to Recurrent Sinusitis. *Endoscopy.* 1986;18(06):213-218.

276. Chambers DW, Davis WE, Cook PR, Nishioka GJ, Rudman DT. Long-term outcome analysis of functional endoscopic sinus surgery: correlation of symptoms with endoscopic examination findings and potential prognostic variables. *Laryngoscope.* Apr 1997;107(4):504-510.

277. Kennedy DW. Functional endoscopic sinus surgery. Technique. *Archives of otolaryngology (Chicago, Ill. : 1960).* 10/ 1985;111(10):643-649.

278. Higdon JJ. Stokes flow in arbitrary two-dimensional domains—shear flow over ridges and cavities. . *J Fluid Mech.* 1985;159 195–226.

279. Shankar PN, Deshpande MD. Fluid mechanics in the driven cavity. *Annual review of fluid mechanics.* 2000;32:92-136.

280. Tutty OR. Flow in a tube with a small side branch. . *J Fluid Mech* 1988;191:79-109.

281. Lund VJ. Fundamental considerations of the design and function of intranasal antrostomies. *Rhinology.* 1985 1985;23(3):231-236.

282. Gaston B, Drazen JM, Loscalzo J, Stamler JS. The biology of nitrogen oxides in the airways. *Am J Respir Crit Care Med.* Feb 1994;149(2 Pt 1):538-551.

283. Mancinelli RL, McKay CP. Effects of nitric oxide and nitrogen dioxide on bacterial growth. *Appl. Environ. Microbiol.* July 1, 1983 1983;46(1):198-202.

284. Croen KD. Evidence for antiviral effect of nitric oxide. Inhibition of herpes simplex virus type 1 replication. *The Journal of Clinical Investigation.* 1993;91(6):2446-2452.

285. Runer T, Lindberg S. Effects of nitric oxide on blood flow and mucociliary activity in the human nose. *Ann Otol Rhinol Laryngol.* Jan 1998;107(1):40-46.

286. Furukawa K, Harrison DG, Saleh D, Shennib H, Chagnon FP, Giaid A. Expression of nitric oxide synthase in the human nasal mucosa. *Am J Respir Crit Care Med.* Feb 1996;153(2):847-850.

287. Melillo G, Taylor LS, Brooks A, Cox GW, Varesio L. Regulation of inducible nitric oxide synthase expression in IFN-gamma-treated murine macrophages cultured under hypoxic conditions. *J Immunol.* Sep 15 1996;157(6):2638-2644.

288. Kirihene RKDRA, Rees G, Wormald P-J. The Influence of the Size of the Maxillary Sinus Ostium on the Nasal and Sinus Nitric Oxide Levels. *Am. J. Rhinol.* 2002;16:261-264.

289. Qian W, Chatkin JM, Djupesland PG, et al. Unilateral nasal nitric oxide measurement after nasal surgery. *Ann Otol Rhinol Laryngol.* Oct 2000;109(10 Pt 1):952-957.

290. Nakano H, Ide H, Ogasa T, et al. Ambient oxygen regulates epithelial metabolism and nitric oxide production in the human nose. *J Appl Physiol.* Jul 2002;93(1):189-194.

291. Haight JS, Qian W, Daya H, Chalmers P, Zamel N. Hypoxia depresses nitric oxide output in the human nasal airways. *Laryngoscope.* Mar 2000;110(3 Pt 1):429-433.

292. Arnal JF, Flores P, Rami J, et al. Nasal nitric oxide concentration in paranasal sinus inflammatory diseases. *Eur Respir J.* Feb 1999;13(2):307-312.

293. Baraldi E, Azzolin NM, Biban P, Zacchello F. Effect of antibiotic therapy on nasal nitric oxide concentration in children with acute sinusitis. *Am. J. Respir. Crit. Care Med.* May 1, 1997 1997;155(5):1680-1683.

294. Colantonio D, Brouillette L, Parikh A, Scadding GK. Paradoxical low nasal nitric oxide in nasal polyposis. *Clin Exp Allergy.* May 2002;32(5):698-701.

295. Balfour-Lynn IM, Laverty A, Dinwiddie R. Reduced upper airway nitric oxide in cystic fibrosis. *Arch Dis Child.* Oct 1996;75(4):319-322.

296. Andersson JA, Cervin A, Lindberg S, Uddman R, Cardell LO. The paranasal sinuses as reservoirs for nitric oxide. *Acta Otolaryngol.* Dec 2002;122(8):861-865.

297. Menzel L, Hess A, Bloch W, et al. Temporal nitric oxide dynamics in the paranasal sinuses during humming. *J Appl Physiol.* June 1, 2005 2005;98(6):2064-2071.

298. Haight JS, Djupesland PG, Qjan W, et al. Does nasal nitric oxide come from the sinuses? *J Otolaryngol.* Aug 1999;28(4):197-204.

299. Dubois AB, Douglas JS, Stitt JT, Mohsenin V. Production and absorption of nitric oxide gas in the nose. *J Appl Physiol.* Apr 1998;84(4):1217-1224.

300. Lindberg S, And AC, Runer T. Nitric Oxide (NO) Production in the Upper Airways is Decreased in Chronic Sinusitis. *Acta oto-laryngologica.* 1997;117(1):113-117.

301. Lund VJ. The results of inferior and middle meatal antrostomy under endoscopic control. *Acta Otorhinolaryngol Belg.* 1993 1993;47(1):65-71.

302. Ramadan HH. Surgical causes of failure in endoscopic sinus surgery. *Laryngoscope.* Jan 1999;109(1):27-29.

303. Weitzberg E, Lundberg JO. Humming greatly increases nasal nitric oxide. *Am J Respir Crit Care Med.* Jul 15 2002;166(2):144-145.

304. Lundberg JO, Maniscalco M, Sofia M, Lundblad L, Weitzberg E. Humming, nitric oxide, and paranasal sinus obstruction. *JAMA.* Jan 15 2003;289(3):302-303.

305. Maniscalco M, Weitzberg E, Sundberg J, Sofia M, Lundberg JO. Assessment of nasal and sinus nitric oxide output using single-breath humming exhalations. *Eur Respir J.* Aug 2003;22(2):323-329.

306. Guillerm R, Badre R, Flottes L, Riu R, Rey A. [A new method of aerosol penetration into the sinuses]. *Presse medicale.* May 30 1959;67(27):1097-1098.

307. Maniscalco M, Sofia M, Weitzberg E, Carratu L, Lundberg JO. Nasal nitric oxide measurements before and after repeated humming maneuvers. *Eur J Clin Invest.* Dec 2003;33(12):1090-1094.

308. Granqvist S, Sundberg J, Lundberg JO, Weitzberg E. Paranasal sinus ventilation by humming. *J Acoust Soc Am.* May 2006;119(5 Pt 1):2611-2617.

309. Eby GA. Strong humming for one hour daily to terminate chronic rhinosinusitis in four days: a case report and hypothesis for action by stimulation of endogenous nasal nitric oxide production. *Medical hypotheses.* 2006;66(4):851-854.

List of publications and contributions

Rennie CE, Gouder KA, Taylor DJ, Tolley NS, Schroter RC, Doorly DJ. Nasal Inspiratory Flow: At Rest and Sniffing. International Forum of Allergy and Rhinology 2011; 3: 128-135.

Rennie CE, Hood CM, Blenke EJSM, Schroter RC, Doorly DJ, Jones H, Towey D, and Tolley NS. Physical and computational modelling of ventilation of the maxillary sinus. Otolaryngology-Head and Neck Surgery 2011; 145 (1): 165-170.

Hood CM, Schroter RC, Doorly DJ, Rennie C, Blenke EJ and Tolley NS. 'Modelling of Human Maxillary Sinus Nitric Oxide Transport' Oral presentation at the 6th World Congress of Biomechanics, Singapore, August 2010. 'Best Young Investigator' prize in Respiratory Mechanics stream. The paper was published in the IFMBE Proceedings, 2010, 31.

Published abstracts

Cetto R, Rennie CE, Bates AJ, Schroter RC, Doorly DJ, Tolley NS. Regional Patterns of Nasal Decongestion. Otolaryngology - Head and Neck Surgery 2012; 147: 116.

Blenke E, Rennie CE, Hood CM, Schroter RC, Doorly DJ, Tolley NS. The effects of sinonasal mophology on transport mechanisms in the maxillary sinus. Clinical Otolaryngology, 2011, 36 (2), 202.

Rennie CE, Blenke EJSM, Hood CM, Towey D, Jones HA, Schroter RC, Doorly DJ, Tolley NS. Analysis of Maxillary Sinus Ventilation. Otolaryngology-Head and Neck Surgery 2010;143(S2)24.

Blenke E, Rennie C, Hood C, Schroter RC, Towey D, Jones H, Doorly D, Tolley NS. Analysis of sinonasal airflow using Krypton81m; a pilot study. Clinical Otolaryngology 2009; 34(s1): 2.

Oral Presentations

Rennie CE, Gouder K, Cetto R, Bates A, Tolley NS, Doorly DJ. Current concepts of nasal airflow mechanics. EAORL Nice, France, April 2013.

Cetto R, Rennie CE, Bates AJ, Schroter RC, Doorly DJ, Tolley NS. Regional Patterns of Nasal Decongestion. American Academy of Otolaryngology and Head and Neck Surgery Annual Meeting. Washington Sept 2012.

Doorly DJ, Taylor DJ, Houzeaux G, Rennie CE, Tolley NS. Computational Modelling of Airflow in the Respiratory Tract. Parallel CFD 2011 conference (http://parcfd2011.bsc.es/), 23rd International Conference on Parallel Computational Fluid Dynamics. 16-18 May 2011, Barcelona, Spain.

Rennie CE, Taylor DJ, Cetto R, Doorly D, Schroter R, Gedroyc W, Tolley N. Patterns of Nasal Congestion. Oral Presentation at the European Rhinitis and Asthma Meeting (ERAM)/Symposium on Experimental Rhinology and Immunology of the Nose (SERIN), 4th – 6th November 2010, Brussels, Belgium.

Rennie CE, Blenke EJSM, Hood CM, Towey D, Jones HA, Schroter RC, Doorly DJ, Tolley NS. Analysis of Maxillary Sinus Ventilation. Oral presentation at the American Academy of Otolaryngology and Head and Neck Surgery Annual Meeting. 26-29th September 2010. Boston USA.

Rennie CE, Gouder KA, Taylor DJ, Tolley NS, Schroter RC, Doorly DJ. Characterizing Patterns of Nasal Inspiration. Oral presentation at the American Rhinology Society's Annual Meeting September 25th 2010 Boston USA.

Doorly DJ, Taylor DJ, Schroter RC, Rennie C, Gambaruto A. Upper Airway Flow and Transport: The Reality of Modelling. Oral Presentation. 6th World Congress of Biomechanics, 1st – 6th August 2010, Singapore Suntec Convention Centre, Singapore.

Rennie CE, Blenke EJSM, Hood CM, Towey D , Jones H , Doorly DJ, Schroter R, Tolley NS. Experimental and computational analysis of gas exchange between the nose and maxillary sinus. Oral presentation at the 23rd Congress of the European Rhinology Society and the 29th International Symposium of Infection and Allergy. Geneva Switzerland June 20-24th 2010.

Rennie C, Blenke EJSM, Hood CM, Towey D, Doorly DJ, Tolley NS. Investigation of maxillary sinus ventilation. Oral presentation prize at the British Rhinology Society Annual Meeting, Solihull, May 2010.

Blenke EJSM, Rennie CE, Hood CM, Schroter RC, Doorly DJ, Tolley NS. The effects of sinonasal morphology on transport mechanisms in the maxillary sinus. Oral presentation at the Annual Irish Otolaryngology Society meeting, Cork, October 2009.

Poster presentations

Rennie CE, Gouder K, Cetto R, Schroter R, Doorly D, Tolley N. Investigating nasal inspiratory air flow. 14th British Academic Conference in Otolaryngology and ENT Expo, Glasgow July 2012.

R. Cetto, C.E. Rennie, A.J. Bates, R.C. Schroter, D.J. Doorly, N.S. Tolley. Regional Patterns of Nasal Decongestion. 14th British Academic Conference in Otolaryngology and ENT Expo, Glasgow July 2012.

Blenke E, Rennie CE, Doorly D, Tolley N. Analysis of the relation between sinonasal airway geometry and gaseous exchange processes14th British Academic Conference in Otolaryngology and ENT Expo, Glasgow July 2012.

Rennie CE, Taylor DJ, Cetto R, Doorly D, Schroter RC, Gedroyc W, Tolley NS. Investigation of Nasal Congestion with 3T MRI. Poster Presentation at the European Rhinitis and Asthma Meeting (ERAM)/Symposium on Experimental Rhinology and Immunology of the Nose (SERIN), 4th – 6th November 2010, Brussels, Belgium.

Blenke EJSM, Rennie CE, Hood CM, Doorly DJ, Schroter RC, Jones H, Towey D, Tolley NS. Analysis of sinonasal airflow using Kr81m, a pilot study. Poster presentation at the British Academic Conference in Otolaryngology, Liverpool, 2009. 1st Prize for best poster presentation.

Appendices

Protocol for Acoustic Rhinometry

The unit must be calibrated each time it is switched on.

Turn the unit on it will be in calibration mode with the word calibrate highlighted.

Place calibration tube firmly on wave tube.

Press enter on the keyboard to begin calibration. You will hear clicking noises as the unit is calibrated.

The word Acquire is highlighted when calibration is finished.

Remove the calibration tube.

Prepare for a test

Select Patient

Enter all patient data

Select Acquire

Sit the patient in a straight backed chair facing straight ahead and remove glasses

Always place the chair in a consistent location (give the subject an X to focus on).

Explain the test and run through the motions with the patient so they are familiar with the sound and breathing techniques and the feel of the tube against their nose.

The patient should rest and acclimatize first for 30mins before measurement.

Perform Test

Determine nose tip size (2 available standard or small).

Place nose tip on wave tube.

Put gel on the edge of the nose tip avoiding the lumen.

Ensure the downward slant of the nose tip is towards septum.

Gently place the nose tip against the subject's nostril.

Ensure no distortion of the nostril by the tube and no gel in tip.

Hold the wave tube on the same plane as the bridge of the subject's nose and fix position with clamp.

Tell the patient to pause in breathing on the count of 3

Press start/stop on the wave tube

Collect data until you hear an audible bleep or see red dot on right hand corner of the screen (about 4 seconds) and press start /stop again. The test result is shown on the monitor.

Rotate the tip 180 to do the other nostril.

MRI Study Protocol

1. Anterior rhinoscopy and nasoendoscopy to ensure normal anatomy
2. 30mins to acclimatise at rest in test room
3. SNOT 22 questionnaire and visual analogue score whilst acclimatising.
4. A pre decongestant Acoustic Rhinometry reading is taken (as per AR protocol)
5. First MRI scan taken supine with head and neck coil (head in fixed position)
6. While the subject is lying on the MRI table, the decongestant (otrivine) is sprayed three times into each nasal cavity until the subject tasted or noticed traces of the spray in the throat. (The atomizer delivers a mean volume of 0.3 ml of decongestant per spray active ingredient xylometazoline hydrocholride 0.1%.) 1 Spray repeated after 5 minutes.
7. Allow 20 minutes for the decongestant to take effect. Take care not to move the subject during this period.
8. The post-decongestant MRI scans are then performed without changing the window contrast or other settings.
9. Post decongestant AR measurements are taken after the MRI scan.
10. The same positioning and alignment coordinates that were used for the pre decongestant readings are used for the post decongestant measurements.

Krypton Study Protocol

Date

Time

Room Temperature

Check ostial configuration

Check sinus size

Ensure model lid tightly screwed down

Place model in scanner ensure horizontal

Ensure tight fit between cameras

Connect medical air

Connect Krypton

Connect flow meter

Check flow rates

Start Medical Air

Start gamma camera

Start Krypton

Image every 2 seconds for 5 or 10 mins

Stop Krypton

Reconfigure model and repeat

Volunteer information sheet: Measuring nasal function.

- This study invites you to help us improve our clinical assessment of patients' noses and improve our understanding of healthy nasal physiology.

- The way we do this is to look at and analyse images of the inside of your nose and take measurements of your nose using an **acoustic rhinometer, rhinomanometer, nasal inspiratory peak flow meter and hot wire anemometer:**
  - **Acoustic rhinometry** entails placing a small tube on the end of each nostril while a computer measures the internal dimensions of your nose using sound waves. It doesn't hurt and takes a couple of minutes to do. Then we will spray your nose with decongestant (the same spray used to examine your nose in the ENT outpatient clinic) and will repeat the measurement. While the spray is working we will ask you to fill out a simple questionnaire about your nasal symptoms (SNOT-22).
  - **Rhinomanometry** entails placing a mask over your face with tube on the end of your nostril. A computer measures the pressure changes in your nose while you breathe.
  - **Nasal Inspiratory Peak Flow** entails placing a mask over your face and you taking 3 sharp breaths in through your nose. A small dial indicates the maximum flow rate.
  - **Hot wire anemometry** entails breathing through a tube placed against each nostril. The tube contains a tiny probe linked to a computer which records the flow rates.
  - **MRI Scan** entails lying still in a scanner for 5 minutes the scanner is noisy and some people find it claustrophobic.

- You have been selected for this study because you are a normal volunteer.
- In terms of your time, we are asking you to come to the outpatient department on 1 occasion to undergo the above measurements and to have an MRI scan of your nose before and after a decongestant is administered. To perform hot wire anemometry an additional visit to Imperial College London will be required. One of the doctors will telephone you to confirm the dates of these and where to come.
- Your data, when gathered will be coded and stored on a database - nobody will be able to recognise your nose from the data we have!
- You are not obliged to participate in this study, but obviously any participation on your part and information we can gather will be most gratefully received.
- If you decide to take part you will be given this information sheet to keep and asked to sign a consent form. If you decide to take part you are still free to withdraw at any time and without giving a reason.
- Imperial College London holds insurance policies which apply to this study. If you experience serious and enduring harm or injury as a result of taking part in this study, you may be eligible to claim compensation without having to prove that Imperial College is at fault. This does not affect your legal rights to seek compensation.
- If you are harmed due to someone's negligence, then you may have grounds for a legal action. Regardless of this, if you wish to complain, or have any concerns about any aspect of the way you have been treated during the course of this study then you should immediately inform the Investigator Miss Catherine Rennie. The normal National Health Service complaints mechanisms are also available to you. If you are still not satisfied with the response, you may contact the Imperial AHSC Joint Research Office.

Thank you for your time.

Volunteer Consent Form

Study Protocol Number: 2

Full Title of Project: Investigation of sinonasal airflow and transport

Name of Principal Investigator: Mr N S Tolley

Please initial box

1. I confirm that I have read and understand the subject information sheet for the above study and have had the opportunity to ask questions which have been answered fully. ☐

2. I understand that my participation is voluntary and I am free to withdraw at any time, without giving any reason, without my medical care or legal rights being affected. ☐

3. The compensation arrangements have been discussed with me. ☐

4. I agree to take part in the above study. ☐

_____ _____ _____

Name of Subject Signature Date

_____ _____ _____

Name of Person taking consent Signature Date

(if different from Principal Investigator)

_____ _____ _____

Principal Investigator Signature Date

1 copy for subject; 1 copy for Principal Investigator; 1copy to be kept with hospital notes

Sino-Nasal Outcome Test-22 Questionnaire v4

Below you will find a list of symptoms and social/emotional consequences of your nasal disorder. We would like know more about these problems and would appreciate you answering the following question to the best of your ability. There are no right or wrong answers, and only you can provide us with this information. Please rate your problems, as they have been over the past two weeks. Thank you for your participation.

Considering how severe the problem is when you experience it and how frequently it happens, please rate each item below on how 'bad' it is by circling the number that corresponds with how you feel using this scale ➔	**No problem**	**Very mild problem**	**Mild or slight problem**	**Moderate problem**	**Severe problem**	**Problem as bad as it can be**
1. Need to blow nose	0	1	2	3	4	5
2. Sneezing	0	1	2	3	4	5
3. Runny nose	0	1	2	3	4	5
4. Cough	0	1	2	3	4	5
5. Post nasal discharge (dripping at the back of your nose)	0	1	2	3	4	5
6. Thick nasal discharge	0	1	2	3	4	5
7. Ear fullness	0	1	2	3	4	5
8. Dizziness	0	1	2	3	4	5
9. Ear pain/pressure	0	1	2	3	4	5
10. Facial pain/pressure	0	1	2	3	4	5
11. Difficulty falling asleep	0	1	2	3	4	5
12. Waking up at night	0	1	2	3	4	5
13. Lack of a good night's sleep	0	1	2	3	4	5
14. Waking up tired	0	1	2	3	4	5
15. Fatigue during the day	0	1	2	3	4	5
16. Reduced productivity	0	1	2	3	4	5
17. Reduced concentration	0	1	2	3	4	5
18. Frustrated/restless/irritable	0	1	2	3	4	5
19. Sad	0	1	2	3	4	5
20. Embarrassed	0	1	2	3	4	5
21. Sense of taste/smell	0	1	2	3	4	5
22. Blockage/congestion of nose	0	1	2	3	4	5
TOTAL:	_____	_____	_____	_____	_____	_____

For Medical Use Only **GRAND TOTAL:** _____

Patient No.: d.o.b.: Date:

M F

Diagnosis: Aims of Treatment:

Today's treatment: L-M score:

MRI scanner settings

CUBE 3D TSC with variable flip angle

Slice thickness 1.2mm

T2 weighted

Repetition time 2500ms

Echo time 89.248ms

CT scanning parameters

Subject	1
Scanner	Philips Mx8000
Scan option	Helix
Protocol	Sinus 1mm/Head/HX
Acquisition	Axial
Slice thickness	1.3
Increment	0.7
Data collection diameter	200
Reconstr diameter	200
Matrix	512x512
Tube voltage	
Tube current	88
kVP	120
Samples per pixel	1
Content	512x512x134 short stacked coordinates
Pixel spacing	0.390625\0.390625
Window centre	-0200\-0200
Data window	-200 200

Correcting for the effects of entry flow

When the value of Re for the ostium flow is above 30, entry flow effects will be significant and this must be taken into account when estimating ostium flow rate. An empirical correction developed by Loudon and McCulloh (1999) was used to estimate the effects of entry flow in the ostia on the flow rate through a double ostium sinus.

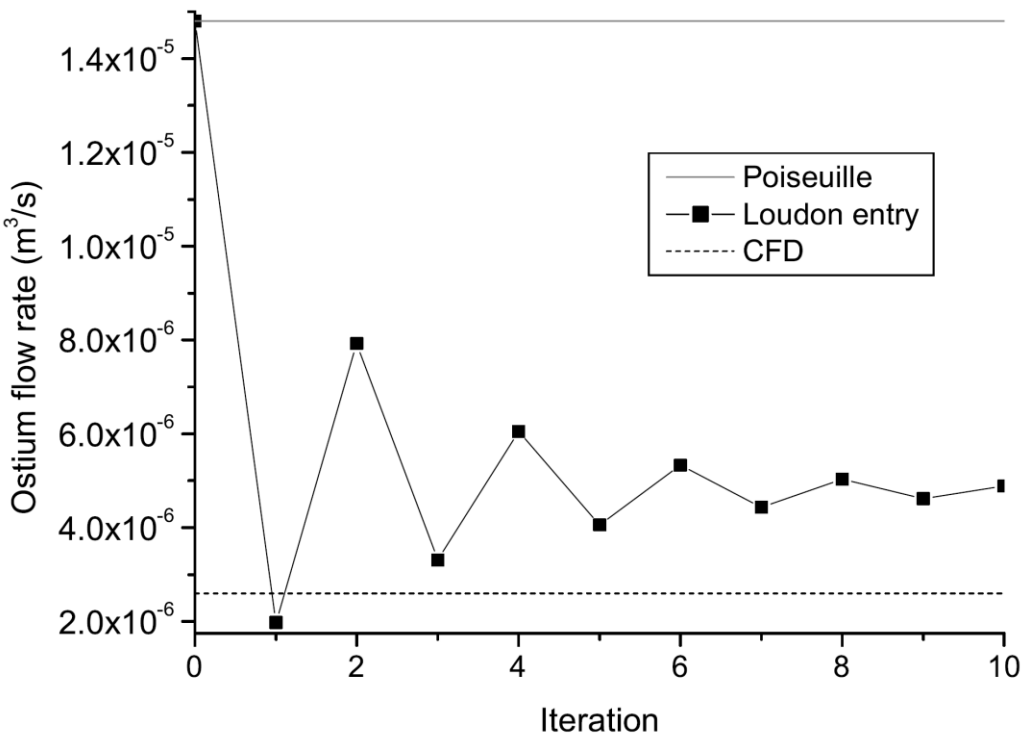

Convergence of Equation 3.12 applied over ten iterations. The Poiseuille and CFD flow rates are also shown. Figure provided courtesy of Dr C.M. Hood [47].

Determining an average waveform for a single subject

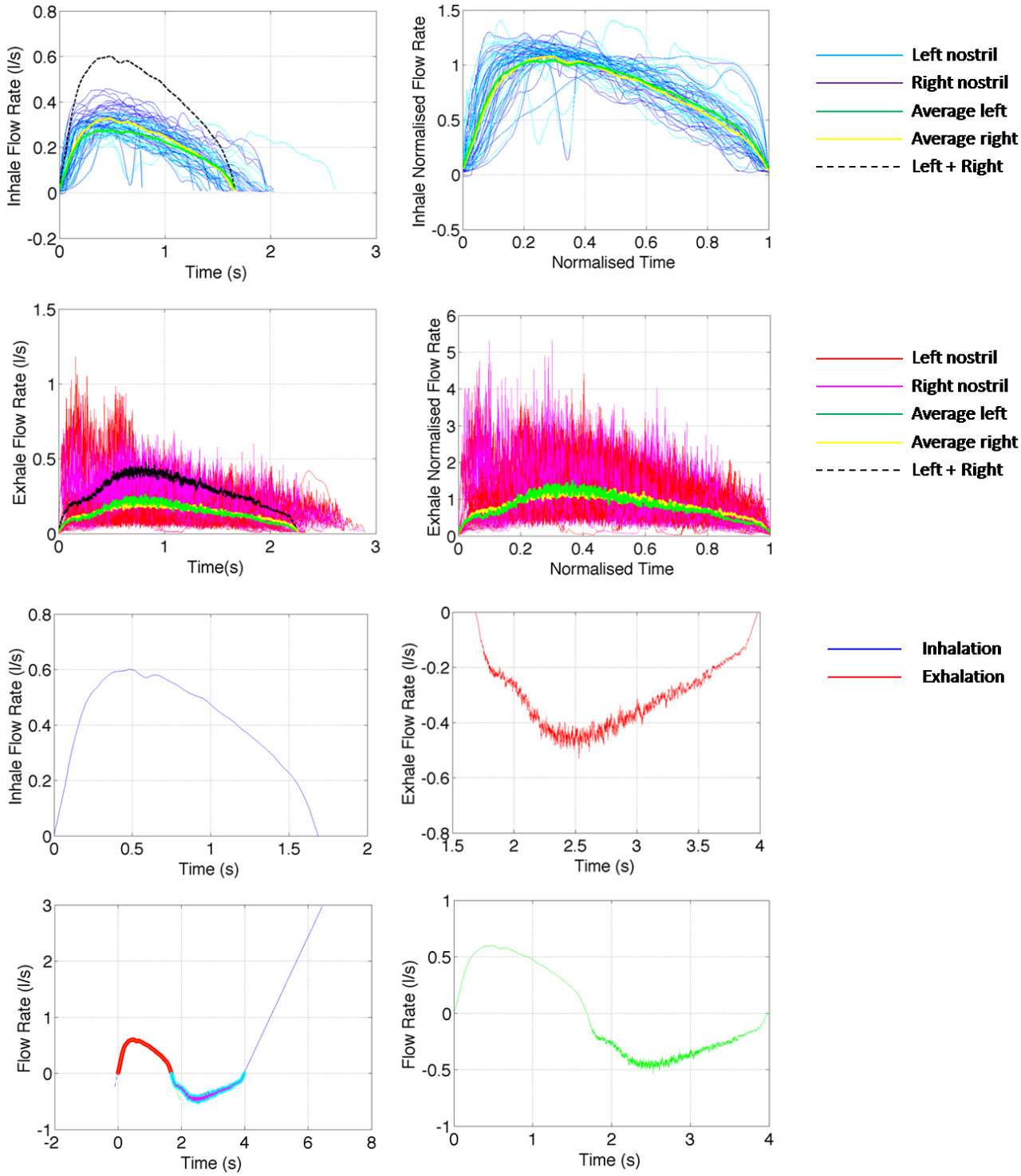

The figures above demonstrate the steps taken in determining an average waveform for a single subject going from the raw data top left to final waveform bottom right.

Gamma scintigraphy image processing detail

Closer detail of the change in total count number of ROI 3 and the difference between ROI 2 and 4 (identified in Figure 3.13) associated with moving the ROI to the left or right on the image (figure 3.13), corresponding to the left and right of the vertical axis.

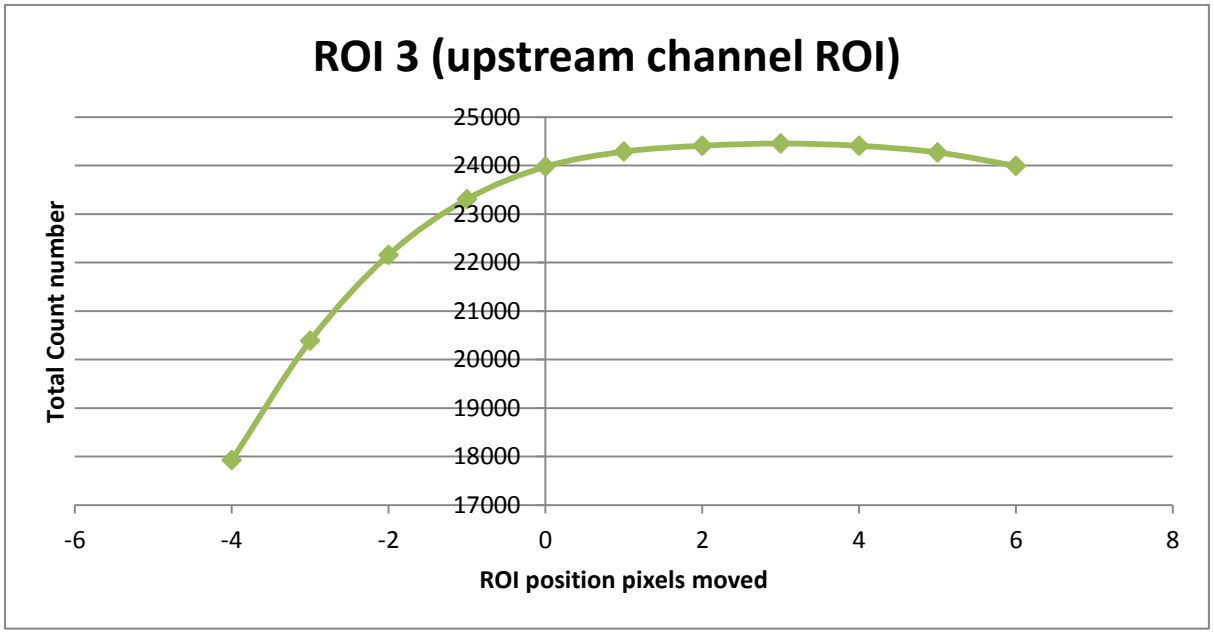

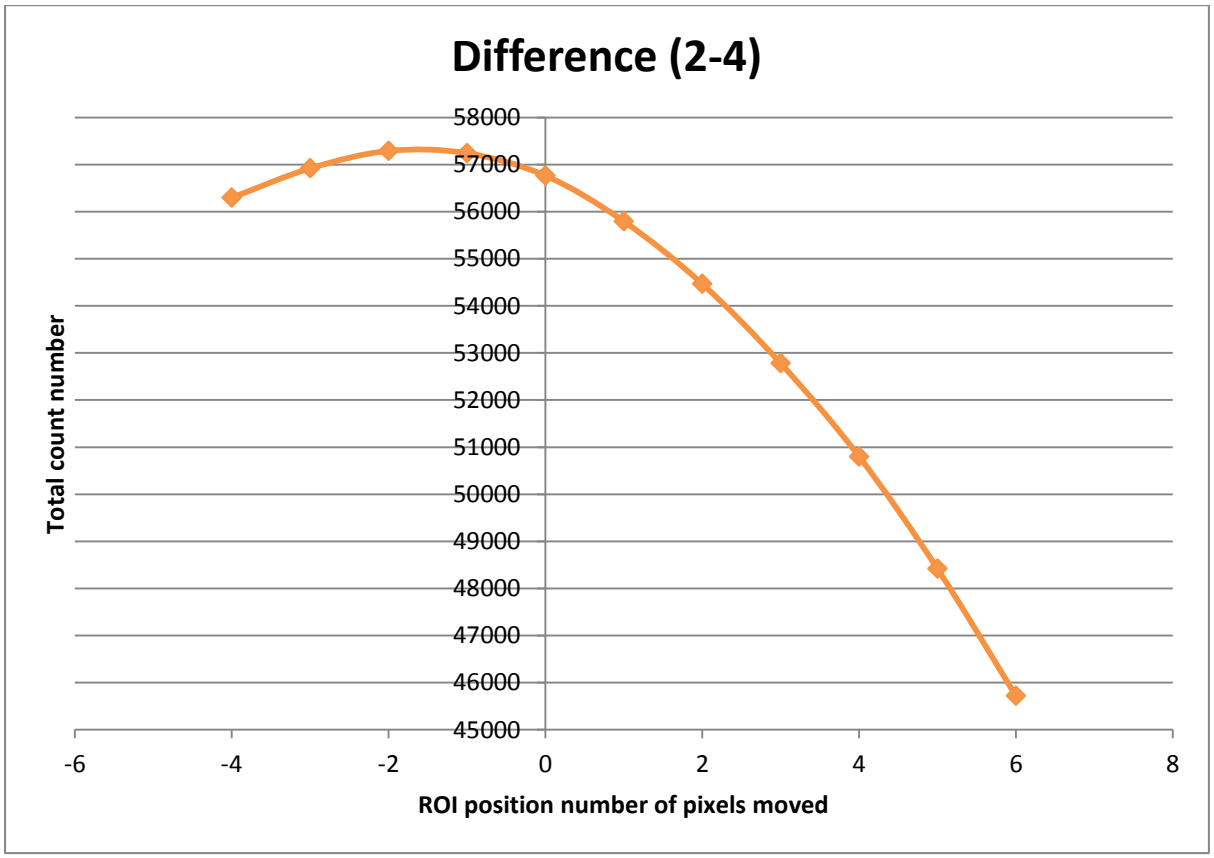

Determining the optimum position of the ROI in the gamma scintigraphy images. (Compare with figure 3.14 pg 69)

Computational model and solver settings

• Double Precision: Selected for increased numerical accuracy in handling very small variations of pressure and other flow variables, and also its suitability for geometries with wide length scale variations. It means that each value is stored as 64 bits rather than the default 32 bits, increasing the overall memory requirement.
• Higher-order Discretisations: Third-order spatial discretisation and second order implicit temporal discretisation were chosen to improve the accuracy and stability of the numerical solutions.
• Pressure-Based Solver: The nasal cavity and sinuses have very low flow velocities, so compressibility effects are expected to be negligible. Hence the pressure-based rather than density-based solver was chosen for sinus ventilation modelling.
• Laminar: The Reynolds' number (Re) in the channel at the standard flow rate is approximately 250, while the maximum Re in an accessory ostium with through-flow is 20. These values of Re are too high to allow the assumption of inertia-free Stokes' flow, but low enough to indicate that the flow will be fully laminar, with no transition to turbulence.
• Steady flow: Although breathing is a bi-directional process, during quiet breathing the time for flow reversal and the energy available for mixing is unlikely to be significant. The experimental findings of identical pressure changes in the sinus and nose and very small volume changes due to Boyle's law indicate that the role of flow reversal in sinus ventilation is likely to be minor, so all the models were run with steady flow along the channel.
• Residuals: The errors in the values of each primary flow variable (velocity, continuity [conservation of mass] and species concentration when relevant) which remained at the end of each iteration, were monitored for convergence. These errors are collectively known as residuals. Convergence was considered to have occurred when the residuals had dropped significantly and then maintained
a low level, rather than by setting an arbitrary convergence threshold.

The physical model simulations were run with a uniform velocity at the inlet, based on the volume flow rate used in the experiments. Applying a more complex velocity profile at the inlet would have no influence on the ostial flow, as the channel is long enough for the flow to develop a classic parabolic profile before approaching the ostia, regardless of the inlet velocity profile. The channel flow profile 1 cm upstream from the large ostium and a parabolic profile are plotted in the figure below for comparison. The very close matching shows that the inlet velocity profile and the details of the ends of the model geometry do not affect the flow past the

ostia and thus the ostium gas transport, justifying the simplification of the geometry in order to reduce computational expense[47].

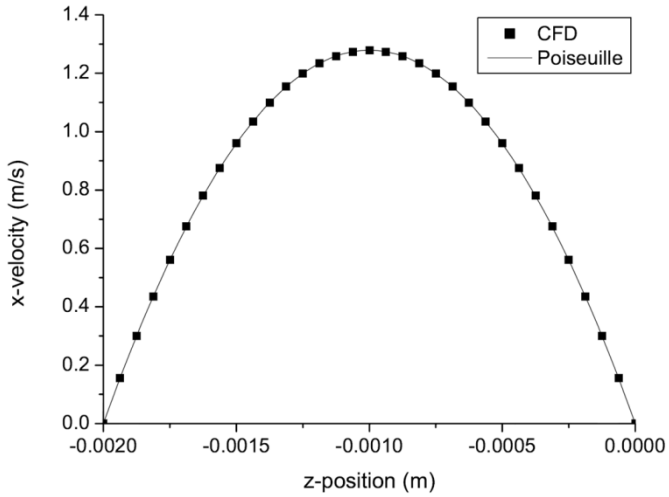

Velocity profile in the centre of the physical model channel, 1 cm upstream of large ostium, from CFD simulation (squares) and as predicted by Poiseuille flow (line). Figure provided courtesy of Dr C.M. Hood [47].